INFORMATION TO USERS

This manuscript has been reproduced from the microfilm master. UMI films the text directly from the original or copy submitted. Thus, some thesis and dissertation copies are in typewriter face, while others may be from any type of computer printer.

The quality of this reproduction is dependent upon the quality of the copy submitted. Broken or indistinct print, colored or poor quality illustrations and photographs, print bleedthrough, substandard margins, and improper alignment can adversely affect reproduction.

In the unlikely event that the author did not send UMI a complete manuscript and there are missing pages, these will be noted. Also, if unauthorized copyright material had to be removed, a note will indicate the deletion.

Oversize materials (e.g., maps, drawings, charts) are reproduced by sectioning the original, beginning at the upper left-hand corner and continuing from left to right in equal sections with small overlaps.

Photographs included in the original manuscript have been reproduced xerographically in this copy. Higher quality 6" x 9" black and white photographic prints are available for any photographs or illustrations appearing in this copy for an additional charge. Contact UMI directly to order.

Bell & Howell Information and Learning
300 North Zeeb Road, Ann Arbor, MI 48106-1346 USA
800-521-0600

UMI®

SYNTHETIC AND COMPUTATIONAL STUDIES ON ORGANOSULFUR RADICAL CATIONS AND α-METALATED SULFIDES

by

Edward Donald Lorance

A Dissertation Submitted to the Faculty of the

DEPARTMENT OF CHEMISTRY

In Partial Fulfillment of the Requirements
For the Degree of

DOCTOR OF PHILOSOPHY

In the Graduate College

THE UNIVERSITY OF ARIZONA

2000

Bell & Howell Information and Learning Company
300 North Zeeb Road
P.O. Box 1346
Ann Arbor, MI 48106-1346

THE UNIVERSITY OF ARIZONA ®
GRADUATE COLLEGE

As members of the Final Examination Committee, we certify that we have read the dissertation prepared by Edward Lorance

entitled Synthetic and Computational Studies on Organosulfur Radical Cations and α-Metalated Sulfides

and recommend that it be accepted as fulfilling the dissertation requirement for the Degree of Doctor of Philosophy

	8/11/2000 Date
	8/11/2000 Date
	8/11/2000 Date
	8/11/2000 Date
	8/11/2000 Date

Final approval and acceptance of this dissertation is contingent upon the candidate's submission of the final copy of the dissertation to the Graduate College.

I hereby certify that I have read this dissertation prepared under my direction and recommend that it be accepted as fulfilling the dissertation requirement.

Dissertation Director	8/18/2000 Date

STATEMENT BY AUTHOR

This dissertation has been submitted in partial fulfillment of requirements for an advanced degree at The University of Arizona and is deposited in the University Library to be made available to borrowers under rules of the Library.

Brief quotations from this dissertation are allowable without special permission, provided that accurate acknowledgment of source is made. Requests for permission for extended quotation from or reproduction of this manuscript in whole or in part may be granted by the head of the major department of the Dean of the Graduate College when in his or her judgment the proposed use of the material is in the interests of scholarship. In all other instances, however, permission must be obtained from the author.

SIGNED: 

ACKNOWLEDGMENTS

I would like to thank the faculty and staff of the Department of Chemistry at the University of Arizona for all their help over the course of my graduate education. In particular, I would like to thank Dr. Richard S. Glass, my research advisor, for his kind and patient help. I would also like to thank Dr. Nadine Gruhn for her assistance and advice. My graduate education was supported in part by a graduate fellowship from the National Science Foundation.

DEDICATION

My stay in Arizona, and in particular the last year of my graduate education, was difficult in ways that no one could have foreseen. My mother and father and my good friends made it both possible and desirable to see this through to the end, and I dedicate this work to them.

TABLE OF CONTENTS

LIST OF FIGURES 9
LIST OF SCHEMES 11
LIST OF TABLES 12
ABSTRACT 13

CHAPTER 1. INTRODUCTION 15
RADICAL CATIONS AND EXCITED STATES 15
SULFUR-CONTAINING COMPOUNDS 16
3,6-DISUBSTITUTED-1,2-DICHALCOGENINS 17
α-THIOCARBANIONS AND α-STANNYL SULFIDES 18
COMPUTATIONAL SIMULATION AND ANALYSIS 19
PHOTOELECTRON SPECTROSCOPY 20
ELECTROCHEMISTRY 22

CHAPTER 2. CONFORMATION AND ELECTROCHEMISTRY OF 1,2-DICHALCOGENINS 25
GENERAL PROPERTIES OF 1,2-DICHALCOGENINS 25
EFFECTS OF OXIDATION AND REDUCTION ON CONFORMATION 26
ELECTROCHEMICAL RESULTS 28
COMPUTATIONAL RESULTS 29
DISCUSSION 33
CONCLUSIONS 39

CHAPTER 3. COMPUTATIONAL SIMULATION AND ANALYSIS OF 1,2-DITHIINS: IONIZATION ENERGIES, ORBITAL ASSIGNMENTS, AND AN EXPLANATION OF THEIR COLOR 40
PREDICTING EXPERIMENTAL PROPERTIES BY COMPUTATION 40
COMPUTATIONAL RESULTS 40
DISCUSSION 62
Dithiin Electronic Structure 62
Geometry, Substitution, and Other Disulfides 63
Ionization Potentials and Substitution 64
The Nature of 1,2-Dichalcogenin Radicals 64
Electronic Transitions and Substitution 65
An Explanation of the Color of 1,2-Dichalcogenins 66
CONCLUSIONS 68

CHAPTER 4. AROMATICITY OR ANTI-AROMATICITY OF 1,2-DICHALCOGENINS AND THEIR RADICAL CATIONS: COMPUTATIONAL AND EXPERIMENTAL ANALYSIS 69
ASSESSMENT OF AROMATICITY AND ANTI-AROMATICITY 69
COMPUTATIONAL RESULTS 71
EXPERIMENTAL RESULTS 73
DISCUSSION 74
Computational Analysis of the Excited State 74
Experimental Indications of Aromaticity 76
CONCLUSIONS 80

TABLE OF CONTENTS – *Continued*

CHAPTER 5. α-DEPROTONATION OF DIALKYL SULFIDES: SYNTHESIS, REACTIONS, STABILITY, AND DECOMPOSITION MECHANISM OF α-THIOCARBANIONS 81
HISTORY AND PROGRESS IN α-THIOCARBANION SYNTHESIS 81
THEORIES OF α-THIOCARBANION STABILIZATION 84
CONFIGURATION OF α-THIOCARBANIONS 89
RESULTS 90
DISCUSSION 95
CONCLUSIONS 101

CHAPTER 6. α-STANNYL DIALKYL SULFIDES: COMPUTATIONAL ANALYSIS AND CORRELATION WITH ELECTROCHEMICAL OXIDATION POTENTIALS 102
NEIGHBORING-GROUP EFFECTS 102
COMPUTATIONAL RESULTS AND DISCUSSION 108
ELECTROCHEMICAL RESULTS 125
ELECTROCHEMICAL DISCUSSION 126
CONCLUSIONS 128

CHAPTER 7. COLLECTED METHODS 129
COMPUTATIONAL METHODS 129
Chapters 2-4: 1,2-Dichalcogenins 131
Chapter 6: α-Substituted Sulfides 132
Appendix A: Tetrathiatetraasterane 133
SYNTHETIC METHODS 133
Synthesis of Starting Sulfides 134
tert-Butyl Cyclohexyl Sulfide by Nucleophilic Substitution 134
tert-Butyl Cyclohexyl Sulfide by Photoreaction 134
Diisobutyl Sulfide from Sodium Sulfide 135
Diisobutyl Sulfide from Isobutyl Thiol 136
Dineopentyl Sulfide from Thiourea 136
Methylation of Alkyl Mercaptans 136
Synthesis of 4-*tert*-Butylthiane 138
4-*tert*-Butylpiperidine 138
N-Benzoyl-4-*tert*-butylpiperidine 140
1,5-Dibromo-3-*tert*-butylpentane 140
4-*tert*-Butylthiane 141
2-Trimethylstannyl-4-*tert*-butylthiane 141
General Procedure for the Trial Deprotonation of Sulfides 142
Summary of Previous Work 143
ELECTROCHEMICAL METHODS 144
General Electrochemical Procedure for 1,2-Dichalcogenins and Thioethers 144
General Electrochemical Procedure for Tetrathiatetraasterane 146

TABLE OF CONTENTS – *Continued*

APPENDIX A. ASTERANE: COMPUTATIONAL SIMULATION, ANALYSIS AND EXPLORATORY ELECTROCHEMICAL STUDIES 148
SIGMA AROMATICITY 148
HÜCKEL VS. MÖBIUS AROMATICITY 149
COMPUTATIONAL RESULTS 151
EXPERIMENTAL RESULTS 168
DISCUSSION 173
CONCLUSIONS 178

REFERENCES 179

LIST OF FIGURES

Figure 1.1. Franck-Condon Transitions for Molecules with Small Geometric Relaxation Energies (left) and Large Geometric Relaxation Energies (right). 22
Figure 2.1. 3,6-Disubstituted-1,2-Dichalcogenins (left) with a Perspective View (right). X = S, Se. 25
Figure 2.2. Valence Tautomerism in 1,2-Dithiins. 25
Figure 2.3a. Thiarubrine A. 26
Figure 2.3b. Thiarubrine B. 26
Figure 2.4. Critical Points of 1,2-Dithiin. 30
Figure 2.5. Critical Points of 3,6-Dimethyl-1,2-Dithiin. 32
Figure 3.1. 1,2-Dithiin Electronic Structure. 62
Figure 4.1. 10,11-Dihydrodibenz[b,f]oxepin, Dibenz[b,f]oxepin, Dibenz[b,f]thiepin, and Suberene. 70
Figure 4.2. Excitation-Induced Changes in the Bond Alternation of Biphenylene. 75
Figure 5.1. Mechanisms of α-Thiocarbanion Stabilization. 85
Figure 5.2. Acyclic vs. Bicyclic Trithioorthoformates. 87
Figure 5.3a. α-Elimination of Diethyl Sulfide, Free Carbene Mechanism. 96
Figure 5.3b. α-Elimination of Diethyl Sulfide, Concerted Mechanism. 96
Figure 5.4. α',β-Elimination of Diethyl Sulfide. 96
Figure 5.5. β-Elimination of Diethyl Sulfide. 97
Figure 5.6. Electrocyclic Decomposition of Thiolane α-Thiocarbanion. 98
Figure 5.7. Conformers for α',β-Elimination in Thiolane and Thiane α-Thiocarbanions. 99
Figure 6.1. Hydrogen Model of α-Stannylated Thioethers, Illustrating the Varied Dihedral Angle. 108
Figure 6.2. Hydrogen and Yoshida's Models' Ionization Potentials. 109
Figure 6.3a. Factors Affecting Ionization Potential: O-Si Model. 109
Figure 6.3b. Factors Affecting Ionization Potential: S-Sn Model. 110
Figure 6.4. Spin Densities on Heavy Atoms in the Cation Radical. 112
Figure 6.5. Charge Densities with Hydrogen Charges Summed into the Heavy Atoms in the Cation Radical. 112
Figure 6.6. α-Carbon-Tin Bond Length. 114
Figure 6.7. α-Carbon-Sulfur Bond Length. 114
Figure 6.8. Cleavage of the C-Sn Bond as the Thione System Develops. 116
Figure 6.9. Methylated Model of α-Stannylated Thioethers, Illustrating the Varied Dihedral Angle (M = C, Si, Sn). 117
Figure 6.10. Methylated Model Adiabatic Ionization Potentials. 118
Figure 6.11. Methylated Model Non-Adiabatic Ionization Potentials. 118
Figure 6.12. Effects of α-Carbon on the Energy of the Sulfide, Sulfur Radical Cation and Corresponding HOMOs. 120
Figure 6.13. Effects of α-Silicon on the Energy of the Sulfide, Sulfur Radical Cation and Corresponding HOMOs. 121
Figure 6.14. Effects of α-Tin on the Energy of the Sulfide, Sulfur Radical Cation and Corresponding HOMOs. 121
Figure A.1. p-Type Orbitals in Benzene: π-Type Overlap with No Interatomic Nodes. 150
Figure A.2. Barrelene Maximum Overlap Model. 150
Figure A.3. Hexaiodobenzene and Tetrathiaasterane Maximum Overlap. 151

LIST OF FIGURES – *Continued*

Figure A.4a. Exploded Overhead View: HOMO. 154
Figure A.4b. Exploded Overhead View: HOMO-1. 155
Figure A.4c. Elevated Side View (left) and Overhead View (right): Doubly-Degenerate HOMO-2. 155
Figure A.4d. Elevated Side View: HOMO-3. 155
Figure A.5. Cyclic Voltammograms of Asterane in Dichloromethane with Trifluoroacetic Anhydride. 170
Figure A.6. Carbon-Paste Cyclic Voltammograms. 172
Figure A.7. Photoelectron Spectra of Asterane. 174

LIST OF SCHEMES

Scheme 2.1. Photodecomposition of 1,2-Dithiins. 26
Scheme 7.1. 4-*tert*-Butylthiane. 138
Scheme 7.2. Synthesis of 3-Trialkylstannyl-2-thiabicyclo[2.2.1]heptane. 144
Scheme A.1. Asterane Desulfuration Pathways. 167

LIST OF TABLES

Table 2.1. Oxidation Peak Potentials of Various 1,2-Dichalcogenins. 28
Table 2.2. Electrochemical Parameters of 1,2-Dithiins. 29
Table 2.3. Taft Parameters for 3,6-Substituents of 1,2-Dithiins. 34
Table 3.1. Comparison of 1,2-Dithiin Bond Lengths. 42
Table 3.2. Comparison of 1,2-Dithiin Bond Angles. 43
Table 3.3. Comparison of 1,2-Dithiin Dihedral Angles. 44
Table 3.4. Comparison of 1,2-Dithiin Ionization Parameters. 45
Table 3.5. 1,2-Dithiin Molecular Orbitals. 49
Table 3.6. Computed Geometric Parameters of 1,2-Dithiins. 52
Table 3.7. Computed Geometric Parameters of Some Other Disulfides. 52
Table 3.8. Molecular Orbital Energies and Symmetries: 1,2-Dithiins. 53
Table 3.9. Molecular Orbital Energies and Symmetries: Selected Disulfides. 54
Table 3.10. Ionization Potentials of 1,2-Dithiins. 55
Table 3.11. Comparison of Charge and Spin Distribution in the Non-Adiabatic Cation Radicals of 1,2-Dithiin and 1,2-Diselenin. 55
Table 3.12. Electronic Transitions: Symmetries, Energies, Oscillator Strengths, and Contributing Transitions for 1,2-Dithiins. 56
Table 3.13. Electronic Transitions: Symmetries, Energies, Oscillator Strengths, and Contributing Transitions for Selected Disulfides. 58
Table 3.14. Calculated S-S Bond Lengths and Stretching Frequencies for Ground State and Electronic Excited States of Selected Disulfides. 61
Table 4.1a. Calculated Planarity Indicators for 1,2-Dithiins. 72
Table 4.1b. Calculated Bond Alternations and Substituent Participation for 1,2-Dithiins. 72
Table 4.2. Ring ^{1}H NMR, ^{13}C NMR, and ^{77}Se NMR Chemical Shifts of 1,2-Dichalcogenins and Related Compounds. 73
Table 5.1. Deprotonation of Thioethers. 90
Table 6.1. Basic Oxidation Potentials and Orbital Ionization Potentials. 103
Table 6.2. Oxidation Potentials of Derivatized Ethers. 104
Table 6.3. Oxidation Potentials and Ionization Potentials of 6-Substituted-1-Azadecalins and Substituent A Values. 105
Table 6.4. Ionization Potentials of Acyclic Ethers and Thioethers, Oxiranes, and Thiiranes. 105
Table 6.5. Oxidation Potentials of 2-Substituted-1,3-Dithianes. 107
Table 6.6. Oxidation Potentials of Selected Sulfides and Derivatives. 125
Table A.1. Comparison of Asterane Geometric Parameters. 153
Table A.2. Asterane Eigenvalues and PES Comparison. 154
Table A.3. Asterane Ionization Potentials and Oxidized State Geometries. 156
Table A.4. Vibrational Frequencies of Asterane. 157
Table A.5. Vibrational Frequency Comparison. 162
Table A.6. Electronic Transitions of Asterane: Symmetries, Energies, Oscillator Strengths, and Contributing Transitions. 164
Table A.7. Asterane Dication Calculated Geometric Parameters and Heavy-Atom Charges. 164
Table A.8. Parameters of Various "Interrupted" Asteranes. 166
Table A.9. Strain Energy in the Desulfuration of Tetraasterane. 167

ABSTRACT

The oxidation potentials and electrooxidation mechanism of 3,6-disubstituted-1,2-dichalcogenins was investigated by cyclic voltammetry. An EC mechanism was found experimentally and the basis for the chemical step was found computationally to be a change in the planarity of the ring on electron transfer.

Photoelectron spectra were obtained of 3,6-disubstituted-1,2-dichalcogenins a different ionizing photon energies. The interpretation of the photoelectron spectra was assisted by computational simulation. A narrow ionization band was found, and was assigned as the sulfur-sulfur σ orbital by computation and comparison of ionization cross-sections. Computational simulation of the excited state determined that this orbital is paired with a low-energy σ^* orbital. Electronic transitions to the σ^* orbital were found to be common in disulfides, and the low energy of the σ^* orbital in 1,2-dichalcogenins causes their unusual color. The computed geometry of the excited state, coupled with ^{1}H NMR and ^{77}Se NMR data, also provided evidence of the limited anti-aromaticity of 1,2-dithiins.

A systematic study of the α-deprotonation of dialkyl sulfides was made with Lochmann's/Schlosser's base. The products were analyzed by GC/MS, and the extent of both deprotonation and decomposition was assessed. Mechanisms of decomposition were evaluated. 4-*tert*-Butylthiane was α-deprotonated and stannylated in good yield, in a 38:1 cis:trans ratio.

The oxidation potentials of various α-stannylated dialkyl sulfides were analyzed by cyclic voltammetry. The dependence of oxidation and ionization potential on the C-S-C-Sn dihedral angle was investigated computationally, and was found to obey a Karplus-Barfield-type relationship, with an ionization potential minimum near 90°. The computational predictions were borne out in the oxidation potential of cis-2-trimethylstannyl-4-*tert*-butylthiane (1.17 V), which was found to be slightly lower than the

underivatized sulfide but much higher than other α-stannylated sulfides due to the 180° C-S-C-Sn dihedral angle.

Various computational techniques were used to find evidence of the cyclic interaction of p-type lone pair orbitals in tetrathiatetraasterane. The neutral species and the radical cation were computationally predicted to be possess the same symmetry (D_{4h}) and cyclic interaction of sulfur lone pair orbitals, but oxidation to the dication was predicted to break a carbon-carbon bond.

CHAPTER 1

INTRODUCTION

RADICAL CATIONS AND EXCITED STATES

Radical cations and excited states are interesting species for a variety of reasons. Both are reactive species, and their reactivity is due to an unpaired electron. Therefore both would be expected to, and generally do, engage in a variety of reactions with a variety of substrates. Though this can make them difficult molecules with which to work, it also allows them to participate in reaction processes available to few if any other types of molecules.

Radical cations in particular are of synthetic interest and have potential as useful materials. Unlike excited states, which have very limited lifetimes, many radical cations can persist for extended periods of time. Though they tend to be very reactive they can be preserved if they are isolated from potential reactants. This often includes a need to be isolated from other molecules of the radical cation, to prevent dimerization or disproportionation. Some radical cations can even be used in materials, such as tetrathiafulvalene radical cation, which forms a moderately stable salt with various counterions. These salts have a variety of interesting properties, including conductivity and superconductivity, as well a few which are semi-conductors.

Beyond their utility in and of themselves, radical cations and excited states can provide a great deal of information on the electronic structure of the neutral, ground-state species, including details of both bonding and non-bonding interactions. The changes that occur when electrons are removed from a molecule, particularly by methods such as photoelectron spectroscopy, but also in electrochemistry, can be used to elucidate the electronic structure of the molecule. Many interactions are reversed or negated upon the

removal of an electron participating in the interaction, while other interactions only occur when half-filled orbitals are involved. Thus useful information is sometimes provided by the contrast between the properties and behavior of the radical cation or excited state and the neutral ground state.

SULFUR-CONTAINING COMPOUNDS

In this field of research, sulfur-containing molecules are often used; their use is significant for several reasons. Sulfur makes studies of radical cations more feasible, since it has an oxidation potential generally well within the range of electrochemical detection. This relatively low oxidation potential also tends to make sulfur radical cations less sensitive to stray environmental effects, solvents, and other potentially reactive contaminants. In addition, sulfur has many electronic features worth exploring. The two lone pair orbitals of divalent sulfur are not degenerate; one can be best characterized as a p-type orbital oriented perpendicular to the plane containing the sulfur atom and its substituents, while the other is more of an sp^2-type orbital and is oriented in the aforementioned plane. Since the orbitals are not degenerate, they can be distinguished by ionization potential; the orbital of higher ionization potential (the HOMO of simple sulfides) is the p-type orbital. Sulfur can be though of as an isosteric replacement for a double bond, as in the aromatic species thiophene, in which the p-type lone pair takes the place of the π orbital of an ethylenic unit. This interaction may also involve the empty d-orbitals of sulfur, or may be related to polarizable filled orbitals, or both. As a polarizable atom, sulfur stabilizes a wide variety of adjacent charge features. Large spin-orbit coupling both improves the efficiency of triplet excitation processes and stabilizes sulfur-centered spin. This allows sulfur to act both as a stabilizing factor for adjacent cations or anions, and also stabilizes sulfur-centered radicals, radical cations and closed-shell cations. Sulfur has the

final advantage of being relatively easy to work with, synthetically speaking. It is nucleophilic, but not particularly basic, when used as the mercaptide, which often eases the synthesis of desirable compounds.

3,6-DISUBSTITUTED-1,2-DICHALCOGENINS

The 3,6-disubstituted-1,2-dichalcogenins present many fascinating theoretical aspects and experimental opportunities. Chalcogens are atoms of the oxygen group (Group 16). In our studies, we considered 1,2-dithiins, which of course contain sulfur, and 1,2-diselenins, which contain electronically similar selenium atoms. Selenium is more easily oxidized and is more polarizable than sulfur, but does not make quite as good an isostere for a double bond, presumably due to poorer overlap and energy matching with carbon 2p orbitals. In a similar fashion to thiophenes, the chalcogen atoms are expected to participate in the conjugated circuit; in this case, the circuit should contain 8π electrons, making it formally anti-aromatic. The overlap might involve a twist, which could make it a Möbius circuit, which would stabilize 8π electrons rather than destabilize. The electronic structure of this molecule should therefore be very interesting, and it was explored by computation and photoelectron spectroscopy. Serendipitous experimental discovery led to the computational solution of the "color mystery" of 1,2-dithiins.

Since both sulfur and selenium are easily oxidizable, it was also possible to explore these unique molecules by electrochemical means. Often, seven-electron cyclically-delocalized species exhibit unusual stability. There was the potential of both discovering new properties of these molecules, and of investigating a species which could display unusual electrochemical behavior. Indeed, computational and electrochemical analysis yielded insight into the conformation of both the neutral and cation radical species, providing another piece of this intriguing electronic puzzle.

Though these methods may seem disparate, it will be demonstrated that they are in fact the best means possible for investigating fundamental electronic issues such as these, and are in fact necessary to the discovery of some of the more interesting features.

α-THIOCARBANIONS AND α-STANNYL SULFIDES

At first glance, other than the fact that all three molecules contain sulfur the topics of α-thiocarbanions and α-stannyl sulfides may not seem related to 1,2-dichalcogenins. However, the interest is still in the fundamental electronic structure and the effect that sulfur can have on it. In this study α-thiocarbanions were the chosen route to the α-stannyl sulfides, but they do have electronic issues of their own. It turns out, in fact, that they may be related to those of the α-stannyl sulfides.

Though not, in this case, participating in a conjugated circuit, the sulfur atom still possesses the p-type lone pair and empty d-orbitals, and the sulfur atom is still quite polarizable. Some of these effects have an angular dependency, their efficacy varying with the dihedral angle between the sulfur atom and the investigated substituent or adjacent center. In the case of α-thiocarbanions, the stability of both the adjacent carbon-hydrogen bond and the carbanionic lone pair which would result from the removal of a proton are affected by the presence of the sulfur atom in what seems a geometry-dependent fashion. Likewise, the stability of an α-stannyl sulfide radical cation varies with the sulfur-α-carbon dihedral angle. While an extensive synthetic survey allowed certain conclusions to be drawn about the stability of α-thiocarbanions, computational simulation filled in the experimental gaps in investigating the stability and ionization potentials of α-stannyl sulfides.

COMPUTATIONAL SIMULATION AND ANALYSIS

Due to the high reactivity of radical cations and excited states, and the short lifetimes of the latter group, it is often difficult to obtain all the information about said states that an investigator would desire. In addition, and often for the same reasons, when data is obtained it is not always as clear or as rich in information content as an investigator would hope. It is therefore often useful, if not necessary, to fill in the gaps in available experimental data, even when a large number of experiments have been conducted successfully.

Computational simulation of a physical process or state has limitations in the information which can be obtained, its ease of calculation, and its accuracy. Even when highly accurate, computation may not compare well with experiment due to differences between the environment of the computational simulation and the environment of the experiment. For example, many experiments are conducted in solvent, and the solvent is known to exert various attractive and repulsive forces on the analyte. Computational simulations tend to be conducted in what would experimentally be a very high vacuum; that is to say, the molecule is in total isolation in the simulation. This is due to constraints of poor models for solvents and a lack of computing power to consider solvent specifically. Often the interesting molecules are sufficiently large that it is a challenge to model them accurately by themselves, much less in the company of dozens of solvent molecules or a dielectric field. This computing-power limitation is also seen in the difficulty of modeling radicals, since the open-shell calculations are much more involved, and excited states, since any consideration of the population of orbitals which are empty in the ground state increases the size and difficulty of the calculations by at least an order of magnitude.

However, while direct comparison of computational simulation to experiment is often disappointing, the computed relative changes from species to species and state to state

tend to be much more reliable, and it is with such comparisons that most computational analysis is carried out. Modern computational chemistry is almost always qualitatively correct, but the quantitative accuracy varies widely from method to method and property to property.

PHOTOELECTRON SPECTROSCOPY

Photoelectron spectroscopy is a process in which molecules are bombarded with monochromatic radiation of sufficient energy to cause the molecules to expel an electron, forming the radical cation. The energy of the incoming photon is known, and the energy of the expelled electrons are measured, yielding the work function for the electrons in the molecule. All the photoelectron spectroscopy referred to in this work is gas-phase ultraviolet photoelectron spectroscopy.

Photoelectron spectroscopy (PES) provides several types of information not available from many other techniques. Of primary interest to this work is that the electrons are not just expelled from the highest occupied molecular orbital; all molecular orbitals for which the work function is less than the energy of the incoming photon have some chance of losing an electron. Therefore, one can generally see many of the valence molecular orbitals of the molecule. Also, the likelihood of losing an electron depends on the energy of the photon and the nature of the orbital (or the composition of a molecular orbital). With multiple ionizing-photon energies, the rough orbital composition (in terms of contributing atomic orbitals) can be determined.

For many reasons, PES lends itself to both computational simulation and computation-assisted analysis. Since in PES the molecules are analyzed at moderately high vacuum, the experimental and computational environments are nearly identical. Computational simulation is made much more simple, since the radical cation does not need

to be computationally addressed, and even if one chooses to do so, the radical cation does not need to be geometry-optimized because PES measures non-adiabatic (vertical or Franck-Condon) ionization transitions. Computation easily provides orbital compositions and orbital energies, and these can be compared to the PES results. Although the energies of molecular orbitals ought to correspond to their eigenvalues in the wavefunction, they often do not when compared to PES results. This is not so much a failing of the computational simulation as a slight mismatch in what the computer is predicting and what PES is measuring. The computer gives eigenvalues for the neutral species in the ground state. According to Koopman's theorem, these eigenvalues should be the work functions for the molecule. However, these are really the energies for removing electrons from a molecule to an infinite distance without allowing for the reorganization of the electrons left behind. PES, on the other hand, measures the energies difference between the neutral species and cation radical at the same geometry, allowing for electronic relaxation but not geometric relaxation. The Koopman's theorem values would then be expected to be consistently high of the actual ionization potentials.

There is another way to simulate PES ionization. This method, usually referred to as ΔSCF, consists of calculating the total electronic energies of the neutral species at the optimized minimum and the radical cation at the same geometry. This more closely approximates the experimental ionization process. Error can still occur if the geometric change upon ionization is large.

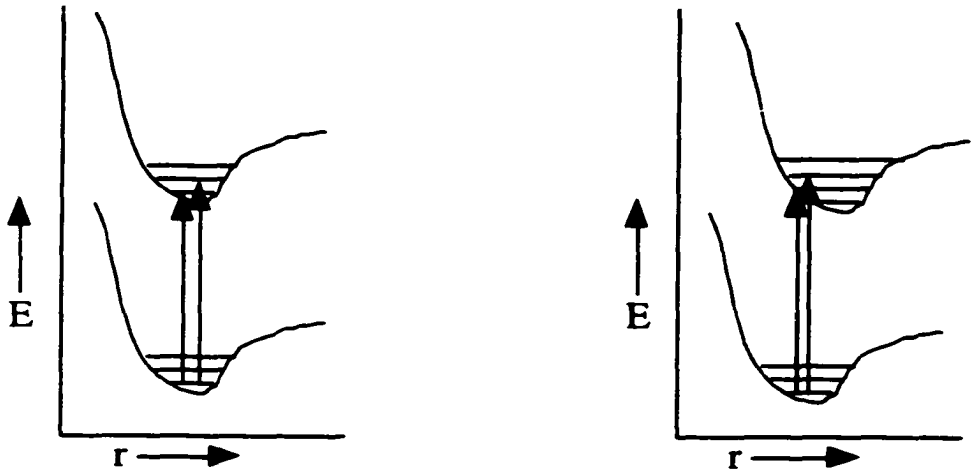

Figure 1.1. Franck-Condon Transitions for Molecules with Small Geometric Relaxation Energies (left) and Large Geometric Relaxation Energies (right).

As can be seen in Figure 1.1, if the geometric relaxation energy is small, the transitions are more likely to be from the neutral vibrational ground state to radical cation vibrational ground state. The possibility of transitions to other vibrational states in the cation radical is always possible, due to the large amount of input energy, and this is observed in the spectrum as ionization band broadening or sometimes, for higher-symmetry or more rigid molecules, as a discrete series of bands separated by the vibrational frequency. However, when the change in geometry is large, the vertical transitions are no longer to the radical cation vibrational ground state; the geometrically-corresponding region of the radical cation potential energy hypersurface is a vibrationally excited state and the measured ionization potential includes this vibrational excitation energy.

ELECTROCHEMISTRY

In contrast with the non-adiabatic ionization potentials provided by PES, electrochemistry provides adiabatic ionization potentials, though it is actually much more complex and solvent effects tend to be very important. Additionally, electrochemistry can

only provide the adiabatic first ionization potential. However, the limitations of electrochemistry can also be its advantages. Electrochemistry is not limited to oxidizing the analyte, so both oxidations and reductions can be investigated. Since electrochemical potentials are sensitive to following processes, detailed electrochemical analysis can yield information about changes in geometry and possible reactions of the oxidized or reduced species. It is fairly easy to investigate multiple electron transfers by electrochemical means, whereas PES is limited to one-electron processes. The methods are therefore often complementary. However, due to the use of conducting solvent which sometimes participates specifically in the redox cycles, electrochemical processes can be much more difficult to computationally simulate.

The electrochemical technique most often used by organic chemists, and the method used throughout this work, is cyclic voltammetry. Cyclic voltammetry consists of immersing three electrodes into a conducting solution (called the supporting electrolyte) of the analyte. Potential is measured by a potentiostat versus the half-cell potential of the reference electrode. The working electrode is where the electron transfer processes of interest occur, and there is a counter-electrode for charge-balance processes. For ease of electrochemical simulation, the working electrode is generally planar or spherical. The potentiostat is a device which regulates the potential of the working electrode versus the reference electrode, while measuring the current flow between the working electrode and counter-electrode. An electron-transfer event will cause a change in the amount of current flow, and this is then seen on the plot as a peak. In cyclic voltammetry, the potential of the working electrode is altered at a known rate, usually from potential A to B, and then back to A, though other patterns are possible. The resulting shape of the peak(s) is dependent on the oxidation (or reduction) potential of the analyte, the concentration of the analyte, and the "sweep rate" (the rate at which the potential is altered). When investigating radical

cations generated from neutral species, the "forward" sweep is an increase in potential from below the oxidation potential to above the oxidation potential, and the "return" sweep is the decrease in potential back to the starting potential.

Cyclic voltammetric peaks have a very particular shape defined by complex equations which mainly involve the interaction of the rate of electron transfer with the rate of diffusion of new analyte to the electrode and the rate of diffusion of oxidized (or reduced) analyte away from the electrode. The shape can change depending upon how far past the oxidation potential the sweep goes, since less oxidized (or reduced) analyte will have diffused away if the sweep is reversed more quickly; the same is true of sweep rate, for the same reason. Some oxidation (or reduction) peaks are irreversible, which means that the oxidized (or reduced) species is not reduced (or oxidized) upon the return sweep. For irreversible oxidation or reduction peaks (sometimes also called waves), the actual standard half-cell potential cannot be determined from the system without knowing the diffusion coefficient. However, the "peak" potentials can be compared between members of a sufficiently similar series of compounds, since their diffusion coefficients would be expected to be similar.

For reversible systems, a great deal more information can be obtained. The true standard half-cell potential can be determined by taking the average of the oxidation and reduction potentials of a reversible redox couple (a pair of oxidation and reduction peaks determined to interconvert a species and its reduced or oxidized form). The separation of the peaks yields the number of electrons in the electron-transfer step. And the exact shape of the reversible couple, acquired at a series of sweep rates and concentrations, can yield detailed mechanistic information about the electron-transfer step and any following processes such as a geometric change or reversible chemical interaction.

CHAPTER 2

CONFORMATION AND ELECTROCHEMISTRY OF 1,2-DICHALCOGENINS

GENERAL PROPERTIES OF 1,2-DICHALCOGENINS

1,2-Dichalcogenins (1,2-dithiacyclohexadienes or 1,2-diselenocyclohexadienes, Figure 2.1) have many interesting properties and raise a variety of unique theoretical issues.

Figure 2.1. 3,6-Disubstituted-1,2-Dichalcogenins (left) with a Perspective View (right). X= S, Se.

They are formally anti-aromatic, possessing 8π electrons. They possess the potential for an interesting tautomerism (Figure 2.2), which may contribute solely as a resonance form, but could also be a discrete species.

Figure 2.2. Valence Tautomerism in 1,2-Dithiins.

Though lacking a conventional chromophore, 1,2-dichalcogenins range from red through orange to yellow, depending on substitution (for example, λ_{max} = 452 for 1,2-dithiin). They are also photosensitive, decomposing into thiophenes when exposed to light (Scheme 2.1).[1]

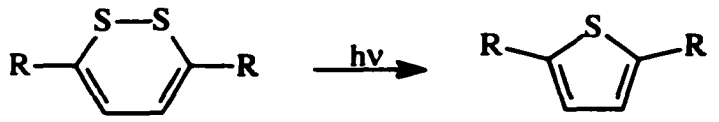

Scheme 2.1. Photodecomposition of 1,2-Dithiins.

1,2-Dithiins are found in nature, in certain members of the sunflower family (*Asteraceae*). Thiarubrines A and B (Figure 2.3) are the most well-known of these natural products.[2-10]

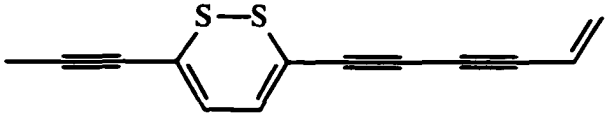

Figure 2.3a. Thiarubrine A.

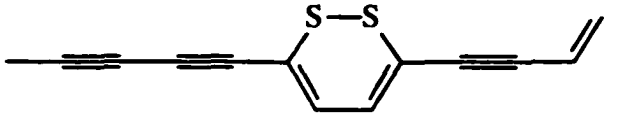

Figure 2.3b. Thiarubrine B.

The thiarubrines show wide-ranging biological activity, including antibiotic, antifungal, antitumor, and nematocidal activity.[11] Thiarubrines A and B are active both in the light and in the dark, while the thiophene decomposition product of thiarubrine A is only active in the light.[7]

EFFECTS OF OXIDATION AND REDUCTION ON CONFORMATION

It is well known that oxidation or reduction of many compounds is accompanied by substantial changes in conformation. For example, tetraarylethylenes undergo two reversible oxidations, to the cation radical and dicationic species. The conformation of tetraanisylethylene in each state of oxidation has been studied by X-ray crystallography. As one would expect, in the neutral species the ethylenic portion is nearly planar (4°

dihedral angle), but in the cation radical the ethylenic portion twists to 31°, and further to 62° in the dication.[12]

It is also known that bianthrones undergo a conformational change both upon oxidation to the cation radical, and again upon reduction. Neutral bianthrone is planar, but when the planar neutral bianthrone is reduced to the anion radical, it changes to the more stable twist anion radical. This twist anion radical is oxidized, upon the return sweep, to a twist neutral species. This twist neutral species then becomes planar once more.[13-17] This type of electron transfer-conformation change scheme is sometimes referred to as a "square scheme".

ELECTROCHEMICAL RESULTS

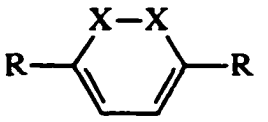

Table 2.1. Oxidation Peak Potentials of Various 1,2-Dichalcogenins.

X	R	E_p [a] in CH_3CN (V) E_1 [b]	E_2 [c]	E_p in CH_2Cl_2 (V) E_1	E_2
S	H	0.70	d	0.85	1.40
	Me	0.65	1.21		
	iPr	0.68	1.22		
	tBu	0.68	1.10		
	CF_3 [d]	1.25	1.40		
	CF_2CF_3 [d]	1.48	1.67		
	CH_2OH	0.58	1.23	0.82	1.13
	Ph	0.75	1.04	0.80	1.23
	TMS	0.58	e		
Se	H [d]	0.53	1.3 [f]		
	Me [d]	0.57	1.1		
	tBu [d]	0.61	0.99		

[a] Peak potentials refer to anodic (oxidation) waves, and are reported at 100 mV/s versus Ag/0.1 M $AgNO_3$ in MeCN.
[b] First anodic wave; part of a reversible redox couple.
[c] Second anodic wave; irreversible.
[d] Due to difficulties including adsorption and electrodeposition, these compounds could not be analyzed with a platinum electrode, but rather a glassy carbon electrode was required.
[e] No second anodic wave observed.
[f] Broad, poorly resolved peak.

For comparison, the oxidation peak potentials were obtained under identical conditions (in MeCN) for diphenyl disulfide (1.29 V) and diphenyl diselenide (1.07 V).

Using experimental data collected by the author, Wilson and co-workers analyzed 3,6-dimethyl-1,2-dithiin and 3,6-diphenyl-1,2-dithiin by simulation to obtain various pertinent electrochemical constants.[1] They determined that, of various possible mechanisms, by far the best fit was obtained for an EC mechanism, in which the electron-transfer step is followed by some type of molecular reorganization. In Table 2.2, $E^{0'}$ is relative to a Ag/0.1 M $AgNO_3$ (MeCN) reference electrode, k_s is the standard heterogenous

electron-transfer rate constant, and k_f is the first-order rate constant for the following chemical reaction.

Table 2.2. Electrochemical Parameters of 1,2-Dithiins.

Parameter	3,6-Dimethyl-1,2-dithiin	3,6-Diphenyl-1,2-dithiin
$E^{0'}$ (V)	0.575 ± 0.001	0.716 ± 0.003
k_s (cm/s)	0.032 ± 0.00	0.014 ± 0.006
k_f (s^{-1})	0.468 ± 0.033	0.318 ± 0.027

COMPUTATIONAL RESULTS

To determine whether 1,2-dichalcogenins undergo a scheme of electrochemical and conformational processes similar to bianthrone, the global minimum geometries of both the neutral species and cation radical were calculated for 1,2-dithiin and 3,6-dimethyl-1,2-dithiin. The energy of the neutral species at the cation radical global minimum geometry and the energy of the cation radical at the neutral species global minimum geometry were also calculated. This process determined the energies of the four critical points of the square scheme (Figure 2.4).

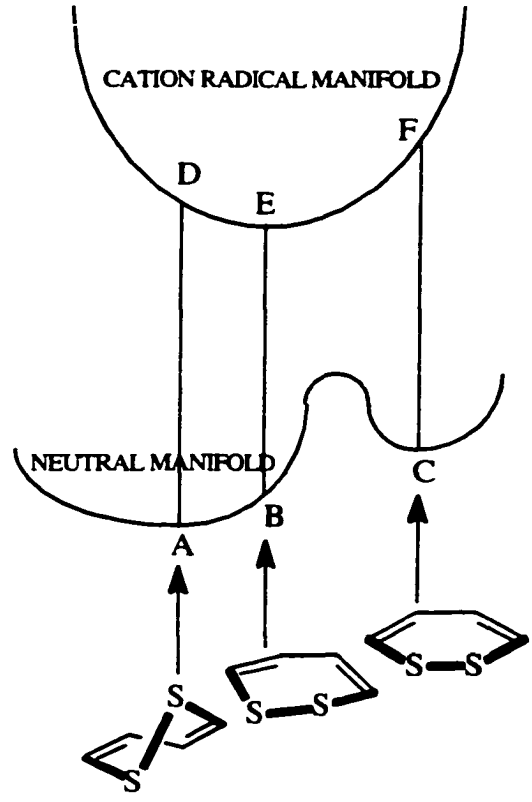

Figure 2.4. Critical Points of 1,2-Dithiin.

In Figure 2.4, the critical points of the 1,2-dithiin neutral and cation radical manifolds are labeled. Geometries do not change along vertical lines in the figure, and a pictorial representation of each geometry is included below neutral manifold. Point A corresponds to the optimized neutral species twist geometry (CSSC dihedral angle = 54.8°). Point D corresponds to the same geometry on the cation radical manifold. Point E represents the optimized cation radical geometry (CSSC dihedral angle = 6.3°) on the cation radical manifold, while Point B is the corresponding point on the neutral manifold. Point C is the optimized planar geometry of the neutral species, while Point F is the corresponding point on the cation radical manifold. Note that the exact shapes of the manifolds in Figures 2.4 and 2.5 are not intended to be quantitative but are designed for clarity of explanation.

It is known that the neutral species of 1,2-dithiin adopts a twisted C_2 geometry.[18] This geometry was well reproduced by the calculations (See Chapter 3). For 1,2-dithiin it was calculated that the non-adiabatic (vertical) ionization potential (energy at D minus the energy at A) was 8.16 eV (experimental: 8.16 eV[19]). The energy difference between the vertical cation radical (D) and the cation radical global minimum geometry (E), which is known as the relaxation energy, was calculated to be 19.6 kcal/mole. While the neutral species is a C_2 twist, the cation radical is nearly planar. The geometry-relaxed cation radical is 7.31 eV higher in energy than the optimized neutral species (E–A); this value is the adiabatic ionization potential of 1,2-dithiin. The neutral species at this optimized cation radical geometry (B) was calculated to have an energy 12.0 kcal/mole higher than the energy of the neutral species at the global minimum neutral geometry (A). The ionization potential at the optimized cation radical geometry was calculated to be 6.79 eV (E–B).

From these data we can construct a square scheme, where the neutral twist (A) is oxidized to the cation radical (D; IP = 8.16 eV) and flattens to the cation radical minimum (E; relaxation energy = 19.6 kcal/mole). This species is reduced to the neutral (B; IP = 6.79 eV) which twists back to the neutral global minimum (A; relaxation energy = 12.0 kcal/mole). Alternatively, the geometric change could be concurrent with the oxidation. The neutral species global minimum (A) could be oxidized with flattening to the cation radical minimum (E; IP = 7.31 eV) which is reduced by the same path. The two possible mechanisms are distinguishable experimentally (see below).

A second, planar, minimum was found for 1,2-dithiin (C). Though a genuine minimum, this conformation is 9.7 kcal/mole higher in energy than the neutral global minimum and is therefore not expected to affect the experimental data. The non-adiabatic ionization potential at this geometry (F–C) was found to be 7.02 eV, while the adiabatic

ionization potential (E–C) was found to be 6.89 eV. The relaxation energy of the cation radical from the planar geometry (F–E) was found to be 2.9 kcal/mole.

The case of 3,6-dimethyl-1,2-dithiin is simpler than for the parent (Figure 2.5).

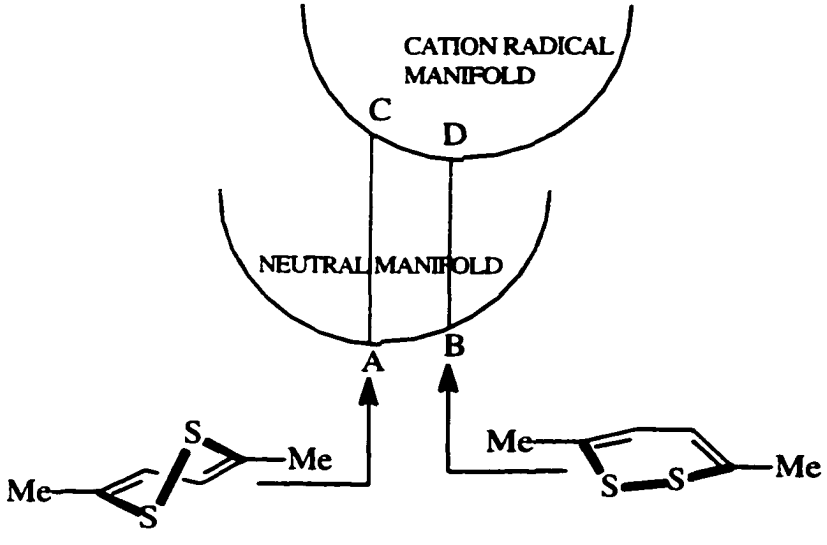

Figure 2.5. Critical Points of 3,6-Dimethyl-1,2-Dithiin.

For 3,6-dimethyl-1,2-dithiin there is no planar minimum on the neutral manifold. Point A is the neutral global minimum; it is a C_2 twist geometry with a CSSC dihedral angle of 56.6°. The same geometry on the cation radical manifold is labelled Point C. The cation radical minimum (Point D) is somewhat flattened (CSSC dihedral angle of 14.2°). The same geometry on the neutral manifold is labelled Point B.

A square scheme for 3,6-dimethyl-1,2-dithiin would involve an oxidation from the neutral minimum to the cation radical (A to C; IP = 7.96 eV; experimental: 7.78 eV[19]) followed by geometric relaxation to the cation radical minimum (C to D; relaxation energy = 19.4 kcal/mole). This flattened cation radical would be reduced to the neutral species (D to B; IP = 6.59 eV) which would twist to the neutral minimum geometry (B to A; relaxation energy = 12.2 kcal/mole). The alternate oxidation with concurrent flattening would have an ionization potential of 7.12 eV (the adiabatic ionization potential).

DISCUSSION

The electrochemistry of 1,2-dithiins and 1,2-diselenins reveals several interesting features of these compounds. The detailed analysis of the first (reversible, one-electron) oxidation of two representative dithiins is best described by an EC mechanism. The possibility of flattening upon oxidation (or twisting upon reduction) concurrent with electron transfer is ruled out by examining the heterogeneous electron-transfer rate constant (k_s), which is seen to be within normal ranges for both dithiins. It would be expected to be much slower if electron transfer occurred concurrently with the geometric change.

The difference between the non-adiabatic and adiabatic ionization potentials is computationally predicted to be fairly large for 1,2-dithiins. This prediction is upheld by comparison to naphtho[1,8-c,d]-1,2-dithiole (1,8-naphthalenedisulfide). The naphthalenedisulfide has an ionization potential of 7.14-7.15 eV[20,21] and a half-wave potential of 0.95 V versus SCE[22] (0.68 V versus silver-silver chloride[23]). 1,2-Dithiin has an ionization potential of 8.16 eV (see also Chapter 3) and a peak potential (corrected for the 300 mV difference between SCE and silver-silver nitrate) of 1.00 V. The similar oxidation potentials suggest similar stabilization of the disulfide cation radical. Since the naphthalenedisulfide is already planar, it has very little relaxation energy, and this is reflected in the 1 eV difference in non-adiabatic ionization potential. Given that the relaxation energy of the naphthalenedisulfide is not zero, and that the compounds are not completely comparable, the 1 eV difference is commensurate with the computationally predicted 12 kcal/mole relaxation energy for 1,2-dithiin.

A comparison of the values for 3,6-dimethyl-1,2-dithiin and 3,6-diphenyl-1,2-dithiin is also enlightening. The diphenyldithiin cation radical would normally be expected to be more stable than the dimethyldithiin cation radical, due to the phenyl groups which

would normally be expected to delocalize both the charge and spin. The methyl groups are expected to stabilize the dithiin via inductive electron donation and hyperconjugation, which in most cases would be the weaker effect. Both by peak potential (generally only useful when compared within as a series, as it is here) and oxidation potential dimethyldithiin is seen to be the more stable cation radical. This suggests that the charge and spin are localized on the ring even in the diphenyl case, and is in keeping with computational survey work done on the diphenyl compound indicating a moderate angle between the plane of the phenyl group and the plane of the ipso carbon and its attached atoms in the neutral species (as in, for example, biphenyl). Inductively, the phenyl groups are slightly electron-withdrawing (Table 2.3), and if charge/spin delocalization is not an issue, they would be expected to slightly raise the oxidation potential as compared to hydrogen.

Table 2.3. Taft Parameters for 3,6-Substituents of 1,2-Dithiins.

Substituent	σ_I	σ^0_R	σ_R	σ^-_R	σ^+_R
H	0.00	0.00	0.00	0.00	0.00
Me	-0.04	-0.11	-0.11	-0.11	-0.25
iPr	-0.06				
tBu	-0.07				
Ph	0.10	-0.11	-0.11	0.04	-0.30
CH_2OH	0.10				
$Si(CH_3)_3$	-0.10	0.06	0.06	0.14	0.06
F	0.50	-0.34	-0.45	-0.45	-0.57
CF_3	0.45	0.08	0.08	0.17	0.08

The Taft parameters are, from left to right: the Taft inductive sigma parameter (log $[k/k_0] = \sigma^*\rho^* + \delta E_s$, $\sigma_{I(X)} = 0.450\ \sigma^*_{(XCH2)}$) [24]; Taft basic resonance parameter (log $[k/k_0]$ or log $[K/K_0] = \sigma_I\rho_I + \sigma_R\rho_R$)[25]; Taft benzoic acid resonance parameter (same equation)[25]; Taft electron-deficient benzene ring resonance parameter (same equation)[25]; and Taft electron-rich benzene ring resonance parameter (same equation)[25].

This is indeed seen in the peak potential comparison. Since the computational survey also predicted a fully planar cation radical (including the phenyl groups' angles with the main ring), it is not unexpected that the chemical step rate constant is smaller for the diphenyl

compound than the dimethyl; the required geometric change is more extensive in the diphenyl case, thereby slowing the transformation.

The peak potentials of 3,6-diisopropyl- and 3,6-di-*tert*-butyl-1,2-dithiin are identical, and only very slightly larger than the peak potential of dimethyldithiin. The effect of the methyl groups as compared to the parent 1,2-dithiin is also small. Insofar as the differences are significant, it may be concluded that hyperconjugation with a C-H bond is much more effective than with a C-C bond. Only in the dimethyl case is there a C-H bond with the proper orientation for hyperconjugation; in the diisopropyl case the two methyl groups force the C-H bond to lie in the plane of the ipso carbon and its attached atoms thereby making hyperconjugation impossible, and there is no C-H bond in the *tert*-butyl case. There is definitely an inductive factor in the overall effect, as shown by the slight decrease in peak potential going from the parent to the di-*tert*-butyl case.

While these explanations seem very neat, and are indeed the best available, they do not account for the observed behavior of the 1,2-diselenins. In the case of selenium, the methyl group causes a slight destabilization, and the *tert*-butyl group about doubles the effect. Since the effect is greater for *tert*-butyl than methyl, the previous discussion would indicate primarily an inductive effect rather than a hyperconjugative one. The inactivity of the hyperconjugative stabilization can be attributed to the different ionization energy, thereby causing a poorer energy match and a less efficient effect. That does not explain the "reverse" inductive effect. Intuitively, one would expect that injecting electrons into a ring with a positive charge could only help. There is a substantial difference between the charge and spin distribution computationally predicted for 1,2-dithiin and 1,2-diselenin (see Chapter 3). Even if one postulates a cation radical centered completely on the selenium atoms (which is not the predicted case), induction should merely lose its stabilizing effect, not become destabilizing. The effect may be related to the available and preferred conformations of 1,2-diselenins; if one applies a similar analysis to the photoelectron

spectroscopic values for the ionization potential (non-adiabatic ionizations; see Chapter 3), one finds the expected trend of decreasing potential with increasing inductive power of the 3,6-substituents, just as for the non-adiabatic ionization potentials of 1,2-dithiins. The search for an adequate explanation of this experimental result is ongoing. The overall difference between the 1,2-dithiins and 1,2-diselenins is nearly identical to that between diphenyl disulfide and diphenyl diselenide, suggesting that the difference is a function of the heteroatoms and the chalcogen-chalcogen bond alone, and not a great change in the electronics of the ring as a whole.

The effects of trimethylsilyl and hydroxymethyl are the most stabilizing in the compounds analyzed. It is expected that the trimethylsilyl group would stabilize the cation radical efficiently, since it is both electron-donating in an inductive sense and a hyperconjugative sense (though the latter would seem not to be in operation, as a much larger decrease in potential would be expected). In fact, according to Table 2.3, the effect seen for trimethylsilyl is in line with the stabilization due to alkyl substitution (smaller in magnitude), the destabilization seen for phenyl (assuming only inductive effects), and the large destabilization seen for trifluoromethyl (corresponding to a large Taft inductive parameter). What is peculiar, in light of this analysis, is that hydroxymethyl stabilizes the cation radical so efficiently. It is inductively as electron-withdrawing as phenyl, so the effect is certainly not inductive. Indeed, the oxidation potential of the hydroxymethyl compound in dichloromethane is nearly identical to that of the phenyl compound in the same solvent. Clearly, a solvent-dependent effect is being observed. There is the possibility of specific interaction between the solvated or non-solvated oxygen lone pair(s) and the ring, but this has not been specifically demonstrated.

Apparently the C-F bond is unsuitable for effective hyperconjugation, as the inductive effects appear unopposed in causing such a large increase in peak potential for the perfluoro compounds. This is verified by the data in Table 2.3 where it can be seen that

trifluoromethyl does exert a slight destabilizing effect via resonance, but it is much smaller than the stabilizing resonance effect of methyl, and is also much smaller than the inductive effect trifluoromethyl exerts. Also impressive is the amount of further destabilization seen in perfluoroethyl as compared to perfluoromethyl; a trifluoromethyl group is often attributed about the same electron-withdrawing power as a fluorine atom (as seen in Table 2.3), but it can be seen that, at least in this case, it is much greater, the perfluoroethyl effect being about half again as great as the perfluoromethyl. This result is especially important when compared to the photoelectron spectroscopic ionization potentials (Chapter 3) which are almost identical for 3,6-bis(trifluoromethyl)-1,2-dithiin and 3,6-bis(pentafluoroethyl)-1,2-dithiin. This suggests that the effect is tied up in the geometric changes the compounds undergo upon adiabatic ionization. It was seen earlier in the *tert*-butyl case that carbon-carbon bonds do not have much of an effect via hyperconjugation, but the fluorine atoms may be withdrawing sufficient electron density from the carbon-carbon bond in perfluoroethyl to have shifted its energy for a more efficient interaction. It is uncertain why this would affect the adiabatic ionization potential and not the non-adiabatic ionization potential, unless the C-C bond's preferred neutral geometry is perpendicular to the ring.

It is known that many 7π electron rings are unusually stable.[26-35] This can be seen in 1,2-dithiins as compared to dibenzo[c,e]dithiin. Just as the 9,10-ethylene unit in phenanthrene behaves more like an isolated double bond than part of an aromatic system, one would expect dibenzodithiin to behave more like a aryl disulfide than an electronically unique heterocycle such as 1,2-dithiins. Electrochemical studies show that the cation radical of dibenzodithiin is less stable and harder to form than that of 1,2-dithiin.[22,23] This is presumably due to the localization of the carbon π electrons in the benzene aromatic overlap, causing decreased availability for the stabilizing seven π-electron interaction.

Finally, it should be noted that the nature of the second oxidation observed for some 1,2-dichalcogenins is unknown. The potential and nature of this oxidation in both acetonitrile and dichloromethane have been compared to those of the primary redox couple of the corresponding thiophene. In dichloromethane, the oxidation potential is substantially different from that of the corresponding thiophene, and the redox couple is reversible for thiophene, while the second oxidation wave of the 1,2-dichalcogenins is irreversible. It can therefore be said conclusively that this wave is not due to thiophene caused by decomposition of the cation radical. It cannot be determined whether the wave is from oxidation to the dication (six π-electrons, but very high charge density and significantly lowered bonding strength) or from some mode of decomposition. The dithiins do possess a reduction wave at or near -0.68 V which can be assigned (by comparison with diphenyl disulfide) to the reduction of the disulfide moiety.

CONCLUSIONS

The square EC scheme computationally predicted for 1,2-dithiins was experimentally verified. This behavior was contrasted with that of similar compounds which do not undergo geometric changes after oxidation and reduction.

The nature and extent of substituent effects in 3,6-disubstituted-1,2-dithiins were examined. In most cases, the effects are limited to induction, with the exception of conformationally available C-H hyperconjugation and the possibility of C-C hyperconjugation in electron-deficient cases. Resonance effects do not play a role in phenyl substitution since the phenyl rings are not properly aligned in the neutral species. The inductive effects of perfluoromethyl and perfluoroethyl groups were found to be very large, suggesting a high sensitivity of the 1,2-dithiin system to electron withdrawal, and the effect of perfluoroethyl was found to be substantially different from that of perfluoromethyl.

Finally, it was noted that increased participation in a seven π-electron circuit in the main dithiin ring increases cation radical stability.

CHAPTER 3

COMPUTATIONAL SIMULATION AND ANALYSIS OF 1,2-DITHIINS: IONIZATION ENERGIES, ORBITAL ASSIGNMENTS, AND AN EXPLANATION OF THEIR COLOR

PREDICTING EXPERIMENTAL PROPERTIES BY COMPUTATION

As mentioned in Chapter 2, 1,2-dithiins have many interesting theoretical aspects. These include the importance of resonance contributions from the acyclic valence tautomer (see Figure 2.2) and the effect of these contributions on bonding, as well as the general electronic structure and the effect of substitution on the electronic structure, and the effect of substitution on both the adiabatic and non-adiabatic ionization energies. Often, even in those cases which can be experimentally determined, a full interpretation is not possible from the data alone. Computation of the experimental properties and their underlying electronic causes can be not only helpful but crucial to the proper interpretation and full use of the experimental data.

It does not often suffice to merely choose method, basis set, and other crucial computational parameters at random. Some guidance can be offered in general as to the failings of certain methods, basis sets, and approaches. The only truly reliable method is to first obtain some experimental data, and then choose a method which accurately reproduces that data, with the expectation that related data arising from the same basic features of the molecule will be accurately predicted as well.

COMPUTATIONAL RESULTS

The first task necessary in computationally analyzing the 1,2-dithiin series was to choose a method and basis set for geometry and general property calculation. Since the gas-phase geometry of 1,2-dithiin has been reported and the gas-phase ionization potential

had been determined as a parallel portion of the collaborative effort which included this work, it was decided that computing the geometry and non-adiabatic ionization potential of 1,2-dithiin by a wide variety of methods would be the best way of determining the optimum basis set and method for use in the 1,2-dithiin series. It has the advantages of being thorough but still being relatively cheap (in terms of computational cycles) since 1,2-dithiin is the simplest member of the series of interest. The results of this analysis are found in Tables 3.1 through 3.4.

Table 3.1. Comparison of 1,2-Dithiin Bond Lengths.

Method[a]	Basis Set[b]	C=C (Å)	C-C (Å)	C-S (Å)	S-S (Å)
HF	6-31G*[c]	1.33	1.47	1.77	2.07
	6-311++G**	1.32	1.47	1.77	2.08
	LANL2DZ	1.33	1.48	1.82	2.24
B3PW91	6-31G*	1.35	1.46	1.77	2.09
	6-311++G**	1.34	1.45	1.77	2.10
	LANL2DZ	1.35	1.47	1.83	2.29
MP2	6-31G	1.36	1.47	1.85	2.29
	6-31+G	1.36	1.47	1.85	2.29
	6-31++G	1.36	1.47	1.85	2.29
	6-31G*	1.35	1.45	1.77	2.07
	6-31+G*	1.36	1.45	1.76	2.07
	6-31++G*	1.36	1.45	1.76	2.07
	6-31G**	1.35	1.45	1.77	2.07
	6-31+G**	1.36	1.45	1.76	2.07
	6-31++G**	1.36	1.45	1.76	2.07
	6-311G	1.35	1.47	1.85	2.28
	6-311+G	1.36	1.47	1.85	2.27
	6-311++G	1.36	1.47	1.85	2.27
	6-311G*	1.35	1.46	1.76	2.08
	6-311+G*	1.36	1.45	1.76	2.08
	6-311++G*	1.36	1.45	1.76	2.08
	6-311G**	1.36	1.45	1.76	2.08
	6-311+G**	1.36	1.45	1.76	2.08
	6-311++G**	1.36	1.45	1.76	2.08
	LANL2DZ	1.38	1.49	1.85	2.32
Experimental value		1.35	1.45	1.76	2.05

[a] HF refers to the Hartree-Fock *ab initio* method. B3PW91 is the Becke-3 Perdew-Wang 91 hybrid density functional method. MP2 is the Hartree-Fock method with second-order Møller-Plesset perturbational corrections.

[b] 6-31G and 6-311G are split valence basis sets constructed of linear combinations of Gaussian functions. They are described in greater detail in Chapter 7. LANL2DZ is the Dunning-Hunziga double-zeta valence basis set employing the Los Alamos National Laboratories relativistic effective core potentials.

[c] These values taken from Mann, M.; Fabian, J. *J. Mol. Struct. (Theochem)* **1995**, *331*, 51-61.

Table 3.2. Comparison of 1,2-Dithiin Bond Angles.

Method[a]	Basis Set[b]	C=C-C (°)	C=C-S (°)	C-S-S (°)
HF	6-31G*[c]	124.6	122.8	99.2
	6-311++G**	124.6	123.0	99.0
	LANL2DZ	126.3	124.6	98.7
B3PW91	6-31G*	124.7	122.5	98.9
	6-311++G**	124.7	122.2	98.6
	LANL2DZ	126.5	124.5	98.0
MP2	6-31G	125.8	123.8	96.5
	6-31+G	125.5	123.7	96.2
	6-31++G	125.5	123.7	96.1
	6-31G*	124.0	122.0	98.0
	6-31+G*	123.9	122.0	97.8
	6-31++G*	123.9	122.0	97.8
	6-31G**	124.0	122.1	97.9
	6-31+G**	123.8	122.0	97.8
	6-31++G**	123.9	122.1	97.7
	6-311G	125.5	123.8	95.8
	6-311+G	125.3	123.6	95.7
	6-311++G	125.3	123.6	95.7
	6-311G*	123.9	122.1	97.5
	6-311+G*	123.9	122.1	97.5
	6-311++G*	123.9	122.1	97.5
	6-311G**	123.8	122.1	97.5
	6-311+G**	123.8	122.1	97.5
	6-311++G**	123.8	122.1	97.5
	LANL2DZ	125.9	124.5	97.3
Experimental value		124.2	121.4	98.7

[a] HF refers to the Hartree-Fock *ab initio* method. B3PW91 is the Becke-3 Perdew-Wang 91 hybrid density functional method. MP2 is the Hartree-Fock method with second-order Møller-Plesset perturbational corrections.

[b] 6-31G and 6-311G are split valence basis sets constructed of linear combinations of Gaussian functions. They are described in greater detail in Chapter 7. LANL2DZ is the Dunning-Hunziga double-zeta valence basis set employing the Los Alamos National Laboratories relativistic effective core potentials.

[c] These values taken from Mann, M.; Fabian, J. *J. Mol. Struct. (Theochem)* **1995**, *331*, 51-61.

Table 3.3. Comparison of 1,2-Dithiin Dihedral Angles[a].

Method[b]	Basis Set[c]	S-C=C-C (°)	C=C-C=C (°)	S-S-C=C (°)	C-S-S-C (°)
HF	6-31G*[d]	1.1	26.2	n/a[e]	49.7
	6-311++G**	1.1	26.3	-38.7	49.5
	LANL2DZ	1.2	24.4	-34.2	43.0
B3PW91	6-31G*	1.1	26.8	-39.5	50.7
	6-311++G**	1.3	26.8	-39.6	50.8
	LANL2DZ	1.3	25.4	-35.0	44.0
MP2	6-31G	1.1	28.6	-39.1	49.0
	6-31+G	1.0	29.2	-39.8	50.0
	6-31++G	1.3	28.9	-40.1	50.2
	6-31G*	1.7	27.6	-42.3	54.2
	6-31+G*	1.6	28.0	-42.6	54.8
	6-31++G*	1.8	27.7	-42.8	54.9
	6-31G**	1.7	27.6	-42.3	54.2
	6-31+G**	1.6	28.0	-42.6	54.7
	6-31++G**	1.8	27.7	-42.8	54.8
	6-311G	2.0	28.3	-40.8	50.6
	6-311+G	1.6	29.0	-41.2	51.3
	6-311++G	2.1	28.5	-41.5	51.5
	6-311G*	2.4	27.3	-43.2	55.1
	6-311+G*	2.3	27.3	-43.2	55.2
	6-311++G*	2.6	27.0	-43.4	55.3
	6-311G**	2.3	27.4	-43.2	55.4
	6-311+G**	2.3	27.4	-43.2	55.2
	6-311++G**	2.5	27.1	-43.3	55.2
	LANL2DZ	1.3	26.7	-36.8	46.2
Experimental value		0.3	29.0	-41.2	53.9

[a] When regarding a dihedral angle 1-2-3-4, if you look down the 2-3 bond, a positive sign indicates a clockwise rotation from 1 to 4, while a negative sign indicates counterclockwise rotation from 1 to 4.

[b] HF refers to the Hartree-Fock *ab initio* method. B3PW91 is the Becke-3 Perdew-Wang 91 hybrid density functional method. MP2 is the Hartree-Fock method with second-order Møller-Plesset perturbational corrections.

[c] 6-31G and 6-311G are split valence basis sets constructed of linear combinations of Gaussian functions. They are described in greater detail in Chapter 7. LANL2DZ is the Dunning-Hunziga double-zeta valence basis set employing the Los Alamos National Laboratories relativistic effective core potentials.

[d] These values taken from Mann, M.; Fabian, J. *J. Mol. Struct. (Theochem)* **1995**, *331*, 51-61.

[e] Value not available.

Table 3.4. Comparison of 1,2-Dithiin Ionization Parameters.

Method[a]	Basis Set[b]	IP[c] (eV)	$<S^2>$[c]
HF	6-31G*	n/a[d]	n/a
	6-311++G**	n/a	n/a
	LANL2DZ	n/a	n/a
B3PW91	6-31G*	n/a	n/a
	6-311++G**	n/a	n/a
	LANL2DZ	8.12	0.754
MP2	6-31G	8.31	0.811
	6-31+G	8.47	0.813
	6-31++G	8.47	0.813
	6-31G*	7.99	0.794
	6-31+G*	8.16	0.796
	6-31++G*	8.17	0.796
	6-31G**	8.03	0.793
	6-31+G**	8.20	0.795
	6-31++G**	8.20	0.795
	6-311G	8.48	0.809
	6-311+G	8.55	0.812
	6-311++G	8.56	0.813
	6-311G*	8.20	0.826
	6-311+G*	8.27	0.801
	6-311++G*	8.27	0.801
	6-311G**	8.25	0.798
	6-311+G**	8.32	0.800
	6-311++G**	8.32	0.800
	LANL2DZ	n/a	n/a
Experimental value		8.16	0.75[e]

[a] HF refers to the Hartree-Fock *ab initio* method. B3PW91 is the Becke-3 Perdew-Wang 91 hybrid density functional method. MP2 is the Hartree-Fock method with second-order Møller-Plesset perturbational corrections.

[b] 6-31G and 6-311G are split valence basis sets constructed of linear combinations of Gaussian functions. They are described in greater detail in Chapter 7. LANL2DZ is the Dunning-Hunziga double-zeta valence basis set employing the Los Alamos National Laboratories relatavistic effective core potentials.

[c] IP refers to the non-adiabatic ionization potential calculated by the ΔSCF method (see Chapter 7). $<S^2>$ refers to the value obtained by operation of the spin-squared operator on the wavefunction obtained in the calculation of the non-adiabatic cation radical energy.

[d] Value not available.

[e] Theoretical expectation value for a pure doublet state.

Tables 3.1 through 3.4 compare the various geometric and ionization-based parameters of 1,2-dithiin. Study of the deviation of geometric parameters, ionization potentials, and measures of spin contamination shows an interesting dependence of the accuracy of certain properties on the inclusion of certain functions in addition to the standard basis set, as well as certain other computational parameters. For all geometric parameters, computed by MP2 with either the 6-31G or the 6-311G basis sets, the deviation from the experimental values was small and rather constant for any level of diffuse function augmentation (none, +, or ++), while the polarization functions were kept constant. There is a marked improvement in the calculated values upon going from no polarization function to one additional set of polarization functions (*); parameters calculated with the heavy-atom set (*) and the full set (**) are practically identical, as would be expected if the hydrogen atoms do not significantly perturb the molecular electronics. In the case of the 6-31G basis set, the C-S-S bond angle and C-S-S-C dihedral angle actually become worse upon the addition of the first diffuse function (+); the increase in deviation is small, but is noticeable in its consistency.

The effect of the diffuse and polarization functions on cation radical-related parameters is more complex. With the 6-31G basis set, the error in ionization potential is moderate without any polarization functions, and shifts from too high when no diffuse functions are included to too low upon the inclusion of diffuse functions. In the presence of one or two sets of polarization functions, the deviation is large and positive without any diffuse functions, nearly zero with one diffuse function, and small and positive with two diffuse functions. The best fit is found to be 6-31+G*. For the 6-311G basis set, the effect is more well-behaved; the deviation is large and positive without diffuse functions, and moderate with diffuse functions. With the exception of the 6-311G (no *) case, the spin contamination is unfortunately large with all combinations of functions, but drops consistently and significantly when at least one diffuse function is included. The

aforementioned exceptional case possesses very large spin contamination which peaks with the addition of a single diffuse function set. It is known that MP2 often has difficulty with spin contamination, tending to mix substantial quartet spin into the calculation; overall, the spin contaminations of these MP2 results are quite acceptable.

A study was also made to compare methods and basis set types. For the prediction of bond lengths and angles the methods seem similar when identical basis sets are compared. For the prediction of dihedral angles Hartree-Fock theory is found to be very poor, and density-functional theory almost as bad. Second-order Møller-Plesset theory is fairly good, but found to be substantially worse for 6-311++G** than 6-31G*. This demonstrates quite eloquently the surprising point that better basis sets do not always give better answers; often the inclusion of extra functions to more fully describe the system overestimates the contribution from the features for which the additional functions account, and throws off the final result. In terms of basis sets, 6-31G* was found to be the same as, or substantially better than, 6-311++G**, except for DFT, which benefited from the additional functions. It is also notable that the B3PW91 predictions of ionization potential often erred on the high side. Even single-point calculations allow orbital reorganization (though not geometric reorganization) when the number of electrons is altered, and this reorganization always lowers the apparent ionization potential. The direction of the B3PW91 error was therefore unexpected and would have cast doubt on an analysis based on the DFT molecular orbitals. The LANL2DZ basis set was found to be uniformly unacceptable for predicting 1,2-dithiin geometry, though it does a surprisingly good job with the ionization potential and spin contamination (IP calc.: 8.12 eV, exp.: 8.16 eV; $<S^2>$ calc.: 0.754, theoretical: 0.75).

The final choice for the computational simulation of the 1,2-dithiin series was 6-31+G*. There was no significant error in the ionization potential, and the error in the geometric parameters was small. Being assured in the method, calculations were

undertaken to visualize the ten highest occupied and eight lowest unoccupied molecular orbitals (Table 3.5). All occupied orbitals were found to be well-behaved, but six out of the eight lowest unoccupied orbitals were found to contain large diffuse orbitals at some distance from the molecule, with only very small contributions near the molecule. The character of these orbitals will therefore not be described. The π-type orbitals will be described as combinations of a pair of sulfur 3p non-bonding orbitals and four carbon 2p π-bonding orbitals; this is essentially the mixing of 1,3-butadiene with a planar disulfide (see Discussion). It should be noted that the disulfide is not planar, and actually possesses significant overlap between the upper lobe of one S 3p orbital with the lower lobe of the other S 3p orbital in all anti-parallel combinations. This overlap will be discussed in greater detail in Chapter 4.

Table 3.5. 1,2-Dithiin Molecular Orbitals.

Orbital	Symmetry	Energy (eV)	Description[a]
LUMO	B	-1.29	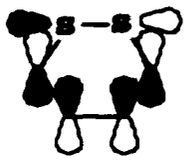 σ*
HOMO	A	8.32	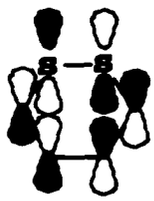 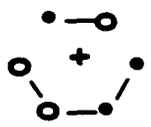 π
HOMO-1	A	10.43	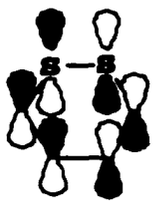 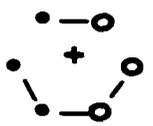 π
HOMO-2	B	10.47	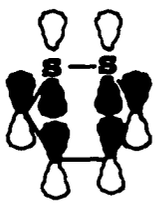  π
HOMO-3	B	12.63	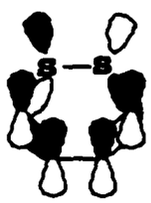 n*
HOMO-4	A	13.02	 σ

Table 3.5. Cont. 1,2-Dithiin Molecular Orbitals.

Orbital	Symmetry	Energy (eV)	Description[a]
HOMO-5	A	14.28	 n
HOMO-6	B	14.38	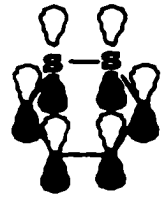 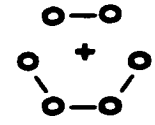 π
HOMO-7	B	16.65	 n*
HOMO-8	A	16.86	 σ
HOMO-9	B	18.74	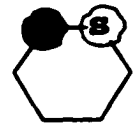 σ*

[a] The diagrams represent the major MO features with s-type, p-type, and sp^3-type orbitals; in addition, the four π-type MOs discussed below are also represented diagrammatically.

The states of greatest concern in the Discussion are the LUMO, HOMO, HOMO-1, HOMO-2, HOMO-4 and HOMO-6. The HOMO-4 and LUMO form the S-S σ/σ^* pair, while the HOMO, HOMO-1, HOMO-2 and HOMO-6 are the various linear combinations of 1,3-butadiene and two sulfur atoms (see dithiin electronic model in Discussion).

Other members of the 1,2-dithiin series were also investigated with the MP2/6-31+G* combination of method and basis (Tables 3.6, 3.8, 3.10, and 3.12). Unfortunately, limited computational resources prevented the simulation of every compound investigated theoretically, and experimental limitations have so far prevented the synthesis of 3,6-difluoro-1,2-dithiin, so there is not a perfect match between the computationally analyzed compounds and the experimentally analyzed compounds. For useful comparison in the Discussion, a few other disulfides have also been computationally simulated (Tables 3.7, 3.9, 3.11, and 3.13). The 3,6-disubstituted-1,2-dithiin excited states were compared to those of other disulfides (Table 3.14). 1,2-Diselenin was also simulated (Tables 3.6, 3.8, and 3.10), but the limited evidence available suggests that the 6-31+G* basis set is not sufficient for a good description of this selenium analogue. The spin and charge distribution of 1,2-dithiin and 1,2-diselenin were compared (Table 3.11).

Table 3.6. Computed Geometric Parameters of 1,2-Dithiins.

Parameter	1,2-Dithiin	3,6-Dimethyl-1,2-dithiin	3,6-Difluoro-1,2-dithiin	3,6-Bis(trifluoro-methyl)-1,2-dithiin	1,2-Diselenin
Bond Lengths (Å):					
S-S (Se-Se)	2.07	2.07	2.07	2.07	2.34
S-C (Se-C)	1.76	1.78	1.76	1.77	1.90
C=C	1.36	1.36	1.35	1.36	1.35
C-C (in ring)	1.45	1.45	1.45	1.45	1.45
C-C (methyl)		1.50		1.49	
C-F			1.36	1.36	
Bond Angles (°):					
S-S-C (Se-Se-C)	97.8	98.3	96.2	96.5	94.1
S-C=C (Se-C=C)	122.0	119.5	124.5	122.1	123.5
S-C-C		115.9		115.9	
S-C-F			114.2		
C=C-C (in ring)	123.9	125.3	122.0	123.1	125.8
C=C-C (methyl)		124.4		122.0	
C=C-F			121.2		
C-C-F				110.4	
Dihedral Angles (°):					
C-S-S-C (C-Se-Se-C)	54.8	56.6	55.0	57.4	52.0
S-S-C=C (Se-Se-C=C)	-42.6	-43.0	-44.2	-45.0	-42.4
S-S-C-C		141.9		138.5	
S-S-C-F			140.0		
C-C=C-S (C-C=C-Se)	1.6	1.5	1.3	1.4	1.3
C-C=C-C		176.1		177.7	
C-C=C-F			176.9		
C=C-C=C	28.0	28.4	29.2	29.7	31.1

Table 3.7. Computed Geometric Parameters of Some Other Disulfides.

Parameter	Dimethyl Disulfide	Dithiirane	1,2-Dithietane
Bond Length (Å):			
S-S	2.06	2.10	2.13
C-S	1.81	1.80	1.84
C-C			1.53
Bond Angle (°):			
S-S-C	102.1	54.1	78.0
S-C-C			96.0
Dihedral Angle (°):			
C-S-S-C	84.0		21.8
S-S-C-C			-26.0
S-C-C-S			30.1

Table 3.8. Molecular Orbital Energies and Symmetries: 1,2-Dithiins.[a]

Molecular Orbital	1,2-Dithiin	3,6-Dimethyl-1,2-dithiin	3,6-Difluoro-1,2-dithiin	3,6-Bis(trifluoro-methyl)-1,2-dithiin	1,2-Diselenin
LUMO+2	0.08023 B	0.07640 B	0.07731 B	0.07153 B	0.06775 B
LUMO+1	0.07340 A	0.07406 A	0.06864 A	0.05863 A	0.05849 A
LUMO	0.04750 B	0.06248 B	0.03724 B	0.01213 B	0.03208 B
HOMO	-0.30589 A	-0.29525 A	-0.33251 A	-0.35486 A	-0.29757 A
HOMO-1	-0.38338 A	-0.36638 A	-0.40561 A	-0.42054 B	-0.36275 A
HOMO-2	-0.38475 B	-0.37632 B	-0.41358 B	-0.42456 A	-0.36432 B
HOMO-3	-0.46415 B	-0.44346 B	-0.48730 B	-0.50802 B	-0.44612 A
HOMO-4	-0.47838 A	-0.46782 A	-0.51223 A	-0.51687 A	-0.45066 B
HOMO-5	-0.52472 A	-0.50024 B	-0.55315 B	-0.56819 B	-0.49636 B
HOMO-6	-0.52837 B	-0.50598 A	-0.58903 A	-0.56897 A	-0.49744 A
HOMO-7	-0.61184 B	-0.53484 A	-0.60643 A	-0.62329 B	-0.59870 A
HOMO-8	-0.61957 A	-0.57025 B	-0.65505 B	-0.64847 A	-0.60820 B
HOMO-9	-0.68875 B	-0.57763 B	-0.69292 B	-0.66608 A	-0.68204 B

[a] The orbital energy (in hartrees) is followed by the orbital symmetry. The 1,2-dithiins were found to possess C_2 symmetry.

Table 3.9. Molecular Orbital Energies Molecular Orbital Energies and Symmetries: Selected Disulfides.[a]

Molecular Orbital	Dimethyl Disulfide	Dithiirane	1,2-Dithietane
LUMO+2	0.08696	0.08716	0.08675
	B	A_1	A
LUMO+1	0.07779	0.06092	0.06363
	B	A_1	A
LUMO	0.07224	0.04406	0.05218
	A	B_2	B
HOMO	-0.35132	-0.33892	-0.32239
	A	A_2	A
HOMO-1	-0.36205	-0.42524	-0.41124
	B	B_1	B
HOMO-2	-0.43980	-0.45546	-0.43624
	A	A_1	A
HOMO-3	-0.49254	-0.46287	-0.45688
	B	B_2	B
HOMO-4	-0.53497	-0.57852	-0.53072
	A	A_1	A
HOMO-5	-0.58110	-0.65676	-0.55362
	B	B_1	A
HOMO-6	-0.59886	-0.85212	-0.62798
	A	B_2	A
HOMO-7	-0.60140	-0.86370	-0.65920
	B	A_1	B
HOMO-8	-0.61431	-1.15714	-0.76970
	A	A_1	B
HOMO-9	-0.78979	-6.66768	-0.93546
	B	A_2	B

[a] The orbital energy (in hartrees) is followed by the orbital symmetry. Dimethyl disulfide and 1,2-dithietane were found to possess C_2 symmetry, while dithiirane was found to possess C_{2v} symmetry.

Table 3.10. Ionization Potentials of 1,2-Dithiins.

Compound:	1,2-Dithiin		3,6-Dimethyl-1,2-dithiin		3,6-Difluoro-1,2-dithiin
Orbital	Exp.[a]	Calc.	Exp.[a]	Calc.	Calc.
IP (ΔSCF)	8.16	8.16	7.78	7.96	8.89
HOMO	8.16	8.32	7.78	8.03	9.05
HOMO-1	9.82	10.43	9.31	9.97	11.04
HOMO-2	10.06	10.47	9.63	10.24	11.25
HOMO-3	11.51	12.63	10.93	12.07	13.26
HOMO-4	12.17	13.02		12.73	13.94
HOMO-5	12.66	14.28		13.61	15.05
HOMO-6	13.15	14.38		13.77	16.03
HOMO-7	14.40	16.65		14.55	16.50
HOMO-8	14.97	16.86		15.52	17.82

Compound:	3,6-Bis(trifluoro-methyl)-1,2-dithiin		1,2-Diselenin	
Orbital	Exp.[a]	Calc.	Exp.[a]	Calc.
IP (ΔSCF)	9.10	8.91	7.93	7.64
HOMO	9.10	9.66	7.93	8.10
HOMO-1	10.57	11.44	9.38	9.87
HOMO-2	10.87	11.55	9.60	9.91
HOMO-3	12.44	13.82	11.22	12.14
HOMO-4	12.97	14.06	11.61	12.26
HOMO-5	13.52	15.46	12.03	13.51
HOMO-6	13.91	15.48	14.19	13.54
HOMO-7	14.54	16.96	15.01	16.29
HOMO-8		17.65		16.55

[a] Photoelectron spectroscopic ionization potentials taken from [19] except those for 3,6-bis(trifluoromethyl)-1,2-dithiin, which are unpublished results from the same collaborative effort.

Table 3.11. Comparison of Charge and Spin Distribution in the Non-Adiabatic Cation Radicals of 1,2-Dithiin and 1,2-Diselenin.[a]

Compound:	1,2-Dithiin		1,2-Diselenin	
Atom	Charge	Spin	Charge	Spin
S or Se	0.18	0.17	0.31	0.40
α C	0.03	0.39	-0.00	-0.00
β C	0.29	-0.03	0.20	0.10

[a] Values calculated with MP2/6-31+G*. Charges reported with hydrogen-centered charges summed into heavy atoms. Signs of values reported even when the magnitude is negligible.

Table 3.12. Electronic Transitions: Symmetries, Energies, Oscillator Strengths, and Contributing Transitions for 1,2-Dithiins.

Transition Symmetry	Transition Energy[a] (nm)	Oscillator Strength	Contributing MOs and Coefficients[b]
1,2-Dithiin			
^{3}B	605[c]	0	**HOMO → LUMO, 0.57454**
^{3}B	357[c]	0	**HOMO-1 → LUMO, 0.44537**
^{1}B	**354**[c]	0.0078	**HOMO → LUMO, 0.64505**
^{3}A	332[c]	0	**HOMO-2 → LUMO, 0.45346**
^{3}A	244	0	**HOMO-2 → LUMO, 0.36667**
^{1}B	**237**[c]	0.0389	**HOMO-1 → LUMO, 0.50774**
^{3}B	226	0	**HOMO-4 → LUMO, 0.34956**
			HOMO-1 → LUMO, -0.35430
^{1}A	**225**[c]	0.0430	**HOMO-2 → LUMO, 0.57423**
^{3}A	215	0	**HOMO → LUMO+4, 0.45933**
^{1}A	**200**	0.0005	**HOMO → LUMO+1, 0.48717**
			HOMO → LUMO+4, 0.36569
^{1}A	**196**	0.0005	**HOMO → LUMO+1, 0.43917**
			HOMO → LUMO+4, -0.37091
^{1}B	**193**	0.0361	HOMO-1 → LUMO, -0.36013
			HOMO → LUMO+5, 0.40951
3,6-Dimethyl-1,2-dithiin			
^{3}B	567[d]	0	**HOMO → LUMO, 0.50013**
^{3}B	350[d]	0	**HOMO-1 → LUMO, 0.41293**
^{1}B	**331**[d]	0.0166	**HOMO → LUMO, 0.57848**
^{3}A	320	0	**HOMO-2 → LUMO, 0.37607**
^{3}A	243	0	**HOMO-2 → LUMO, 0.35562**
^{1}B	**239**[d]	0.0860	**HOMO-1 → LUMO, 0.43392**
^{3}B	223	0	HOMO-4 → LUMO, 0.31164
			HOMO-1 → LUMO+5, 0.31359
^{1}A	**221**[d]	0.0278	**HOMO-2 → LUMO, 0.49584**
^{3}A	219	0	**HOMO → LUMO+1, 0.40353**
^{1}A	**206**[d]	0.0012	**HOMO → LUMO+1, 0.52637**
^{1}A	**197**[d]	0.0413	HOMO-1 → LUMO, -0.33508
			HOMO → LUMO+2, 0.40414
^{1}B	**189**	0.0033	**HOMO → LUMO+5, 0.32589**

Table 3.12. Cont. Electronic Transitions: Symmetries, Energies, Oscillator Strengths, and Contributing Transitions for 1,2-Dithiins.

Transition Symmetry	Transition Energy[a] (nm)	Oscill. Str.	Contributing MOs and Coefficients[b]
3,6-Difluoro-1,2-dithiin			
^{3}B	549	0	**HOMO → LUMO, 0.54471**
^{3}B	348	0	**HOMO-1 → LUMO, 0.48783**
^{1}B	**327**	0.0036	**HOMO → LUMO, 0.62472**
^{3}A	315	0	**HOMO-2 → LUMO, 0.40445**
^{3}A	244	0	**HOMO-2 → LUMO, 0.41641**
^{1}B	**234**	0.0264	**HOMO-1 → LUMO, 0.53997**
^{3}B	225	0	**HOMO-4 → LUMO, 0.35803**
			HOMO-1 → LUMO, 0.33172
^{1}A	**220**	0.0236	**HOMO-2 → LUMO, 0.56729**
^{3}A	212	0	**HOMO → LUMO+1, 0.37736**
^{1}A	**194**	0.0001	**HOMO → LUMO+1, 0.50611**
^{1}B	**189**	0.0439	**HOMO → LUMO+2, 0.53744**
^{1}A	**176**	0.0035	HOMO → LUMO+1, -0.36076
			HOMO → LUMO+4, 0.41249
3,6-Bis(trifluoromethyl)-1,2-dithiin			
^{3}B	582[c]	0	**HOMO → LUMO, 0.58510**
^{3}B	344[c]	0	**HOMO-2 → LUMO, 0.42993**
^{3}A	342[c]	0	**HOMO-1 → LUMO, 0.49337**
^{1}B	**332**[c]	0.0133	**HOMO → LUMO, 0.65108**
^{3}A	242	0	HOMO-1 → LUMO, -0.32628
			HOMO-1 → LUMO+9, 0.26513
^{1}B	**232**	0.0684	**HOMO-2 → LUMO, 0.50646**
^{1}A	**225**	0.0414	**HOMO-1 → LUMO, 0.58738**
^{3}B	221	0	HOMO-4 → LUMO, -0.31349
			HOMO-2 → LUMO, -0.34486
			HOMO → LUMO+2, 0.25487
^{3}A	208	0	**HOMO → LUMO+1, 0.25168**
^{1}A	**189**	0.0022	**HOMO → LUMO+1, 0.33430**
			HOMO → LUMO+3, -0.33523
^{1}B	**188**	0.0237	HOMO-2 → LUMO, -0.42973
			HOMO → LUMO+2, 0.41363
^{1}B	**168**	0.0033	**HOMO → LUMO+21, 0.26690**

Table 3.12. Cont. Electronic Transitions: Symmetries, Energies, Oscillator Strengths, and Contributing Transitions for 1,2-Dithiins.

[a] Wavelengths in bold indicate allowed transitions.
[b] All contributions from MOs with coefficient magnitudes of less than 0.3 not listed (except that the largest contributing MO is always listed); major positively contributing MO is listed in bold.
[c] Compare to experimental transitions: 452 nm (ε = 90), 279 nm (ε = 2000), and 248 nm (ε = 1500).
[d] Compare to experimental transitions: 422 nm (ε = 47), 334 nm (ε = 360), 268 nm (ε = 22000) and 202 nm (ε = 45000).
[e] Compare to experimental transitions: 444 nm (ε = 552) and a broad, flat-topped band of greater absorbance at 250-300 nm.

Table 3.13. Electronic Transitions: Symmetries, Energies, Oscillator Strengths, and Contributing Transitions for Selected Disulfides.

Transition Symmetry	Transition Energy[a] (nm)	Oscillator Strength	Contributing MOs and Coefficients[b]
Dimethyl Disulfide			
^{3}B	273[c]	0	**HOMO → LUMO+2, 0.34598**
			HOMO → LUMO+8, -0.32650
			HOMO → LUMO+14, 0.30545
^{3}A	255	0	**HOMO-1→ LUMO+2, 0.34567**
			HOMO-1 → LUMO+8, -0.30903
			HOMO-1 → LUMO+14, 0.31408
^{1}B	**224**[c]	0.0141	HOMO → LUMO+1, -0.30706
			HOMO → LUMO+2, 0.33436
			HOMO → LUMO+8, -0.31222
^{1}A	**215**	0.0013	HOMO-1 → LUMO+1, -0.31122
			HOMO-1 → LUMO+2, 0.32460
			HOMO-1 → LUMO+8, -0.31212

Table 3.13. Cont. Electronic Transitions: Symmetries, Energies, Oscillator Strengths, and Contributing Transitions for Selected Disulfides.

Transition Symmetry	Transition Energy[a] (nm)	Oscillator Strength	Contributing MOs and Coefficients[b]
Dithiirane			
$^3B_1$	534[d]	0	**HOMO → LUMO, 0.60600**
$^1B_1$	**393**[d]	0.0010	**HOMO → LUMO, 0.61335**
$^3B_2$	265	0	**HOMO → LUMO, 0.59208**
$^3A_2$	265	0	**HOMO-1 → LUMO, 0.51236**
$^3A_2$	235	0	**HOMO → LUMO+1, 0.38432**
$^1A_2$	233	0	**HOMO-1 → LUMO, 0.47538**
			HOMO → LUMO+1, 0.31015
$^3B_1$	217	0	**HOMO → LUMO+3, 0.42897**
			HOMO → LUMO+14, 0.33079
$^1A_2$	204	0	**HOMO → LUMO+1, 0.41926**
$^1B_1$	**188**	0.0198	**HOMO → LUMO+3, 0.52629**
$^1A_2$	180	0	**HOMO → LUMO+2, 0.54934**
1,2-Dithietane			
^3B	513[e]	0	**HOMO → LUMO, 0.56191**
^1B	**380**[e]	0.0010	**HOMO → LUMO, 0.57922**
^3A	295	0	**HOMO-1 → LUMO, 0.33499**
			HOMO → LUMO+1, 0.32769
^1A	253	0	HOMO-1 → LUMO, 0.30409
			HOMO → LUMO+1, 0.37363
^3B	253	0	**HOMO-2 → LUMO, 0.53212**
^3A	237	0	**HOMO-1 → LUMO, 0.45022**
^1A	**204**	0.0002	**HOMO-1 → LUMO, 0.47660**
			HOMO → LUMO+2, 0.34979
^3B	203	0	**HOMO → LUMO+18, 0.31107**
^1A	**184**	0.0136	HOMO → LUMO+1, 0.38352
			HOMO → LUMO+2, 0.46252
^1B	**179**	0.0819	**HOMO → LUMO+3, 0.41745**

Table 3.13. Cont. Electronic Transitions: Symmetries, Energies, Oscillator Strengths, and Contributing Transitions for Selected Disulfides.

[a] Wavelengths in bold indicate allowed transitions.
[b] All contributions from MOs with coefficient magnitudes of less than 0.3 are not listed (except that the largest contributing MO is always listed); major positively contributing MO is listed in bold.
[c] Compare to experimental transition: 254 nm (ε = 275), taken from Percampus, H. H. *UV-Vis Atlas of Organic Compounds*; VCH: New York, 1992.
[d] Compare to experimental transition for related compound:

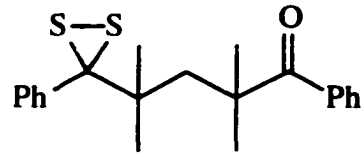

452 nm, taken from Ishii, A.; Akazawa, T.; Maruta, T.; Nakayama, J.; Hosino, M.; Shiro, M. *Angew. Chem., Int. Ed. Engl.* **1994**, *33*, 777-779. Also, previous calculation (CNDO/S-CI): 422 nm, same assignment as current work, taken from Snyder, J. P.; Carlsen, L. *J. Am. Chem. Soc.* **1977**, *99*, 2931.
[e] Compare to experimental transition for related compound:

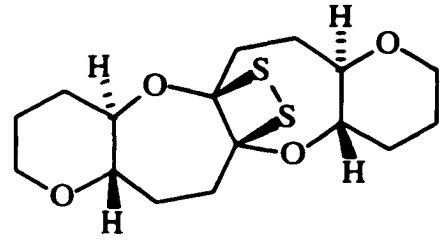

426 nm (ε = 102) and 213 nm (ε = 4074), taken from Nicolaou, K. C.; Defrees, S. A.; Hwang, C. K.; Stylianide, N.; Carroll, P. J. *J. Am. Chem. Soc.* **1990**, *112*, 3029-3039.

Table 3.14. Calculated S-S Bond Lengths and Stretching Frequencies for Ground State and Electronic Excited States of Selected Disulfides.

Compound (State)	S-S Bond Length (Å)	S-S Stretch (cm^{-1})
Dimethyl disulfide		
(S_0)	2.06	554.9[a]
(S_1)	2.59	304.7 (508.5)[b]
(T_1)	2.63	286.5
Dithiirane		
(S_0)	1.80	521.2
(S_1)	2.44	337.5 (508.4)[b]
(T_1)	2.53	308.5
1,2-Dithietane		
(S_0)	2.13	515.6[c]
(S_1)	2.48	347.6 (529.8)[b]
(T_1)	2.59	313.9
1,2-Dithiin		
(S_0)	2.07	556.1
(S_1)	2.66	284.1 (330.7)[b]
(T_1)	2.65	287.4
3,6-Dimethyl-1,2-dithiin		
(S_0)	2.07	564.5
(S_1)	2.64	246.0 (233.8)[b]
(T_1)[d]	2.12	370.1 (515.1)[b]
3,6-Difluoro-1,2-dithiin		
(S_0)	2.07	557.3
(S_1)	2.68	249.6 (318.0)[b]
(T_1)	2.68	260.0
3,6-Bis(trifluoromethyl)-1,2-dithiin		
(S_0)	2.07	545.4
(T_1)[d]	-	(444.8)[b]

[a] Compare to experimental transition: 693.2 cm^{-1}, taken from Pouchert, C. J. *The Aldrich Library of FT-IR Spectra*; First Edition, Aldrich Chemical Co., Inc.: Milwaukee, 1989.
[b] The value in parentheses is the frequency of the excited state at the ground state geometry.
[c] Compare to experimental transition for related compound: 490 cm^{-1}. For details see Footnote E, Table 3.13.
[d] These triplet values calculated with CIS rather than MP2.

DISCUSSION

Dithiin Electronic Structure

1,2-Dithiins can be described as a pair of sulfur atoms interacting with a 1,3-butadiene unit. This allows the π-type orbitals to be viewed as combinations of the two filled butadiene orbitals and the two filled p-type sulfur lone pair orbitals. This generates four filled 1,2-dithiin orbitals (Figure 3.1).

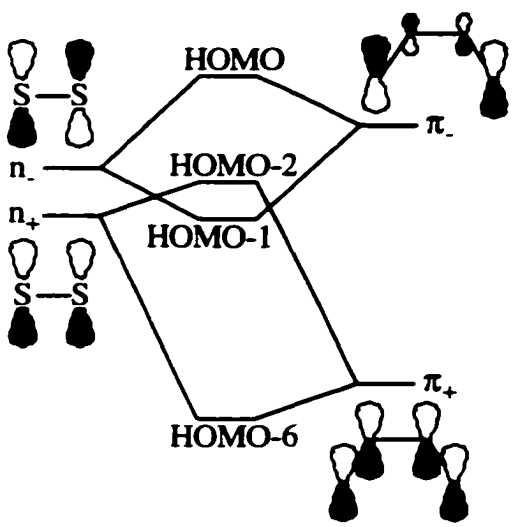

Figure 3.1. 1,2-Dithiin Electronic Structure

The order of the HOMO-1 and HOMO-2 predicted by computational simulation of 1,2-dithiin is found to be reversed by comparison of photoelectron spectroscopic data acquired with helium(I) and helium(II) photon sources, which can provide a measure of participating atomic orbitals in a molecular orbital. The computational splitting between the two orbitals is predicted to be 0.03 eV, and is found to be 0.24 eV in the opposite sense, for a total error of 0.27 eV. This is not really a substantial error even for MP2 eigenvalues, and illustrates the unreliability of the use of Koopman's Theorem in obtaining ionization potentials.

Another feature of 1,2-dithiins which was initially observed by photoelectron spectroscopy is an orbital of nearly complete sulfur character (analyzed as noted in the

preceding paragraph) which possesses a very narrow ionization band. The only orbital in the highest several orbitals expected to be of primarily sulfur character is the sulfur-sulfur σ bond (HOMO-4). Its paired orbital (the S-S σ* orbital) was found to be the LUMO. The full implications of this discovery will be addressed below (see An Explanation of the Color of 1,2-Dichalcogenins).

Geometry, Substitution, and Other Disulfides

As can be seen from Table 3.6, substitution does not affect most geometric parameters of 1,2-dithiins. Most values are also fairly typical of disulfides in general (see Table 3.7) with the notable exception of the C-S bond length. The C-S bond is shorter by a small but consistent amount than the C-S bond in other disulfides, but is fairly typical of aryl sulfides.[36] This may indicate a higher bond order in the case of 1,2-dithiins, which can be attributed to contributions from π-type molecular orbitals such as those discussed above (or to the equivalent valence-bond description such as the valence tautomer seen in Chapter 2).

The difference could also be attributed to hybridization changes, which would be evidenced in the C-S-S bond angle. Indeed, it was found that one of the few geometric parameters observed to be sensitive to substitution was the C-S-S bond angle. This angle was found to be 98.3° for the dimethyl compound, 97.8° for the parent, 96.2° for the difluoro compound, and 96.5° for the diperfluoromethyl compound. Since the bond angle around the sulfur atom should be an indicator of its hybridization, one can determine that the sulfur atom σ bonds increase in p-character as the ring becomes more electron rich. It is also notable that these angles are all substantially smaller than the angle in dimethyl disulfide (102.1°), indicating that 1,2-dithiins possess substantially less p-character in their C-S bonds than other disulfides. This may correlate to the increased importance of π-type

bonding involving sulfur atoms in the case of 1,2-dithiins (thereby increasing the demand for p-character in the p-type lone pair).

Ionization Potentials and Substitution

It is easy to see the effects of various substitutions on the ionization potential of 1,2-dithiins, and they are completely expected. The ionization potential is lowered by electron donating effects such as dimethyl substitution; increased electron density in the already electron-rich ring in which interaction of the various p-type orbitals is destabilizing (Chapter 4) would raise the HOMO and stabilize the cation radical. For the same reasons, electron withdrawing effects such as difluoro or diperfluoromethyl substitution would cause an opposite effect.

Somewhat more difficult to predict is the effect on lower-energy orbitals. Thanks to detailed photoelectron spectroscopic analysis such as that mentioned earlier, it was possible to determine that the 1,2-dithiin orbital labelled HOMO-2 is stabilized more by dimethyl substitution than the orbital labelled HOMO-1, to the extent that the order of the two orbitals is reversed in the dimethyl compound as compared to the parent. The HOMO-1 orbital and HOMO-2 orbitals retain the order of the parent in the perfluoromethyl compound, and the separation increases only slightly.

The Nature of 1,2-Dichalcogenin Radicals

As is discussed in Chapter 2, 1,2-diselenins display an unexpected trend in oxidation potential relative to alkyl substitution. This trend is not observed in the photoelectron spectroscopic studies, in which 1,2-dithiins and 1,2-diselenins display identical ionization potential trends of nearly identical substitution-effect magnitude. A strange difference was found in the nature of the distribution of charge and spin in 1,2-diselenin as compared to 1,2-dithiin. As seen in Table 3.11, the charge in 1,2-dithiins is centered more on the β-carbon than the heteroatom, while the spin is centered more on the α-carbon than the heteroatom. In the case of charge, essentially none is centered on the α-

carbon, while there is essentially no spin centered on the β-carbon. The carbon portion of the non-adiabatic cation radical is therefore essentially distonic. In the case of 1,2-diselenin the charge and spin are distributed similarly, and in a more expected pattern: most of the charge and spin is on the selenium atom, with some charge and spin on the β-carbon in a sort of "allylic" distribution. It is interesting to note that "allylic" charge distribution also seems to be an overriding effect in the proton NMR chemical shifts of 1,2-diselenin-1-oxide (see Chapter 4). That more charge and spin would be centered on the heteroatom in the case of 1,2-diselenin is expected, since the lone pair of selenium is a poorer energy match for the p-orbital of sp^3-hybridized carbon, and therefore the HOMO should resemble a normal diselenide more closely. It is the charge and spin distribution in 1,2-dithiin which seems odd, and may be a product of aromaticity effects (Chapter 4).

Electronic Transitions and Substitution

Substitution has almost no effect on the computationally predicted electronic transitions of 1,2-dithiins. The transitions have a conserved structure, consisting of a triplet progression: 550-600 nm, HOMO → LUMO; 340-360 nm, HOMO-1 → LUMO; 315-345 and 243-244 nm, both HOMO-2 → LUMO. This progression is mirrored by a singlet progression: 330-355 nm, HOMO → LUMO; 225-240 nm, HOMO-1 → LUMO; 220-230 nm, HOMO-2 → LUMO. The lowest triplet transition is often observed in disulfides, since it is far from the other transitions and spin-orbit coupling is fairly efficient in sulfur-containing compounds, allowing forbidden transitions to be observed. The longest-wavelength excitation of dimethyl disulfide is almost certainly a triplet transition. In the case of 1,2-dithiin it is likely but less assured that the longest-wavelength transition is the triplet. The only observed effect of substitution on these transitions was for the case of 3,6-bis(trifluoromethyl)-1,2-dithiin (and notably NOT for the difluoro compound). In the other compounds, the progression of triplet and singlet transitions is in the order given above, but for the perfluoromethyl the HOMO-1 → LUMO and HOMO-2 → LUMO

transitions are reversed in relative energy. There is also only one triplet HOMO-2 → LUMO transition, rather than the two transitions predicted for the other dithiins.

An Explanation of the Color of 1,2-Dichalcogenins

As previously mentioned, the photoelectron spectrum of 1,2-dithiin contains a very sharp ionization which was assigned as the sulfur-sulfur σ orbital. The width of an ionization band is directly related to the bond strength of an orbital.[37] This ionization for 1,2-dithiin is much narrower than is seen for other sulfur-sulfur σ orbitals. For example, the S-S σ bond ionization of dimethyl disulfide measured under the same conditions was found to have an average full-width-at-half-height of 0.38 eV, while for 1,2-dithiin it is 0.26 eV. This narrow ionization band indicates that the S-S σ bond of 1,2-dithiin is substantially weaker than for a typical disulfide. That does not indicate a weaker overall S-S bond, but rather a particular orbital which is more weakly bonding. In fact, as can be seen in Table 3.14, 1,2-dithiin has about the same S-S stretching frequency as dimethyl disulfide, indicating a similar bond strength. The Se-Se σ bond ionization of 1,2-diselenin was also found to be narrow, with an average full-width-at-half-height of 0.30 eV.

A weakly bonding sulfur-sulfur σ orbital necessitates a correspondingly weakly antibonding, lower-energy σ* orbital as compared to a typical disulfide. When this feature is combined with a HOMO which is destabilized compared to a typical disulfide, it might result in a low energy electronic absorption which could account for the unusual color of these compounds. The LUMO of 1,2-dithiin was computed to have an energy 1.29 eV greater than a free electron, while the dimethyl disulfide S-S σ* orbital (found to be the LUMO+2) was computed to have an energy 2.37 eV greater than a free electron. This orbital was located with certainty by comparing S-S bond lengths and stretching frequencies in the ground state and in the excited state. It would seem that, as a general rule, the lowest-energy electronic transitions of disulfides can be characterized as n (or

$n+\pi) \rightarrow \sigma^*_{S\text{-}S}$ (as demonstrated by the increase in S-S bond length and decrease in S-S stretching frequency in the excited state as compared to the ground state), and the unique aspect of dithiins is the low energy of the $\sigma^*_{S\text{-}S}$ orbital, causing the unusual color (unusually long-wavelength absorption). Strain perturbation was computed to have a similar effect on the small cyclic disulfides dithiirane and 1,2-dithietane. These cyclic disulfides are predicted to have only a slightly weaker S-S bond than dimethyl disulfide, but the electronic effect of forcing the sulfur p-type lone pairs to be nearly parallel while enhancing the p-character of the lone pair apparently creates a large perturbation in the electronic nature of the compound. If one considers the Walsh model of cyclopropane, dithiirane could be considered homologous to a 1,2-dithiin locked in a planar conformation.

Certain peculiarities were observed in the comparison of ground and excited state properties of 1,2-dithiins. Although the S-S bond length in the singlet excited state was found to be slightly shorter in the dimethyl compound than the parent and slightly longer in the difluoro compound than the parent, the bond was found to be weaker in both substituted cases. The former result would seem to suggest that the inductive and/or hyperconjugative effects of the substituents interact more with the S-S bond-stabilizing molecular orbitals than with the S-S σ^* antibonding orbital, but the latter result seem inconsistent with this or any other simple explanation. The data are similar if one looks instead at the change in stretching frequency going from the ground state to the singlet excited state. One can see more weakening for the difluoro compound (239.3 cm^{-1}) than for the parent (225.4 cm^{-1}), but by far the greatest weakening is seen for the dimethyl compound (330.7 cm^{-1}). Of the ground-state S-S stretching frequencies, the dimethyl compound is the "odd man out", possessing a value almost 10 cm^{-1} greater than the other two, which were found to be nearly identical to one another. These facts may correlate with the fact that, of the compounds simulated, only 3,6-dimethyl-1,2-dithiin was found to not planarize completely upon excitation to the singlet state (Chapter 4).

CONCLUSIONS

A suitable method was found to computationally simulate electronically complex molecules such as 1,2-dithiins. It was found not to be wholly adequate for the simulation of 1,2-diselenin. In general, the computational simulation compared well to the experimental data, and was of great help in its interpretation. Unlike most geometric features of 1,2-dithiins, the ionization energies of these compounds were both computed and experimentally observed to show a strong dependence on substituents. The charge and spin of the 1,2-diselenin non-adiabatic cation radical was seen to be more localized on the chalcogen than in the 1,2-dithiin non-adiabatic cation radical, and the charge and spin distribution in the carbon portion of the ring was found to be substantially different. This was probably due to poor energy matching between selenium 4p and carbon 2p orbitals as compared to sulfur 3p and carbon 2p orbitals. The photoelectron spectra of 1,2-dithiins and 1,2-diselenins gave experimental evidence for a weak chalcogen-chalcogen σ bond orbital compared to other dichalcogenides. Calculations were used to show that the LUMO of 1,2-dithiins is primarily S-S σ^* in character. They also demonstrated a low energy HOMO $\rightarrow$ LUMO transition ($n+\pi \rightarrow \sigma^*_{S\text{-}S}$) which explains the unusual color of 1,2-dichalcogenins.

CHAPTER 4

AROMATICITY OR ANTI-AROMATICITY OF 1,2-DICHALCOGENINS AND THEIR RADICAL CATIONS: COMPUTATIONAL AND EXPERIMENTAL ANALYSIS

ASSESSMENT OF AROMATICITY AND ANTI-AROMATICITY

A great many methods for assessing the extent of aromatic stabilization or anti-aromatic destabilization have been proposed over the years. The experimental analysis of anti-aromatic molecules is particularly difficult since they tend to be very reactive. Often it is not much easier computationally, since the many "anti-aromatic" molecules could be reactive and high in energy due to certain unstable moieties of the molecule rather than cyclic conjugation of the molecule as a whole; this is particularly true when assessing the properties of reactive species such as radical cations and dications, and transient species such as excited states. Much work in this field is accomplished by analogy to accepted standard molecules and systems.[38-59]

Some of the more classical approaches to assessing aromaticity involve planarity and bond alternation; of course, anti-aromatic molecules tend to undergo any geometric distortion possible to reduce the efficiency of cyclic conjugation. In a discovery with which many may be unfamiliar, Shukla and Wan found an interesting way to allow such geometric factors to verify the aromatic or anti-aromatic nature of molecules by comparing the ground-state behavior of the molecules to the excited state.[60] They found that 10,11-dihydrodibenz[b,f]oxepin (Figure 4.1) undergoes a facile photochemical reaction and exhibits very little fluorescence, though in the ground state it is no more reactive than would be expected of a diphenyl ether. This was found to be in great contrast to the behavior of the fully-conjugated analog dibenz[b,f]oxepin, which is very reactive in the ground state but is photochemically inert and exhibits a strong fluorescence with a large

Stokes shift. Similarly, a Stokes shift is seen for dibenz[b,f]thiepin, but is absent for suberene (1,2,5,6-dibenzocyclohexatriene). These Stokes shifts were determined to be due to planarization of the molecules upon excitation to the singlet state. In addition, the Stokes shifts are also observed at 77K in a glass, indicating a low barrier to the causal ring torsion in the singlet excited state.

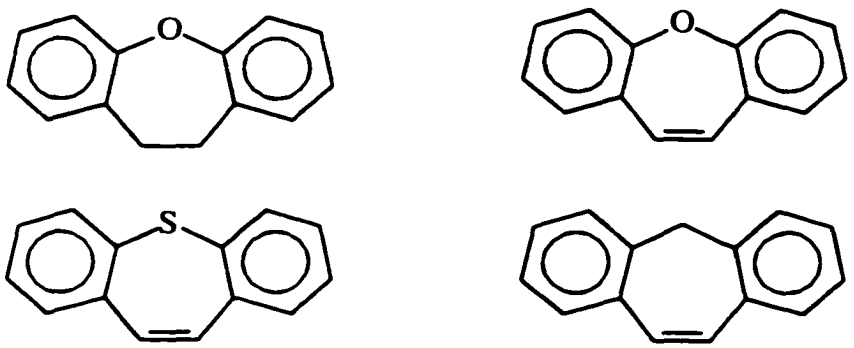

Figure 4.1. 10,11-Dihydrodibenz[b,f]oxepin, Dibenz[b,f]oxepin, Dibenz[b,f]thiepin, and Suberene.

More classical methods of assessing aromaticity via geometry include examining bond alternation; in an aromatic molecule, double bonds have been observed to lengthen and single bonds to shorten along a conjugated cycle, presumably enhancing the overlap and improving the efficiency of conjugation. Conversely, in anti-aromatic molecules bond alternation has been seen to increase where possible; for example, the lowest energy state of cyclobutadiene has been demonstrated to be rectangular, undergoing a Jahn-Teller distortion which reduces overlap between carbon 2p orbitals of adjacent ethylene units. In flexible molecules, aromatic compounds are expected to be planar, such as in the case of the dianion of cyclooctatetraene, which is a planar 10π-electron aromatic molecule; the neutral is a highly-distorted "tub-shaped" 8π-electron molecule in which the dihedral angle between adjacent ethylene units is nearly 90°, thereby effectively breaking the conjugated circuit.[61]

Some of the most popular modern methods for assessing aromaticity and anti-aromaticity, both computationally and experimentally speaking, involve the computational prediction or direct measurement of nuclear magnetic resonance spectroscopic shifts. The theory is simple: aromatic molecules possess a delocalized circuit of electrons which induces a diamagnetic shift moving the NMR signals of atoms outside the circuit downfield and atoms inside the circuit upfield; anti-aromatic molecules induce a paramagnetic shift which moves the NMR signals in exactly the opposite directions. The computational simulation of chemical shifts has been able to remove much of the experimental ambiguity from this process by calculating Nucleus-Independent Chemical Shifts; these shifts can be calculated at any point in space relative to the molecule and can therefore be used to map the ring current via its resultant magnetic field. As one would expect for real chemical shifts, a positive (downfield) shift in the ring center or a negative (upfield) shift outside the ring indicates an anti-aromatic compound, while a negative shift in the ring center or a positive shift outside the ring indicates an aromatic compound. The advantage of NICS is that, since the chemical shift is calculated independently of any particular nucleus, the effects of that nucleus do not need to be considered and the chemical shifts can be analyzed "as-is", without need for a reference compound.

COMPUTATIONAL RESULTS

1,2-Dithiins were analyzed by a number of methods (see Chapters 3 and 7) to determine geometric changes and changes of bond strength in the excited state. The results, in terms of planarity, ring flexibility, and bond alternation are seen in Table 4.1. Also included are the ring-substituent bond lengths. While not directly comparable between molecules, the various states should be comparable in an attempt to assess whether the substituent becomes more or less involved in the ring electronics in each state.

Table 4.1a. Calculated Planarity Indicators for 1,2-Dithiins.

Compound (State)	C-S-S-C Dihedral Angle (°)	C=C-C=C Dihedral Angle (°)	C-S-S-C Torsional Vibration (cm^{-1})
1,2-Dithiin			
(S_0)	54.6	28.0	227.3
(S_1)	-0.1	-0.1	22.7 (280.2)[a]
(T_1)	20.7	11.3	155.1
3,6-Dimethyl-1,2-dithiin			
(S_0)	56.6	-28.4	162.9
(S_1)	-11.6	-6.8	27.9 (124.4)[a]
(T_1)[b]	43.6	-	118.8
3,6-Difluoro-1,2-dithiin			
(S_0)	55.0	-29.2	186.3
(S_1)	0.0	0.0	29.4 (169.8)
(T_1)	24.8	14.3	87.3

[a] The value in parentheses is the frequency of the excited state at the ground state geometry.
[b] These triplet values calculated with CIS rather than MP2.

Table 4.1b. Calculated Bond Alternations and Substituent Participation for 1,2-Dithiins.

Compound (State)	C=C Bond Length (Å)	C-C Bond Length (in ring, Å)	3,6-Ring-Substituent Bond Length (Å)
1,2-Dithiin			
(S_0)	1.36	1.45	1.09
(S_1)	1.36	1.42	1.08
(T_1)	1.38	1.42	1.09
3,6-Dimethyl-1,2-dithiin			
(S_0)	1.36	1.45	1.50
(S_1)	1.37	1.42	1.52
3,6-Difluoro-1,2-dithiin			
(S_0)	1.35	1.45	1.36
(S_1)	1.36	1.41	1.33
(T_1)	1.38	1.41	1.37

EXPERIMENTAL RESULTS

Included here are ^{1}H NMR, ^{13}C NMR, and ^{77}Se NMR results obtained by Block and co-workers.[1]

Table 4.2. Ring ^{1}H NMR, ^{13}C NMR, and ^{77}Se NMR[a] Chemical Shifts of 1,2-Dichalcogenins and Related Compounds.

Compound	Hα, Hα' (Cα, Cα')	Hβ, Hβ' (Cβ, Cβ')	Se
1,2-Dithiin	6.07 (119.43)	6.29 (129.74)	
3,6-Dimethyl-1,2-dithiin	(128.47)	6.05 (125.93)	
3,6-Diisopropyl-1,2-dithiin	(142.06)	6.08 (122.78)	
3,6-Di-*tert*-butyl-1,2-dithiin	(146.52)	6.16 (122.02)	
3,6-Bis(trimethylsilyl)-1,2-dithiin	(139.08)	6.43 (135.47)	
1,2-Dithiin-1-oxide	7.18, 7.03-7.08	6.98, 7.03-7.08	
1,2-Dithiin-1,1-dioxide	7.14, 6.83	6.76, 6.94	
Thiophene	7.18 (125.6)	6.99 (127.3)	
2,5-Diisopropylthiophene	(150.22)	6.57 (120.97)	
2,5-Di-*tert*-butylthiophene	(154.21)	6.58 (120.18)	
2,5-Bis(trimethylsilyl)thiophene	(140.3)	6.98 (134.6)	
Thiophene-1,1-dioxide	6.59 (131.1)	6.79 (129.3)	
1,2-Diselenin	6.10 (112.78)	6.27 (132.22)	119
3,6-Dimethyl-1,2-diselenin	(123.71)	6.06 (128.67)	206
1,2-Diselenin-1-oxide	7.24, 6.87	7.11, 6.95	
Selenophene	7.88 (131.0)	7.23 (129.8)	565
2,5-Di-*tert*-butylselenophene	(162.40)	6.75 (122.37)	565
Dimethyl Diselenide			275

DISCUSSION

Computational Analysis of the Excited State

Examination of Table 4.1 reveals that the behavior of 1,2-dithiins is very similar to the aforementioned cases of dibenz[b,f]oxepin and dibenz[b,f]thiepin. The ground states of the various 1,2-dithiins are twisted; this has the effect of reducing overlap between adjacent non-planar portions (each sulfur atom and each ethylenic unit). Additionally, for 1,2-dithiins it has the bonus of allowing significant overlap between the upper lobe of one sulfur 3p orbital and the lower lobe of the adjacent sulfur 3p orbital. This overlap causes the π conjugation to behave like a Möbius strip. In Appendix A, there is an extensive discussion of Möbius conjugation, and a comparison to the more frequently encountered Hückel conjugation. Suffice it here to say that Möbius conjugation stabilizes cyclic arrays of 4n electrons rather than 4n+2 electrons, so this type of overlap would be expected to stabilize 1,2-dithiins.

The singlet excited state of 1,2-dithiins shows the flattening and weakening of the C-S-S-C torsional motion expected for the excited state of an anti-aromatic molecule which was non-planar in the ground state. By comparison of the excited-state C-S-S-C torsional frequencies of the adiabatic and non-adiabatic excited states, one can see that the weaking of the torsion is dependent on achieving the preferred planar geometry. While the triplet excited state also displays some flattening and weakening of the C-S-S-C torsional vibration, it is not nearly as pronounced as for the singlet excited state. It is not known whether this behavior of the triplet excited state is indicative of anything in particular, since the triplet excited states of most anti-aromatic molecules have not been investigated in this fashion. It is known that biphenylene, a stable analogue of cyclobutadiene, undergoes almost identical changes in the T_1 state as in the S_1 state, relative to the S_0 state.[62] As seen in Figure 4.2, avoidance of the cyclobutadiene moiety fixes the single and double bonds in

the S_0 positions. Excitation causes the bond alternation to change such that the cyclobutadiene moiety becomes "active".

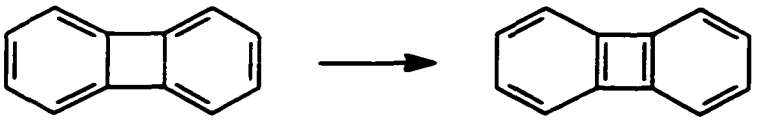

Figure 4.2. Excitation-Induced Changes in the Bond Alternation of Biphenylene.

Insofar as the indication of the previous data is one of anti-aromaticity, the effects of electron donation or withdrawal can be assessed by comparison of the behavior of the substituted 1,2-dithiins to the parent and each other. 3,6-Dimethyl-1,2-dithiin is the electron-donating representative, and it can be seen that the excited state is less planar than either the parent or the difluoro compound. The C-S-S-C torsion is somewhat more difficult to analyze, but it is clear that the torsion in the ground state of the dimethyl compound was found to be the weakest, and therefore it decreased the least; this may or may not be more significant than its final value, which is very similar to that of both of the other 1,2-dithiins. 3,6-Difluoro-1,2-dithiin, on the other hand, was found to be completely planar (the parent was also, within known calculated geometric variance for dihedral angles). This is in agreement with data known for small carbocyclic and heterocyclic anti-aromatic rings, which are stabilized by electron-withdrawing groups such as fluoro and trifluoromethyl. Indeed, there is a small increase in ring-methyl bond length upon singlet excitation, while there is a small decrease in ring-fluorine bond length, which may be a sign of methyl destabilization (and an effort to decrease its effect by lengthening the bond) and fluoro stabilization.

The classical analysis of bond alternation is difficult for heterocycles, since the electronic perturbation and lowered symmetry caused by introduction of heteroatoms

would be expected, in any case, to cause some bond alternation. It is not necessarily expected that the stabilized excited singlet state of anti-aromatic molecules would have less bond alternation. The aforementioned case of biphenylene may behave as it does due to bond fixation in the ground state. 1,2-Dithiin bonds are not similarly fixed (as seen in the contribution of the valence tautomer), and bond alternation might be expected to decrease upon excitation. Benzene symmetrically reduces overlap by increasing C-C bond length in the S_1 state,[63] but desymmetrizes in the T_1 state.[64] At any rate, the C=C bond length in 1,2-dithiins was found to be essentially invariant. However, the C-C (in ring) bond length was found to vary. Two things should be said about the C-C (in ring) bond length. First, the ground-state value is more typical of conjugated C_{sp2}-C_{sp2} bonds (typical value: 1.455 Å[36]) than unconjugated bonds (typical value: 1.478 Å[36]). Secondly, it decreases upon excitation, suggesting an increase in favorable interaction. This interaction may be due to an increase in aromaticity causing an increase in overlap by contracting the bond, or it may be a side effect of planarization of the ring which would also increase overlap. Either indicates increased aromaticity of the 1,2-dithiin ring. The effect is rather small, though it is larger than the known calculated geometric variance for bond lengths. The effect was slightly larger for the difluoro compound than for the parent or dimethyl, but the differences among the three cases are small enough to be uncertain.

Experimental Indications of Aromaticity

There are many data which bear on the aromaticity argument in the NMR chemical shifts of 1,2-dichalcogenins. To begin with, the 1,2-dithiin proton chemical shifts are upfield of those found for analogous thiophenes, while the carbon shifts are essentially identical; this indicates that the additional upfield shift of 1,2-dithiin protons is due to the difference between the thiophene diamagnetic and dithiin paramagnetic ring currents. It is uncertain why the chemical shifts would be more different in the α position than in the β;

such a pattern of variation suggests a difference in disulfide/sulfide chemical shift effects in addition to the difference in ring currents. It could also be another manifestation of diamagnetic versus paramagnetic ring currents; the chemical shift order of the α-protons compared to the β-protons is reversed between 1,2-dithiin and thiophene and could indicate that a similar heteroatomic perturbation on opposite types of ring currents causes opposite distributions of electron density.

Comparing the behavior of the substituted 1,2-dithiins reveals behavior supporting the contention in Chapter 2 that methyl participates in ring electronics more than isopropyl or *tert*-butyl, due to C-H hyperconjugation. As one can see in Table 4.2, the most upfield shift (which should correspond to the most paramagnetic ring current and most destabilizing interaction) is found in the dimethyl compound, while all the dialkyl-substituted compounds, which should be more electron rich than the parent, are found to be more upfield than the parent. The comparison falls down when the bis(trimethylsilyl) compound is considered, since it should be the most electron rich and it is found to have proton chemical shifts downfield of the parent. It should also be noted that for thiophene, alkyl substitution also causes an upfield shift; if one considers the effect to be one of increasing electron density in the delocalized molecular orbital, the ring current should increase with increasing electron donation and the thiophene chemical shifts should move downfield. Also, 2,5-bis(trimethylsilyl)thiophene has about the same chemical shift as thiophene itself, in contradiction to the downfield shift seen for 1,2-dithiins.

In many analyses of aromaticity, it has proved useful to compare the behavior of neutrals and di-ionic species, since the loss or gain of two electrons should reverse the nature of the ring current.[61] To a limited extent, this effect can be seen in the oxidation of a sulfur atom in the dithiin ring. Oxidation to the mono-oxide does put a nearly full unit of formal positive charge on the affected sulfur atom, but does not remove second electron

pair; it is uncertain as to how this electron pair will interact with the rest of the ring, since it should be an sp^3-type lone pair rather than an p-type lone pair as in the parent disulfide. If the lone pair continues to participate, the chemical shifts should move slightly downfield due to the increased positive charge, while if the positive charge participates, the ring current should become diamagnetic and cause a large downfield shift. The effects could be difficult to separate, and could be complicated by the anisotropic shifts sometimes observed for sulfoxides. Oxidation to the dioxide should make the lone pair, whatever its interaction, completely unavailable, thereby constituting a break in the aromatic circuit. The even greater positive charge on the sulfur atom should cause an incrementally greater shift downfield. These effects can be seen in a variety of model sulfur compounds. Dimethyl sulfide has a proton chemical shift of 2.06 ppm, dimethyl sulfoxide 2.52 ppm, and dimethyl sulfone 3.11 ppm.[65] The aromatic protons of phenyl sulfide are found at 7.18 ppm.[65] Phenyl sulfoxide ortho protons are found at 7.59 ppm, while the meta and para protons are at about 7.3 ppm.[65] Phenyl sulfone ortho protons are at 7.99 ppm, while the meta and para protons are at 7.40-7.75 ppm.[65] Perhaps more applicable is data for the disulfide series. Methyl disulfide protons can be found at 2.37 ppm.[66] The protons of the methyl attached to the oxidized sulfur of methyl methanethiosulfinate (MeS(O)SMe) are found at 2.92 ppm, while the other methyl protons are at 2.52 ppm.[66] The protons of the methyl attached to the oxidized sulfur of methyl methanethiosulfonate ($MeS(O_2)SMe$) are found at 3.20 ppm, while the other methyl protons are at 2.60 ppm.[66]

As can be seen from Table 4.2, the protons of the mono-oxide are shifted farther downfield than the protons of the dioxide. The best explanation of this result, according to the analysis in the previous paragraph, is the existence of some diamagnetic ring current in the mono-oxide; without the ring current one would expect the chemical shifts of the mono-oxide to be between the parent and the dioxide. Thiophene, on the other hand, experiences

an upfield shift upon oxidation to the dioxide, demonstrating that the ring current is responsible for a larger downfield shift than is the sulfone moiety.

Once again, 1,2-diselenin can be seen to have proton chemical shifts substantially upfield of selenophene, with the same reversal of α/β chemical shift order. Additionally, for the selenium-bearing compounds ^{77}Se NMR chemical shifts were obtained. Since these atoms would be in the nodal plane of the ring current, it is uncertain how to evaluate the effect of the ring current on them. However, it can be noted that the shift for selenophene (565 ppm) is greater than that for dimethyl diselenide (275 ppm), while that for 1,2-diselenin is less (119 ppm). This may indicate that the atoms experience a slight ring current effect, but the data are far too obscured by other possible effects to be certain.

1,2-Diselenins experience the same upfield change in proton chemical shift upon alkyl substitution as 1,2-dithiins. Selenophenes also display an upfield shift in proton chemical shift, just as do thiophenes. There is a notable difference in that the selenium chemical shift is downfield upon alkyl substitution for 1,2-diselenins, but for selenophenes no shift is observed.

Although the proton chemical shifts of 1,2-diselenin are almost identical to those of 1,2-dithiin, the disparity between those protons on the side of ring nearest the oxidation and those on the far side is substantially greater for 1,2-diselenin-1-oxide than for 1,2-dithiin-1-oxide. Also, the α-proton on the far side of the ring from the oxidation and the β-proton on the near side are shifted farther downfield in the diselenin oxide than in the dithiin oxide, while the other shifts are somewhat more upfield for the diselenin oxide than for the dithiin oxide. This seems to suggest a lessening of the ring current effect for the diselenin case, overlayed with an increase in charge alternation of the positive charge on the oxidized selenium atom. These two effects indicate less of a true cyclic conjugation for the

diselenins, and more of a substituted butadiene behavior. This result was expected from other observations (see Chapter 3).

Finally, preliminary nucleus-independent chemical shift calculations have been made by Dr. Jürgen Fabian (GIAO-SCF/6-31+G*; unpublished results). According to these calculations, the center of the twisted 1,2-diselenin ring was found to have a NICS of -1.1 ppm, while the planar ring was found to have a NICS of 5.2 ppm. As explained in the introduction to this chapter, the data indicate a very weak aromatic ring current at the optimized geometry (probably due to the Möbius overlap), with a much stronger anti-aromatic ring current at the planarized (and therefore purely Hückel) geometry.

CONCLUSIONS

It has been demonstrated via computational simulation and analysis of experimental nuclear magnetic resonance chemical shifts that 1,2-dichalcogenins should be regarded as anti-aromatic, at least to the same extent as oxepins and thiepins. This anti-aromaticity seems to be dependent on the planarity or non-planarity of the dichalcogenin ring, and the anti-aromatic interaction is avoided as much as possible by ring torsion. There are other interesting effects participating in dichalcogenin electronic structure, including Möbius conjugation and electron density alternation effects. Some of these effects remain unidentified or ambiguous, but the overall picture seems clearly in favor of the anti-aromaticity of 1,2-dichalcogenins.

CHAPTER 5

α-DEPROTONATION OF DIALKYL SULFIDES: SYNTHESIS, REACTIONS, STABILITY AND DECOMPOSITION MECHANISM OF α-THIOCARBANIONS

HISTORY AND PROGRESS IN α-THIOCARBANION SYNTHESIS

Both as useful synthetic intermediates[67,68] and as theoretically interesting species,[69] α-metalated sulfides are sought-after chemical entities.

There are quite a few examples of the synthesis of α-metalated sulfides. The inital discovery was made by Corey and Seebach when they found they could α-lithiate thioanisole (phenyl methyl sulfide) with DABCO and n-butyllithium in THF at 0°C (97% yield). Phenyllithium in THF at 25°C was also found to work, though it was slower and slightly less efficient (90% yield).[70] Peterson expanded the synthetic utility of this discovery by α-lithiating dimethyl sulfide with n-butyllithium and TMEDA in hexanes at room temperature; the reaction was essentially quantitative. His attempts to α-lithiate methyl decyl sulfide did not go as well (18% yield with another 38% decomposition product), and methyl 2-methylbutyl sulfide failed completely (42% decomposition product obtained).[71]

It was rapidly determined that phenylthio substituted compounds were much easier to deprotonate, and many discoveries were made in that direction. Shirley and Reeves used n-butyllithium in ether to deprotonate thioanisole (42% yield) and thiophenetole (phenyl ethyl sulfide); the thiophenetole yield was low due to competing ring lithiation and lithium-sulfur exchange.[72] Trost used n-butyllithium in THF at 0°C to α-lithiate cyclopropyl phenyl sulfide (96% yield), but found it necessary to employ *sec*-butyllithium or n-

butyllithium and potassium *tert*-butoxide to α-lithiate vinyl phenyl sulfide. This is the first reported use of Lochmann's/Schlosser's base to deprotonate organic sulfides.[73]

Dolak and Bryson also used stronger bases (*tert*-butyllithium and HMPA), which allowed them to drop the temperature (-78°C) and α-lithiate both methyl and isobutyl phenyl sulfide (quantitative by deuterium oxide quenching). They also α-lithiated 4-methoxy-2-methylbutyl phenyl sulfide quantitatively, and evidence suggested that the methoxy oxygen coordinated the lithium atom. With this effect in mind, Block α-lithiated 2-methylthiotetrahydrofuran and 2-methylthiotetrahydropyran using *tert*-butyllithium in 10:1 THF:HMPA at -90°C. When reacted with TBDMSCl, the yield for the five-membered ring was 44%, while the six-membered ring yielded as much as 87%. As both these rings can be opened to produce the free thiol, these compounds are synthetic equivalents of methanethiol carbanion.[74] McDougal and co-workers also had success with the chelation technique, successfully deprotonating 2R-1-phenylthio-2-methylpropanal 1,2-ethanediol acetal (yield not reported).[75]

To this date, only one method has been found capable of deprotonating alkyl sulfides which do not possess a phenylthio or methylthio group. This method was discovered by Liu and Glass,[76] and its development and scope are the subject of the current study.

It is also possible to generate α-thiocarbanions from various substituted precursors, and to be of more than theoretical interest the method developed here must have advantages over these non-deprotonative methods. The main drawback of non-deprotonating methods is the difficulty of making the necessary precursors. Transmetalation is the most popular of these techniques. (Phenylthio)phenylmethyl bromide was transmetalated with n-butyllithium in THF at -78°C in 75% yield.[67] *p*-Tolylthiomethyl tri-n-butylstannane

underwent lithium-bromine exchange with butyllithium in hexanes at 70°C in approximately 50% yield.[77]

Using chelation assistance, McDougal and co-workers transmetalated 2R-1-phenylthio-1-tri-n-butylstannyl-2-methylpropanal 1,2-ethanediol acetal (yield not reported).[75,78]

Mixed selenothioacetals can be transmetalated to form exclusively the α-thiocarbanions. Reich and Bowe transmetalated cis-3,5-diphenyl-1-phenylthio-1-phenylselenocyclohexane with n-butyllithium in THF at -78°C (yield not reported).[79] 1-Phenylseleno-1-phenylthio-2-methylpropane was transmetalated with butyllithium in THF at -78°C in 96% yield.[67,80]

While most techniques rely on transmetalation, a few rely on cleavage of a leaving group. Kitteringham and Mitchell found that α-silyl sulfides could be treated with tetra-n-butylammonium fluoride to cleave the silyl group and form the α-thiocarbanion. Using this method they formed phenylthiomethyl anion, and were able to do so in the presence of even highly enolizable ketones. The anion was trapped in yields up to 96%.[81] This method was also used by McDougal and co-workers to form the α-thiocarbanion of 2R-2-methyl-3,3-bis(phenylthio)propanal 1,2-ethanediol acetal from the α-silyl precursor. They also formed the α-lithio species from 2R-2-methyl-3,3-bis(phenylthio)propanal 1,2-ethanediol acetal using reductive cleavage of the dithioacetal with lithium naphthalide at -78°C in THF (62% yield).[75,78]

There is also an example of butyllithium being added across the double bond of phenyl vinyl sulfide to form the α-thiocarbanion (in diethyl ether at 20°C, 51% yield).[82,83]

The root of these techniques, in terms of the pathways necessary to form the precursors, is α-halogenation of sulfides. This reaction can be difficult, especially in the sense of regiocontrol, and in many cases may not prove to be advantageous compared to

direct deprotonation, particularly since at least two steps are added to the reaction sequence. The two exceptions are the reductive cleavage of a dithioacetal and the addition of butyllithium across a double bond. The former would stem from the corresponding aldehyde; that synthetic technology is well developed, but still adds steps and may not be the best route in compounds with other reductive functionalities or where it would be necessary to distinguish among multiple carbonyls for derivatization. The latter is a very harsh technique and does not provide a good yield.

THEORIES OF α-THIOCARBANION STABILIZATION

There are many proposed mechanisms by which α-thiocarbanions are stabilized by sulfur. In considering the merits of various theories, the first question is the configuration of the carbanion. It is generally accepted,[68,84] and is supported by studies of various types, that the α-thiocarbanion is tetrahedral, though some studies do indicate some flattening.[84]

Of much greater controversy is the mechanism by which α-thiocarbanions are stabilized. There are three major contributions considered by most studies (Figure 5.1): d-orbital interaction, sulfur atom polarization, and negative hyperconjugation. Presumably effects such as induction are also active, but must play a fairly small role since sulfur compounds are so much more acidic than compounds with much more electronegative atoms.

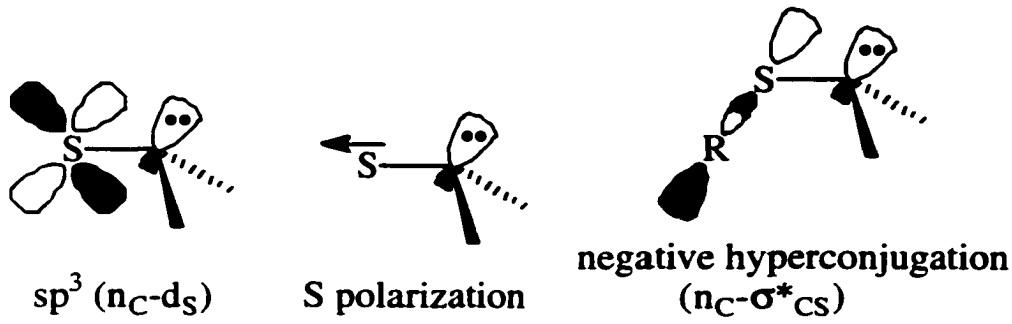

Figure 5.1. Mechanisms of α-Thiocarbanion Stabilization.

d-Orbital involvement has been perhaps the most argued mechanism, both for and against. Some of the major computational studies even argue against their previous findings.[85,86] It is for this reason that, of the many computational studies, only the two most recent, advanced, and hopefully therefore most reliable studies will be considered.[84,87] For dimethyl sulfide Wiberg and Castejon's MP2 study found a flattened but pyramidal α-thiocarbanion which slightly prefers to be anti to the methyl group. They also found a large barrier to rotation of the anionic center. These facts point to negative hyperconjugation as the major stabilizing factor; charge density plot analysis indicated that d-orbitals play a very small role in stabilizing the anion, and serve mostly to transfer charge from lone pairs to bonding regions. Interestingly, the barrier to inversion of the anionic center is neglible, indicating that inversion is the path by which chiral α-thiocarbanions racemize. It was also found to be critical that for good stabilization, the charge must be centered on the carbon. These conclusions were supported by Cuevas and Juaristi's DFT study of 2-lithio-1,3-dithiane, which they found to be quite ionic.

Very few experimental studies are suitable for the analysis of contributions to α-thiocarbanion stability. Recently, however, Bernasconi and Kittredge studied the intrinsic rates of deprotonation and the acidities of several sulfur-bearing compounds and their non-sulfurated analogues.[88] They point out that their study, while examining the same

mechanisms as other studies in the field, actually weighs the importance of the various mechanisms in stabilizing the deprotonation transition state. They find that it is the polarizability of the sulfur atom that is primarily responsible for stabilizing the transition state.

There is a wealth of other experimental evidence, but it must be analyzed carefully, and unlike Bernasconi's study the data are not conclusive. One must distinguish between studies which investigate kinetic acidities (measured by deuterium exchange rates) and thermodynamic acidities (measured by pK_a). In the following discussion, differences in kinetic acidities will be referred to as "faster" or "slower" deprotonation, and should relate to Bernasconi's study, while differences in thermodynamic acidities will be referred to as being "more" or "less acidic", and should relate to the studies of Wiberg and Juaristi.

It is known that sulfur stabilizes adjacent carbanions better than selenium.[67-69] At first this would seem to favor the d-orbital theory, since the size and energy of sulfur d-orbitals is a better match for a carbon sp^3 lone pair orbital than the size and energy of selenium d-orbitals, thereby increasing the interaction with them. Selenium is more polarizable, yet less stabilizing. However, polarization stabilization falls off very quickly with distance, and the selenium-carbon bond is longer than the sulfur-carbon bond. Also, the issue may not be the energy match between the carbanion orbital and sulfur or selenium d-orbitals, but rather between the carbanion orbital and sulfur-carbon or selenium-carbon σ^* orbitals. It is also known that methyl phenyl sulfide deprotonates 10 times faster than methyl phenyl selenide.[89] Deprotonation rates should be governed by polarization effects, and selenium is the more polarizable atom, all of which lends credence to the bond-length argument made previously.

The difference in rate of deuterium exchange for the two trithioorthoformates in Figure 5.2[90] argues for either negative hyperconjugation or for d-orbital participation, but

does not distinguish between the two. Additionally, since it is a difference in deprotonation rate, Bernasconi predicts that it should be affected by transition-state effects; that is, it should be governed by polarization of the sulfur atom and therefore not show a geometric effect. It is possible that the bicyclic constraints shorten the carbon-sulfur bonds thereby enhancing the kinetic acidity, but this has not been demonstrated.

relative rate of deuterium exchange 1:1200

Figure 5.2. Acyclic vs. Bicyclic Trithioorthoformates.

On the other hand, the pK_a of tri(propylthio)methane was found to be 31.3, while the bicyclic compound with a methyl group at the β bridgehead has a pK_a of 30.5.[91] The difference in acidities is much smaller than the difference in rates, though the alignment of the C-S bonds seems perfect for negative hyperconjugation.

Many studies have been conducted with cis-4,6-dimethyl-1,3-dithianes. When trans-2-methyl-cis-4,6-dimethyl-1,3-dithiane (equatorial 2-hydrogen) was deprotonated at -25°C and quenched with DCl, the configuration at the 2 position was not altered, but 80% of the compound was deuterated in 2.5 hours. The all-cis compound (axial 2-hydrogen) was deprotonated at -20°C and quenched with DCl. After 4 hours, 31% of the compound reacted and had been converted to the trans,cis-compound and deuterated; after 24 hours the fraction was increased to 75%.[92,93] These studies indicate that the equatorial hydrogen is kinetically more acidic than the axial hydrogen, the equatorial carbanion is more stable, and the carbanion configuration is not stable, but rather converts rapidly to the lowest-energy form. By NMR spectroscopic studies, Seebach and co-workers determined

that the equatorial hydrogen in the 2 position of cis-4,6-dimethyl-1,3-dithiane is abstracted 10 times faster than the axial hydrogen and that the resulting lithiated species is at least 6 kcal/mole more stable.[94] These compounds have, in addition to the aforementioned mechanisms of stabilization, the additional complication of destabilizing n_C-n_S interactions for the axial carbanion.[87,94] These data are particularly confusing in the light of the hydrogen preference; the preferred (equatorial) hydrogen is perfectly aligned for negative hyperconjugation, but the crystal structure of the anion obtained by Seebach showed essentially no lengthening of the C-S bonds that would be involved in negative hyperconjugation; instead it shows a decrease in the C-S bond to the anionic center, suggesting d-orbital participation or possibly polarization effects.

Methyl *tert*-butyl sulfide deprotonates more than 13 times faster than dimethyl sulfide, while cyclohexyl methyl sulfide deprotonates 200 times faster than dimethyl sulfide.[89] This is not explained at all by polarization effects, and seems to indicate some rate-enhancing effect of β C-C bonds with certain geometric orientations. No interpretation has been made of these data.

α-Thiocarbanions also seem to be very sensitive to substitution at the carbanionic center. Methyl phenyl sulfide deprotonates 100 times faster than ethyl phenyl sulfide; ethyl phenyl sulfide in turn deprotonates 100 times faster than isopropyl phenyl sulfide (10,000:100:1 over the three compounds). The corresponding ratios for methyl-, ethyl-, and isopropylbenzene are 35:5:1, respectively.[89]

Finally, it must be mentioned that phenylthio groups seem to be much more stabilizing than alkylthio groups. While this is not suprising, it is unclear as to the origin of this enhancement. Wiberg noted that d-orbitals seemed to be mainly transferring charge, and in phenylthio groups they could be transferring charge to the benzene ring where it is delocalized. However, charge delocalization in methylthiomethyl anion accompanied

destabilization of the system. The phenyl-sulfur bond may be better for negative hyperconjugation. The phenyl group might also enhance the polarizability of the sulfur atom. Other possible acidifying effects of the phenyl group include electron withdrawal by induction and the possibility of lithium cation solvation by the π cloud. In any case, there is no guarantee that the mechanism(s) of greatest importance for the stabilization of dimethyl sulfide α-thiocarbanion are the same as those for phenyl methyl sulfide α-thiocarbanion.

CONFIGURATION OF α-THIOCARBANIONS

While there have been a great number of studies on the configurational stability and preference of various α-thiocarbanions,[87,94-98] this discussion will be limited to those of greatest applicability to the current study, where the sulfur is in a six-membered ring and therefore the C-S-C-H/C-S-C-: dihedral angle is constrained.

As was discussed in the preceding section, there is a strong preference for abstraction of the equatorial hydrogen in 1,3-dithianes, and a strong preference for the equatorial configuration of the anionic center. The strength of this preference is fairly large. All-cis 2-*tert*-butyl-cis-4,6-dimethyl-1,3-dithiane is converted with butyllithium and TMEDA, followed by quenching with water, to the isomer with an axial *tert*-butyl group.[92,99] Even in 2-phenyl-1,3-dithiane, the anionic lone pair/C-Li bond is equatorial, forcing the phenyl group to be axial.[94] The equilibration of the anion configurations in the conformationally-locked cis-4,6-dimethyl-1,3-dithianes must proceed via inversion, which is in agreement with the calculated large rotational barrier and small inversion barrier.

RESULTS

The results of the deprotonation surveys are presented in Table 5.1. Except for 2-trimethylstannyl-4-*tert*-butylthiane, the products were not further isolated from the crude product mixture. In the examples from previous work (see Table 5.1, Footnote D), R_4 is cyclohexyl. In the synthesis of 2-trimethylstannyl-4-*tert*-butylthiane, R_4 is methyl. In all other cases, R_4 is n-butyl.

Table 5.1. Deprotonation of Thioethers.

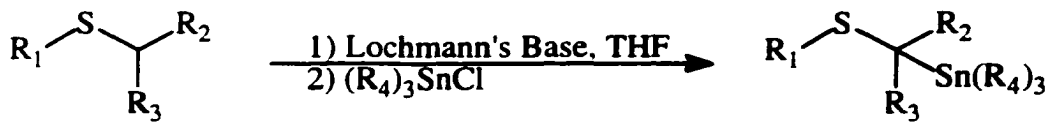

Compound			Deprotonation Time (h)	Deprotonation Temperature (°C)	Deprotonation Yield[b]	Decomposition Yield[c]
R_1	R_2	R_3				
Me	H	H	1-2	-40	97[d]	not determined
Et	H	H	0.33	-78	23[d]	not determined
iBu	H	H	1-2	-40	58[d]	not determined
Dc[a]	H	H	1-2	-40	86[d]	not determined
$-(CH_2)_3-$		H	1-2	-40	70[d]	not determined
$-(CH_2)_3-$		H	1-2	-30	62[d]	21
$-(CH_2)_3-$		H	1-2	5	not determined[d]	100
$-(CH_2)_4-$		H	1-2	-40	55[d]	not determined
iBu	H	H	0.1	-40	100	0
iBu	H	H	2	-40	100	15
iBu	H	H	2	-78	100	3
iPr	H	H	0.1	-40	100	0
iPr	H	H	2	-40	100	4
iPr	H	H	2	-78	100	0
tBu	H	H	0.1	-40	100	0
tBu	H	H	2	-40	100	0
tBu	H	H	2	-78	100	0

[a] Dc = Decyl.
[b] Percent relative to starting sulfide, determined by GC/MS.
[c] Percent of all products resulting from deprotonation, determined by GC/MS.
[d] Isolated yield from previously published work[76]; tricyclohexylstannyl examples selected for consistency.

Table 5.1. Cont. Deprotonation of Thioethers.

Compound			Deprotonation Time (h)	Deprotonation Temperature (°C)	Deprotonation Yield[a]	Decomposition Yield[b]
R_1	R_2	R_3				
Et	Me	H	0.1	-40	97	87
Et	Me	H	1	-40	100	100
Et	Me	H	0.1	-78	80	0
Et	Me	H	2.5	-78	100	12
nPr	Et	H	0.1	-40	6	100
nPr	Et	H	1	-40	39	100
nPr	Et	H	0.1	-78	24	0
nPr	Et	H	2.5	-78	63	0
iBu	iPr	H	2.5	-78	47	0
iBu	iPr	H	4	-78	77	0
iBu	iPr	H	12	-78	not determined	≤16.5 mol%
iPr	Me	Me	0.1	-40	0	-
iPr	Me	Me	1	-40	27	100
iPr	Me	Me	0.1	-78	0	-
iPr	Me	Me	2.5	-78	0	-
$-(CH_2)-$		H	0.1	-40	35	100
$-(CH_2)-$		H	1	-40	42	100
$-(CH_2)-$		H	0.1	-78	58	100
$-(CH_2)-$		H	1	-78	34	100
$-(CH_2)_2-$		H	0.1	-78	16	100
$-(CH_2)_2-$		H	1	-78	5	100
$-(CH_2)_3-$		H	2	-40	100	0
$-(CH_2)_4-$		H	0.1	-40	91	0
$-(CH_2)_4-$		H	1	-40	100	0
$-(CH_2)_4-$		H	1	-78	0	-
$-(CH_2)_2$ CH(tBu) CH_2-		H	1	-40	74	0

[a] Percent relative to starting sulfide, determined by GC/MS.
[b] Percent of all products resulting from deprotonation, determined by GC/MS.

At some temperatures the α-thiocarbanions decompose to varying extents. This decomposition product is $R_1SSn(nBu)_3$ for all acyclic sulfides. For thiolane the decomposition product is $H_2C{=}CHSSn(nBu)_3$. $H_2C{=}CHCH_2SSn(nBu)_3$ is a major decomposition product of thietane. It appears that thiirane mainly decomposes into oligomers or polymers of the formula $nBu[(CH_2)_2S]_nH$ or $H_2C{=}CHS[(CH_2)_2S]_nH$.

A few trials were conducted that do not appear in Table 5.1 due to difficulty in analysis of the product mixture. Trials of various deprotonation times at -40°C were conducted with diisobutyl sulfide; none of the desired product was formed, which was not surprising, but the products that were obtained could not be satisfactorily identified and may have stemmed from reactivity of stannylated primary decomposition products with the unstannylated products. It is also possible that anionic 1,2-rearrangements of the Wittig type, which are known for some higher phenyl alkyl sulfides,[100] may have occurred. It is uncertain why the 12-hour trial at -78°C gave such poor results. It is possible that over long enough time, very slow unknown decomposition paths may prevail. It is also possible that over the 24 hours of the run (12 for deprotonation, 12 for reaction with the electrophile) the temperature control was not good.

Similarly, trials were made with *tert*-butyl cyclohexyl sulfide at both -40 and -78 °C. Visual evidence of the reaction seemed to indicate fairly rapid deprotonation, but other than *tert*-butyl stannyl sulfide no products could be reliably identified. Conspicuously absent from the product mixture was any desired product or cyclohexyl stannyl sulfide.

Evidence in some of the diethyl sulfide trials seemed to indicate that the decomposition product ethyl stannyl sulfide was acting as a stannyl transfer agent. To test this supposition, ethyl stannyl sulfide (formed pure in one of the previous trials) was deprotonated at -40°C. Since it is very difficult to add the Lochmann's/Schlosser's base because it is an inhomogenous mixture, it is prepared in the presence of the sulfide.

Generally potassium *tert*-butoxide is added first (being the weaker base and a solid), followed by the solution of n-butyllithium in hexanes. In a very few cases the yellow color, which was generally taken to indicate deprotonation, appeared upon addition of the butoxide, while in most cases this color did not appear until the addition of the butyllithium. It has been previously demonstrated that n-butyllithium alone is insufficient to deprotonate thiolane,[76] so species which reacted with butoxide were assumed to be unstable to base. Thiirane was one of these species. The other was ethyl stannyl sulfide, though its behaviour was even stranger. The yellow color which developed upon addition of butoxide disappeared upon addition of butyllithium. In addition, not all the ethyl stannyl sulfide was recovered; this fact has several interesting implications.

It is known that benzyl trialkylsilyl and trialkylgermyl sulfides undergo a rearrangement similar to the anionic 1,2-Wittig rearrangement; this rearrangement is known as the Wright-West rearrangement.[101] It was expected that if the ethyl stannyl sulfide was α-deprotonated, it would rearrange to the 1-tri-n-butylstannylethyl thiolate, which would then react with tri-n-butylstannyl chloride just as ethyl thiolate did to form 1-tri-n-butylstannylethyl tri-n-butylstannyl sulfide. This product was not detected. If, on the other hand, the stannyl group was transmetalated (or the stannyl group nucleophilically displaced by butylide) the eventual product should be the same as the starting material. Since less ethyl stannyl sulfide was recovered than was initially present, something happened for which these processes could not account. Unfortunately, it was impossible to determine what that might be.

It is worth a few words to explain how the relative configuration of the major isomer of 2-trimethylstannyl-4-*tert*-butylthiane was determined. It has long been known that the vicinal ^{119}Sn-^{13}C coupling is both larger than the geminal, and shows a good Karplus-Barfield relationship.[102] Kuivila and co-workers determined the governing

equation to be $^3J_{Sn-C} = 30.4 - 7.6 \cos \theta + 25.2 \cos 2\theta$. By computing the axial and equatorial geometries (trans and cis isomers, respectively) using B3PW91/LANL2DZ,[103] the Sn-C-C-C dihedral angles were found to be 68.7° and 176.0°, respectively. The computed dihedral angles correspond to a ^3J = 9.1 Hz for the axial isomer and ^3J = 62.9 Hz for the equatorial isomer. The observed ^3J was 47.1 Hz. According to Kuivila's equation, that ^3J value corresponds to either 7.8 or 147.1°. This seems to demonstrate some ring distortion or perhaps a coupling-reducing effect of the sulfur is in operation.

If the former, it cannot be assured that this is the proper geometric assignment, since there are a large number of possible twist conformers. However, they are all of much higher energy than the chair conformers (according to SYBYL molecular mechanics[104]). It seems more likely that the reduction in the coupling constant is an effect of the sulfur. It is known that sulfur significantly alters the s character of other orbitals on the carbon to which it is bound,[105] and it is also known that vicinal coupling constants are sensitive to changes in s character.[106] 2-Trimethylstannylthiane, which can be presumed to exist with equatorial tin in a chair conformation, has vicinal couplings to the carbon at the 4 position of 50.8 and 48.1 Hz (the ^{119}Sn and ^{117}Sn couplings are resolved). These are almost identical to the vicinal coupling constants in 2-trimethylstannyl-4-*tert*-butylthiane, and indicate that whatever the dihedral angle is in the latter compound, it is only slightly nearer to 90° than in the former. The coupling constant across the sulfur (to the carbon at the 6 position) could be expected to be even less reliable due to the drastically different s character and bond lengths of the C-S bonds. In 2-trimethylstannyl-4-*tert*-butylthiane it is 43.0 Hz, while the value for 2-trimethylstannylthiane is only 37.2 Hz. While the differences in the two compounds could be due to changes in s character, this seems unlikely considering the difference between the compounds is the minor change from a C-H bond to a C-C bond at the distant 4 position. The differences are consistent with a shift

of the stannyl group induced by steric effects of the *tert*-butyl group. A crude analysis with SYBYL[104] demonstrates that from 2-trimethylstannylthiane, the addition of a 4-*tert*-butyl group increases the dihedral angle through sulfur and decreases the dihedral angle through carbon, which is exactly what is observed. Furthermore, comparison of the stannylated and non-stannylated 4-*tert*-butylthianes with SYBYL indicates that the change is entirely due to the *tert*-butyl group (that is, that the same dihedral angle differences are observed for the equatorial hydrogen in the non-stannylated compounds). It can therefore be concluded with few reservations that the major isomer is equatorial-equatorial chair; that is, cis-2-trimethylstannyl-4-*tert*-butylthiane.

DISCUSSION

The first notable difference between the sample of previous results, found at the head of Table 5.1, and the current results is a non-uniform increase in yield. This is due to an early discovery that the efficiency of the reaction is very sensitive to concentration. While the previous work paid close attention to the number of equivalents present, it did not maintain a consistent concentration. The current work uses concentrations of approximately 0.67 M sulfide and 0.83 M base. Of course, Lochmann's/Schlosser's base is not soluble in tetrahydrofuran; 0.83 M is what the concentration would be if it were completely dissolved. In many cases, this increase in concentration alone vastly improved the yield.

Also obvious from a cursory examination of Table 5.1 is the importance of limiting decomposition. The mechanism of this decomposition was not immediately apparent, but there have been some gas phase studies on thioether deprotonation that shed some light.[107] The case of gas phase deprotonation of thioethers with NH_2^- has several features in common with the low temperature solution deprotonation of thioethers with a strong

heterogenous base. Among these are the irreversibility of deprotonation and kinetic control of the reaction. The main differences are the greatly increased chances of intermolecular interactions between protonated and deprotonated thioethers in the case of solution reactions and the higher energy of the gas phase collisions versus low-temperature solution collisions.

The possible mechanisms to be considered are demonstrated in Figures 5.3 through 5.5 with diethyl sulfide.

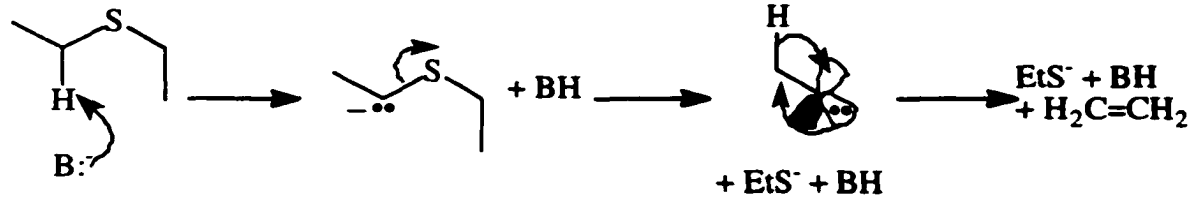

Figure 5.3a. α-Elimination of Diethyl Sulfide, Free Carbene Mechanism.

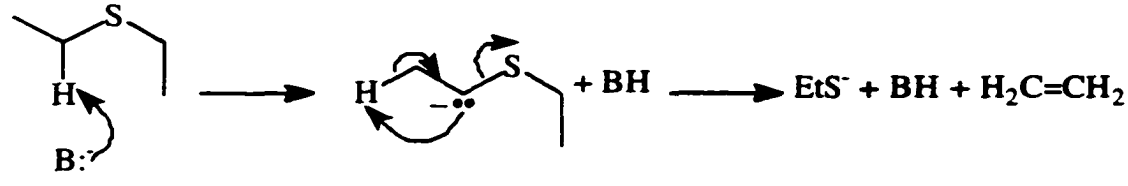

Figure 5.3b. α-Elimination of Diethyl Sulfide, Concerted Mechanism.

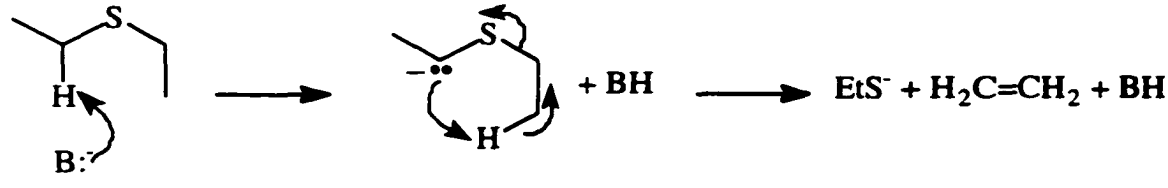

Figure 5.4. α',β-Elimination of Diethyl Sulfide.

Figure 5.5. β-Elimination of Diethyl Sulfide.

The study measured the product ratios of different reactions between NH_2^- anion and various deuterated diethyl sulfides. The product-ratio-determining step for both α-elimination and α',β-elimination is α-deprotonation, and therefore the two mechanisms should show the same isotope effect. Since β-elimination in sulfides was shown in the study to be concerted, its ratio-determining step will be the E2 removal of a β-hydrogen. It would not be expected to exhibit the same isotope effect.

There is no isotope effect observed for α',β-elimination in the case of $CD_3CH_2SCH_2CH_3$ since all the α-hydrogens are protons. Forty-eight percent of the product was observed to be CH_3CHDS^- + HB + $C_2H_2D_2$ and must arise from α',β-elimination with α-deprotonation of the undeuterated chain. Presumably, another 48% of the product should be from α',β-elimination with α-deprotonation of the deuterated chain. Fifty percent of the mixture is this product ($CD_3CH_2S^-$ + HB + C_2H_4); the extra 2% probably arises from β-elimination of the undeuterated chain. This is in accord with the observed 2% which must come from β-elimination of the deuterated chain ($CH_3CH_2S^-$ + DB + $C_2H_2D_2$). A greater portion of the product was expected from β-deprotonation than β-dedeuteration. This suggests that β-elimination shows little or no isotope effect. While this is not in accord with the literature,[108] it compares well to other examples within the gas phase study, and may be an effect of the method. For example, nearly equal product ratios are observed for the reaction of $CD_3CD_2SCH_2CH_3$; 3% β-dedeuteration and 4% β-deprotonation. These cases cannot be distinguished from α-elimination, but since no α-

elimination was detected in the former case, it is reasonable to assume no α-elimination occurs in the latter.

The rest of the $CD_3CD_2SCH_2CH_3$ product mixture is clearly from α',β-elimination: 28% CD_3CHDS^- + DB + C_2H_4 and 65% CH_3CHDS^- + HB + C_2D_4. This allows us to observe the gas-phase isotope effect for α-deprotonation, which is 2.3:1. While this also seems a bit low, both this value and the β value could be due to an excessively high impact energy; it is known in collisional mass spectrometry that isotope effects can become more muted as the collision energy rises.[109]

It is also known that at significantly high energies, processes which require the least energy are not necessarily the fastest, especially if the low-energy processes require the breaking or forming of several bonds while the higher energy processes require fewer such transformations.[109] This would seem to be a reasonable explanation for the large differences in behaviour observed between the gas phase and low-temperature solution studies of thiolane. As mentioned in the Results, thiolane is observed to decompose to vinyl stannyl sulfide. This presumably occurs by a mechanism known for the basic decomposition of tetrahydrofuran (Figure 5.6).[110]

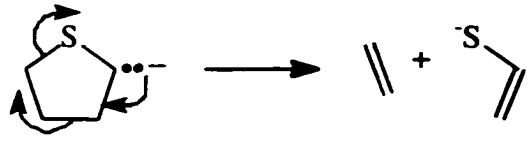

Figure 5.6. Electrocyclic Decomposition of Thiolane α-Thiocarbanion.

This reaction is not observed in the gas phase study of thiolane,[111] where it was found that 54% of the product mixture was the β-elimination product (completely unobserved in solution) and the other 46% was the α-thiocarbanion. 12% of these α-thiocarbanions decomposed via α',β-elimination while the other 88% were reactive towards starting

thiolane (via β-elimination). In light of the aforementioned known effects of collisional energy, this does not seem too peculiar. It does throw some doubt on the validity of applying the results of the gas phase study to the low-temperature solution results, though the gas phase studies, other than in the matter of the isotope effect, agree with what solution studies have been done, especially in the *syn* nature of the elimination.[107,108,111]

If one assumes that such application is sufficiently valid it can be answered why the anions of cyclic thioethers are so much more stable than the seemingly analogous acyclic compounds. While the acyclic compounds have freedom to obtain the optimal transition state geometry for α',β-elimination, cyclic compounds are more restrained. Thiolane can achieve an envelope conformation through which the anion may undergo α',β-elimination (Figure 5.7); the absence of this product in the solution study suggests that the necessary conformer and/or the best transition state are fairly high in energy relative to an acceptable conformer for the electrocyclic decomposition.

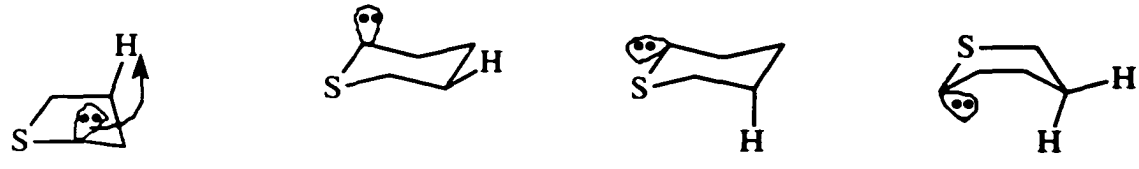

Figure 5.7. Conformers for α',β-Elimination in Thiolane and Thiane α-Thiocarbanions.

It has been predicted computationally, observed for 1,3-dithiane carbanions, and observed in the current study (*vide infra*) that the carbanionic lone pair in six-membered-ring α-thiocarbanions is equatorially disposed, even at fair steric conformational cost. This has not been demonstrated for five-membered rings, and so we must give credence to the proposed thiolane transition conformer. Since it has been demonstrated for six-membered

rings, the axial-lone-pair chair conformer shown above for thiane is very unlikely, and the geometry is poor even so. The geometry is equally poor for the more likely equatorial-lone-pair chair conformer. The geometry of the boat conformer is better, but the conformer itself is even less likely. It would seem, therefore, that the stability of cyclic thioether α-thiocarbanions is due to their inability to efficiently undergo α',β-elimination. This also explains both the instability of the anion and the observed product in thietane deprotonation. It is uncertain whether thiirane undergoes electrocyclic ring opening, α',β-elimination, or direct nucleophilic displacement of the sulfur, but it is certainly sensitive to the latter as evidenced by the polymerization observed in its treatment with Lochmann's/Schlosser's base.

Understanding of the mechanism involved also allows one to draw certain conclusions about the effect of more remote substituents on α-thiocarbanion stability. It is obvious that the methyl sulfide α-thiocarbanions are much more stable than the ethyl sulfide α-thiocarbanions. This should not be due to either compound type's propensity for α',β-elimination, since they should be very similar in this respect. One can only conclude that the methyl α-thiocarbanions are inherently more stable (more thermodynamically acidic).

Those differences do not explain the difference in decomposition rates for the methyl alkyl sulfide α-thiocarbanions, since the rate-limiting step for the decomposition of the anion (if there is any) would be the E2 β-elimination, which should increase in rate-per-hydrogen from isopropyl to isobutyl to *tert*-butyl, but instead shows no decomposition for the *tert*-butyl. This may stem from the same underlying cause as the increase in kinetic acidity of methyl *tert*-butyl sulfide as compared to dimethyl sulfide.

Among the primary sulfides we can see the effects of β-groups on acidity and stability. Going from diethyl sulfide (no β-groups) to di-n-propyl sulfide (1 β-methyl) causes a drastic drop in deprotonation rate. Diisobutyl sulfide (2 β-methyls) is even slower (though not by as much). It would appear that the decomposition rate also rises a bit going

from ethyl to n-propyl, though the ethyl is so close to complete decomposition that this should not be overinterpreted.

The acidity of secondary sulfides is very low; diisopropyl sulfide did not deprotonate at all at -78°C, and only deprotonated very slowly at -40°C. Its decomposition was also very rapid, though it is impossible to say whether it is more or less rapid than the primary cases.

Finally, the deprotonation of 4-*tert*-butylthiane proved that the equatorial anion is more stable for the case of one stabilizing sulfur (as was already known for two sulfurs). It cannot be determined from this experiment whether the equatorial or axial hydrogen is more acidic as conversion to a more stable anion would be expected to be very rapid.

CONCLUSIONS

The low-temperature deprotonation of dialkyl sulfides with a mixture of n-butyllithium and potassium *tert*-butoxide in THF is a versatile method capable of deprotonating methyl and primary sulfides in good yield with minimal decomposition. Unfortunately, while secondary sulfides could be deprotonated, they proved too unstable for synthetic use. Cyclic primary sulfides showed much greater stability than similar acyclic compounds. This is probably a result of there being no good geometry by which the cyclic compounds can undergo the preferred α',β-elimination. Thiolane was observed to undergo the electrocyclic decomposition observed for tetrahydrofuran. The method was employed to form the α-thiocarbanion of 4-*tert*-butylthiane, and the anion was found to produce the equatorial isomer when reacted with trimethylstannyl chloride.

Certain improvements were made to the synthesis of simple dialkyl sulfides, and dineopentyl sulfide was synthesized, though the yield was too poor for full characterization.

CHAPTER 6

α-STANNYL DIALKYL SULFIDES: COMPUTATIONAL ANALYSIS AND CORRELATION WITH ELECTROCHEMICAL OXIDATION POTENTIALS

NEIGHBORING-GROUP EFFECTS

It has long been known that various functional groups exert an non-bonding electronic influence on the tendency for nearby centers to undergo reactions.[112-136] Perhaps one of the more well known effects is the β-silicon effect on carbocation stability; it is known that a vicinal silyl group greatly increases the stability of a carbocation. It is probably this effect that led Yoshida and co-workers to try stabilizing an ether cation radical with an α-silyl group.[130] They found computationally that the stabilization is geometry-dependent, as it is for the case of the carbocation β-silicon effect. The stabilization of the carbocation is greatest when the β-C-Si bond is coplanar with the adjacent empty carbon p-orbital; in the case of α-silyl ethers the stabilization is similarly greatest when the α-C-Si bond is coplanar with the adjacent half-filled oxygen 2p lone pair orbital. The stabilization of the α-silyl ethers was found to be about 0.3 eV, about a third of the stabilization found for β-silylcarbocations. The lesser stabilization was attributed to the C-Si bond hyperconjugation being less effective at lowering the overall energy when it interacted with a half-filled orbital, as in a cation radical, as opposed to a completely empty orbital, as in a carbocation. The lowering of the oxidation and ionization potentials was attributed more to destabilization of the neutral species HOMO than stabilization of the cation radical. The neutral species HOMO is most destabilized when the α-C-Si bond is coplanar with the adjacent oxygen 2p lone pair orbital, so the effects would work in tandem. As it happens, this explanation is flawed in part, and in another part while true for oxygen-silicon interactions, it is not true in general (see Results).

The question then arises, if silicon affects adjacent lone pair orbitals, can other Group 14 elements do the same? Since silicon, by all evidence, is acting by hyperconjugative electron donation, presumably any Group 14 element would be able to likewise participate; the efficiency of the participation would depend on the energy matching of the α-C-M bond (where M is the Group 14 element) and the adjacent oxygen lone pair. Table 6.1 lists the ionization potentials of various oxygen and sulfur lone pairs, along with the ionization potentials of C-M bonds for various Group 14 elements. Oxidation potentials, which can sometimes be interpreted as adiabatic ionization potentials, are included where known.

Table 6.1. Basic Oxidation Potentials and Orbital Ionization Potentials.

Compound	Oxidation Potential (V)	Ionization Potential (eV)
Dimethyl ether	-	10.04[a]
Dimethyl sulfide	1.66[b]	8.72[a]
Neopentane	-	
Tetramethylsilane		10.57[a]
Tetraethylsilane	2.56[c]	9.78[c]
Tetraethylgermane	2.24[c]	9.41[c]
Tetraethylstannane	1.76[c]	8.93[c]
Tetraethylplumbane	1.26[c]	8.13[c]

[a] Taken from [137].

[b] Potential obtained via pulse radiolysis, versus SHE, taken from [129].

[c] Versus SCE, taken from [134].

It would appear that the best match for oxygen, and therefore the most efficient interaction, would be silicon, and this has been argued by Yoshida. A less efficient interaction with an even lower-energy bonding orbital can yield lower overall ionization potentials, as can be seen in Table 6.2.

Table 6.2. Oxidation Potentials of Derivatized Ethers.[a]

Compound	$E_{1/2}$ (V vs. Ag/AgCl)
Methyl trimethylsilylmethyl ether	1.85
Menthyl trimethylsilylmethyl ether	1.83
Menthyl trimethylgermylmethyl ether	1.67[b]
Methyl trimethylstannylmethyl ether	1.14
Menthyl trimethylstannylmethyl ether	1.09
Methyl bis(trimethylsilyl)methyl ether	1.54
Methyl (trimethylsilyl)trimethylgermylmethyl ether	1.31[b]
Methyl (trimethylsilyl)trimethylstannylmethyl ether	1.00

[a] Unless otherwise noted, values taken from [132].

[b] Taken from [131].

The oxidation potential drops from the silyl-substituted ethers to the germyl-substituted ethers, and yet further to the stannyl-substituted ethers. Additionally, it was computed that in the mixed silicon-tin case, the preferred conformation of the cation radical (by 0.1-0.2 eV) was that where the oxygen 2p lone pair is parallel to the C-Sn bond, not the C-Si bond, suggesting that the tin substituent is providing significantly more stabilization than the silicon.[135]

It might seem that it would be more appropriate to consider the oxidations and ionizations as chalcogen-stabilized carbon-metal (carbon-metalloid, etc.) ionizations. Both computation (see below) and experiment[134] indicate that despite the apparently easier ionization of the carbon-metal bond, the spin is localized on the chalcogen. Even in the most delocalized cases, the spin is still mainly chalcogen-centered. It is correct to consider the ionization a chalcogen lone pair ionization affected by an adjacent carbon-metal bond.

Table 6.3. Oxidation Potentials and Ionization Potentials of 6-Substituted-1-Azadecalins and Substituent A Values.[a]

Substituent	Oxidation Potential (V vs. NHE)	Ionization Potential (eV)	A value of Substituent (kcal/mole)
H	1.18	8.3	-
Me_3Si	0.61	7.3, 7.5	10-11
Me_3Ge	0.45	7.4	8.8
Me_3Sn	0.39	7.5	4

[a] Taken from [138].

A similar trend can be observed in the oxidation potentials of 1-azadecalins, but for some reason the effect is not seen in the ionization potentials, though all are significantly lower than the parent compound.

Table 6.4. Ionization Potentials of Acyclic Ethers and Thioethers, Oxiranes, and Thiiranes.[a]

Oxygen Compound	Ionization Potential (eV)	Sulfur Compound	Ionization Potential (eV)
Dimethyl ether	10.04[b]	Dimethyl sulfide	8.72[b]
Methyl t-butyl ether	9.64	Methyl t-butyl sulfide	8.46
Methyl trimethylsilylmethyl ether	9.40 9.67[c]	Methyl trimethylsilylmethyl sulfide	8.35
Methyl bis(trimethylsilyl)-methyl ether	8.49[c]		
Methyl tris(trimethylsilyl)-methyl ether	8.23[c]	Methyl tris(trimethylsilyl)-methyl sulfide	7.66
Oxirane	10.57	Thiirane	9.03
Methyloxirane	10.26	Methylthiirane	8.88
tert-Butyloxirane	10.04	*tert*-Butylthiirane	8.58
		trans-2,3-*tert*-Butylthiirane	8.39
2,2-Dimethyloxirane	10.00		
trans-2,3-Dimethyloxirane	9.98		
Trimethylsilyloxirane	9.67	Trimethylsilylthiirane	8.44
trans-2-Trimethylsilyl-3-*tert*-butyloxirane	9.33		
trans-2,3-Bis(trimethylsilyl)oxirane	9.07	trans-2,3-Bis(trimethylsilyl)thiirane	8.19

[a] Unless otherwise noted, values taken from [139].

[b] Taken from [137].

[c] Taken from [140].

Collected here are a few ionization potentials of substituted ethers and thioethers. The data provide several interesting observations. In going from methyl *tert*-butyl ether to methyl

trimethylsilylmethyl ether, there is a drop in ionization potential of 0.24 eV, while for the corresponding sulfides, the change is 0.11 eV. This supports Yoshida's contention that silicon does not interact as strongly with sulfur as with oxygen. In both cases it can be seen that additional substitution is not linearly additive in effect. The disilyl oxygen compound ionizes at 0.65 eV less than the unsubstituted compound (0.41 eV less than one silicon), while the trisilyl compound is a full 1.41 eV lower in ionization potential (0.76 eV less than two silicons). The trisilyl sulfur compound is 0.8 eV lower in ionization potential than the unsubstituted sulfur compound. For the oxiranes, the first silyl lowers the potential 0.37 eV while a second silyl lowers the potential 0.6 eV more. The thiiranes once again exhibit smaller effects, showing a 0.14 eV drop for a single silyl group and a further 0.25 eV drop for the second silyl group.

With the three-membered saturated heterocycles, the effect of the substituent should be near maximum since the substituents are approximately parallel to the heteroatom p-type lone pairs. Variations may be seen if the substituent is bulky enough to force it to bend outward from the ring center, which not only changes its interaction angle with the heteroatom, but affects the hybridization of the substituent-bearing ring carbon. This effect can be seen in the 0.22 eV drop in ionization potential going from methyloxirane to *tert*-butyloxirane, and similarly in the 0.3 eV drop in potential going from methylthiirane to *tert*-butylthiirane. Since the C-S bonds are longer, the steric effect of the *tert*-butyl group should be less, and this may mean that the differences in oxidation potential are more inductive or hyperconjugative than due to steric/rehybridization effects.

Table 6.5. Oxidation Potentials of 2-Substituted-1,3-Dithianes.[a]

Parent Compound	R[b]	R´[c]	E_p (V)
1,3-Dithiane	H	H	1.18
	H	2-Trimethylsilyl	0.99
	tert-Butyl	2-Trimethylsilyl	0.95
	Phenyl	2-Trimethylsilyl	0.85
	2-Trimethylsilyl	2-Trimethylsilyl	0.70
	H	2-Trimethylstannyl	0.75
	tert-Butyl	2-Trimethylstannyl	0.54
	Phenyl	2-Trimethylstannyl	0.81
	2-Trimethylstannyl	2-Trimethylstannyl	0.19
	2-Trimethylsilyl	2-Trimethylstannyl	0.44
3,5-cis-Dimethyl-1,3-Dithiane	2-Trimethylstannyl	H	0.75
	H	2-Trimethylstannyl	0.40
	2-Trimethylstannyl	2-Trimethylstannyl	0.35

[a] Taken from [128,136].
[b] In the conformationally-fixed 3,5-cis-dimethyl-1,3-dithianes, the R substituent is equatorial.
[c] In the conformationally-fixed 3,5-cis-dimethyl-1,3-dithianes, the R´ substituent is axial.

The variations of oxidation potentials seen in Table 6.5 could be attributed to the same effects as those at work in Table 6.4. However, an attractive alternate explanation can be made. As the bulk of the "other" 2-substituent increases, the population of axial 2-silyl and 2-stannyl conformers rises. Since the C-S-C-M dihedral angle (M = Si, Sn) is approximately 60° for the axial conformer and 180° for the equatorial conformer, the axial conformer would be expected to have a much larger interaction and therefore a lower oxidation potential. This would appear to be supported by the data for 3,5-cis-dimethyl-1,3-dithianes, but there is a complication, since it was determined that the axial 2-stannyl compound in this series is not in fact a chair but rather something like a twist-boat. It was decided that the study could benefit from simplification and sophisticated computational simulation.

COMPUTATIONAL RESULTS AND DISCUSSION

The methods used to acquire these computational results are detailed in Chapter 7, but for clarity it should be explained how certain terms are being employed in the results. All calculations of ionization potentials are done by taking the difference in the total electronic energy of the cation radical and the neutral species. This method is known as ΔSCF and is more reliable than methods based on Koopman's Theorem which employ the HOMO. The terms adiabatic and non-adiabatic (or vertical) are used to denote calculations where the geometry of the cation radical was optimized or fixed at the optimal neutral value, respectively. HOMO refers to the highest occupied molecular orbital, while SOMO refers to the singly-occupied molecular orbital (which is generally assumed to be the HOMO of a cation radical, though this is not necessarily the case).

The computational studies began with a simple model of α-stannylated sulfides, seen below and referred to as the Hydrogen Model.

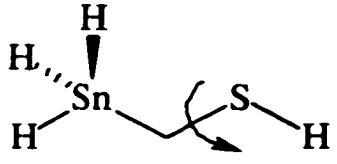

Figure 6.1. Hydrogen Model of α-Stannylated Thioethers, Illustrating the Varied Dihedral Angle.

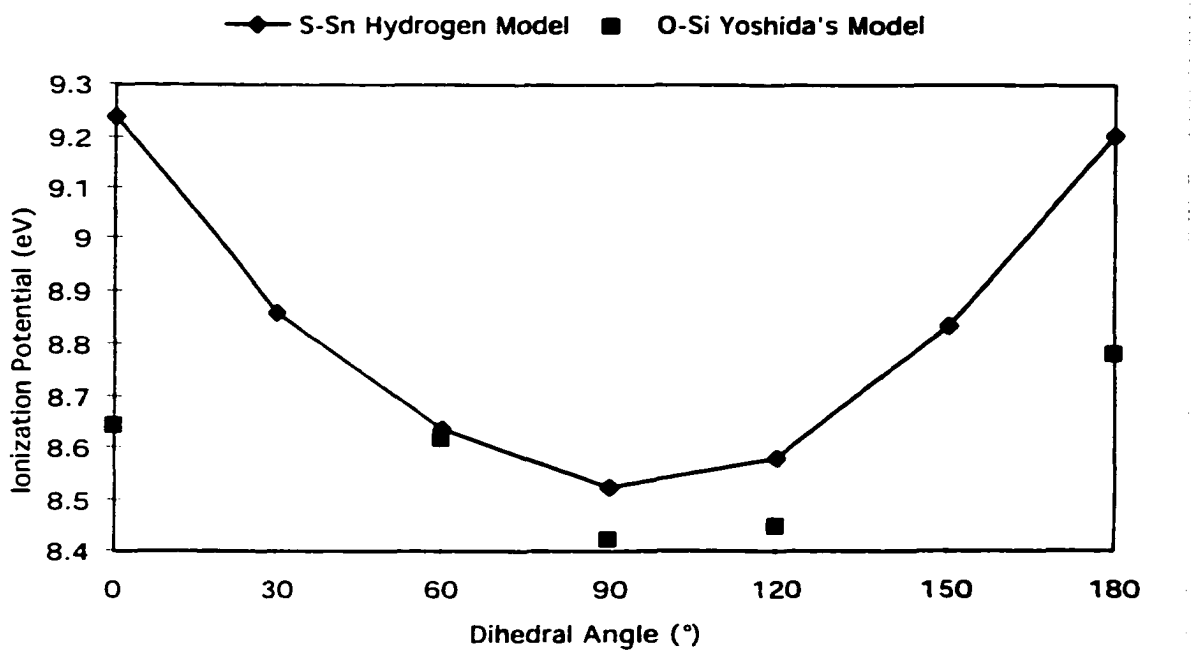

Figure 6.2. Hydrogen and Yoshida's Models' Ionization Potentials.

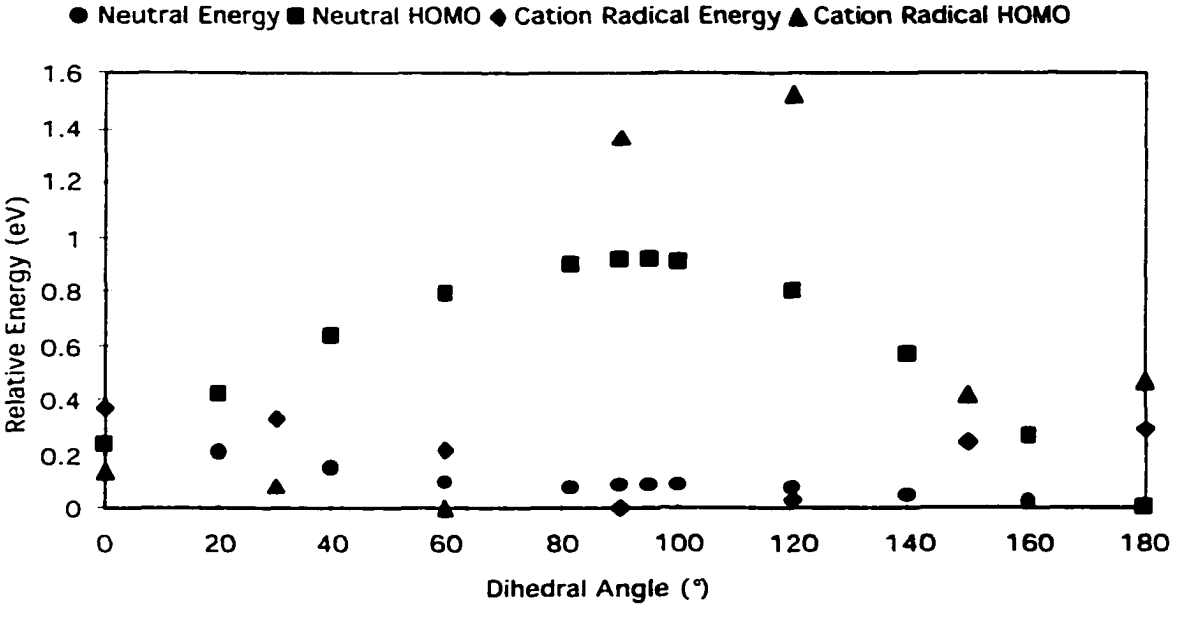

Figure 6.3a. Factors Affecting Ionization Potential: O-Si Model.

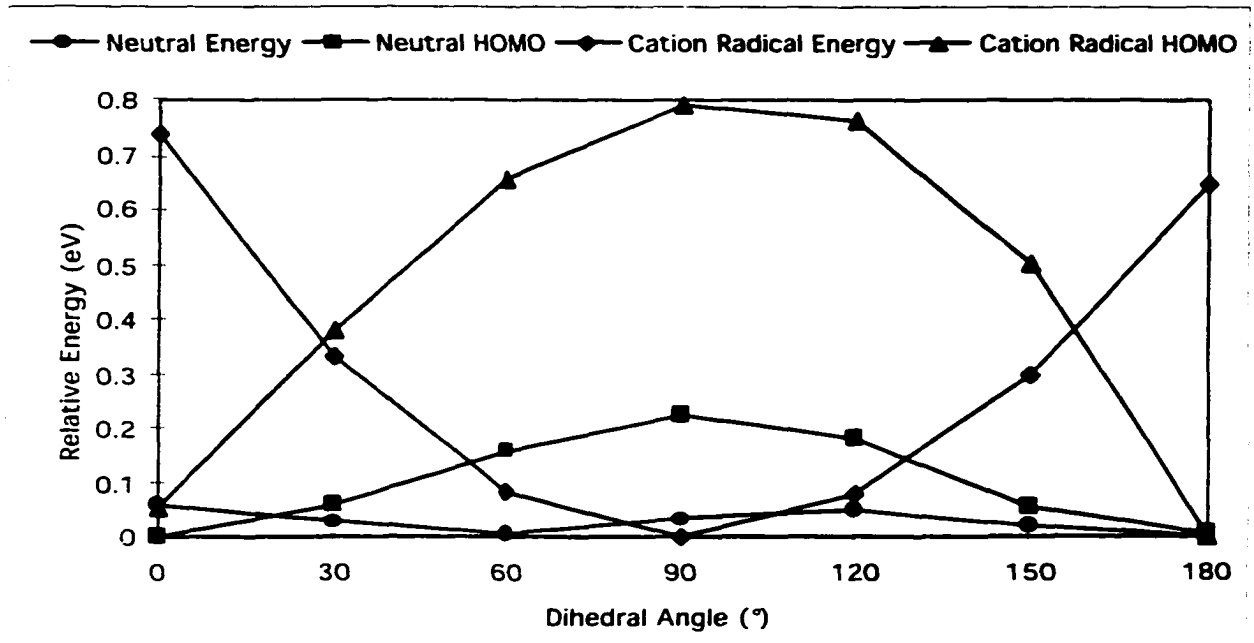

Figure 6.3b. Factors Affecting Ionization Potential: S-Sn Model.

As was expected, the tin substituent caused a large decrease in ionization potential when the substituent was parallel to the sulfur p-type lone pair.

To answer the important question of why the ionization potential is lowered, we returned to Yoshida's model. Since there were various things about Yoshida's claims it was desirable to verify, calculations of Yoshida's original model compound (identical to the Hydrogen Model, but with oxygen and silicon rather than sulfur and tin) were undertaken in the same fashion as Yoshida and co-workers reported (HF/3-21G*).[130] These were compared to the Hydrogen Model calculations (B3PW91/LANL2DZ; unfortunately, not of the same type due to the limited number of basis sets which describe tin).

As can be seen in Figure 6.3a, the variation of the energy of the HOMO in Yoshida's O-Si compound is indeed much larger than the variation of either the neutral species or the cation radical. His assumption of the large silicon effect (approx. 1.1 eV) using Koopman's theorem is not justified, since at best the actual ionization potential

change is no more than 0.4 eV by ΔSCF. It seems reasonable that the difficulty of ionizing a species should be the difference in energy between the HOMO and a free electron, but sometimes electronic reorganization effects can be very large, and this appears to be one of those cases. Also, claims that the cation radical SOMO is stabilized by interaction with the C-Si bond[134] are incorrect. As can be seen, the destabilization of the SOMO at 90° (as compared to 0°) is even larger than the destabilization of the HOMO. This is in accord with the explanation of the interaction (the SOMO should logically be raised by interaction with a filled C-Si orbital). It is easy to see how one might be misled, since the overall cation radical energy is minimized at 90°.

The effects for tin are even more dramatic. As can be seen in Figure 6.3b, the destabilization of the SOMO (at 90° as compared to 0°) is fully four times the destabilization of the HOMO, but the lowering of the ionization potential is almost entirely due to stabilization of the cation radical (at 90° as compared to 0°). The variation of neutral species total energy is almost neglible and mainly sterically derived.

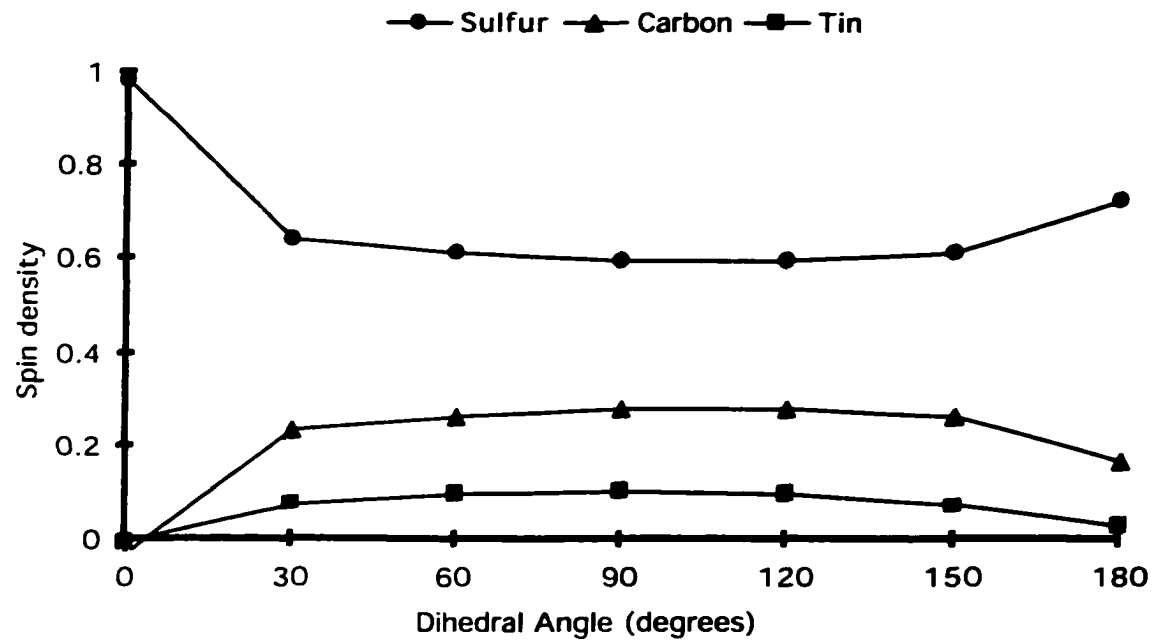

Figure 6.4. Spin Densities on Heavy Atoms in the Cation Radical.

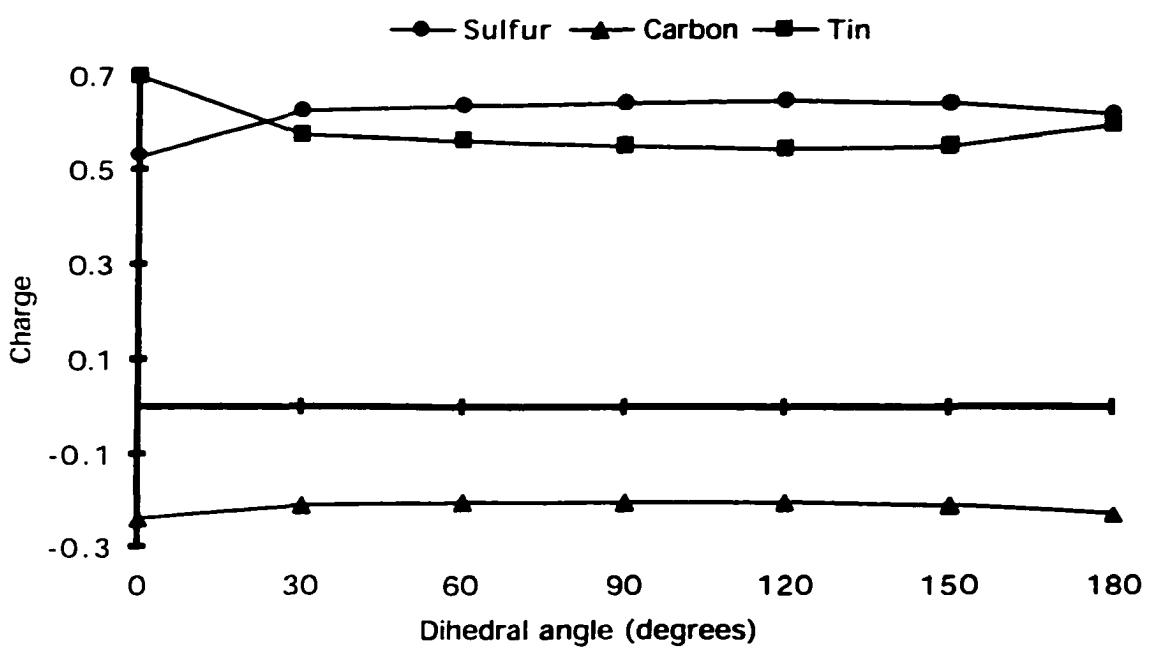

Figure 6.5. Charge Densities with Hydrogen Charges Summed into the Heavy Atoms in the Cation Radical.

The nature of the cation radical was also investigated, and it was hoped that this investigation might shed light onto anomalies such as those in Table 6.3, since it was still unclear why germanium and tin lowered ether oxidation potentials more than silicon. It was thought that the start of the explanation might be that the orbital energy of the SOMO is not the same as that of the HOMO and the energy matching efficiency would be different; since the SOMO does not seem to have a drastic effect on the overall cation radical energy, other electronic effects and certain geometric effects were considered. What can be seen at a glance in Figure 6.4 is that when the C-Sn bond is orthogonal to the sulfur 3p lone pair, the cation radical is purely sulfur-centered, but the radical becomes more delocalized as the C-Sn bond comes into alignment with the 3p orbital. Very little overlap is apparently necessary for substantial delocalization, leading to a plot which changes very steeply near 30° and 150°, especially when compared to the ionization energy. The charges follow a similar pattern, though they do not alter as much; one would expect the charges in compounds of this type to be polarized and distributed mainly by induction, which would not show such a strong geometric effect. Figures 6.4 and 6.5 begin to suggest that there are two kind of α-stannylated thioethers: the kind with no interaction (a 0° dihedral and, to a lesser extent, a 180° dihedral) and the kind with some interaction (any non-parallel orientation). This suggestion is born out in the geometric features.

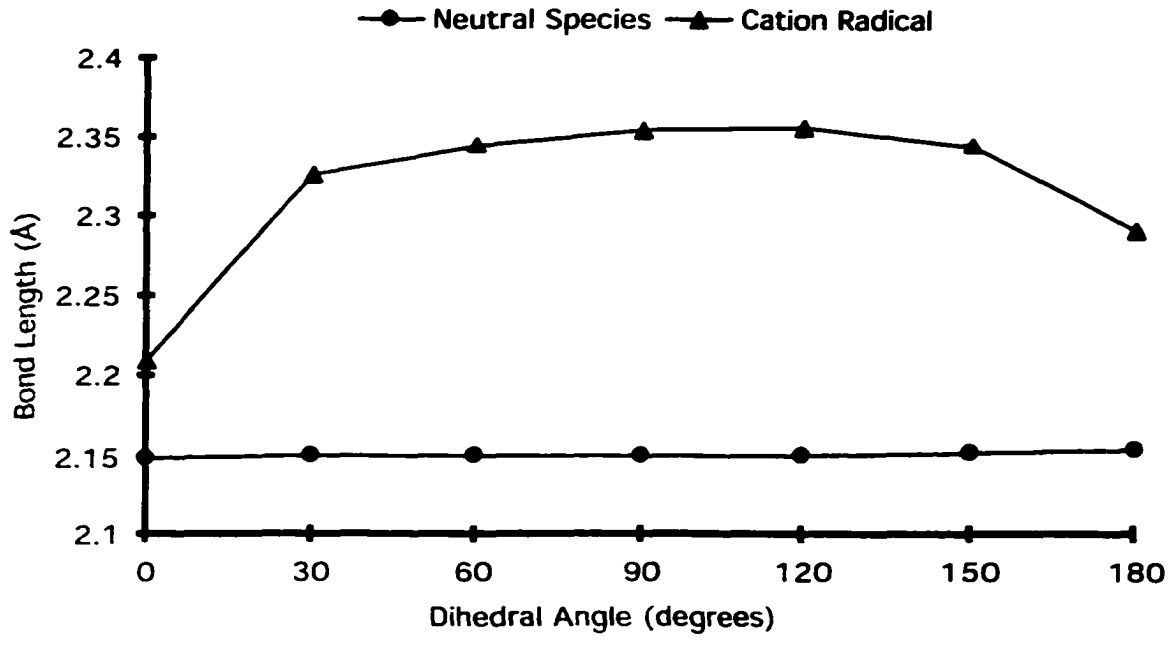

Figure 6.6. α-Carbon-Tin Bond Length.

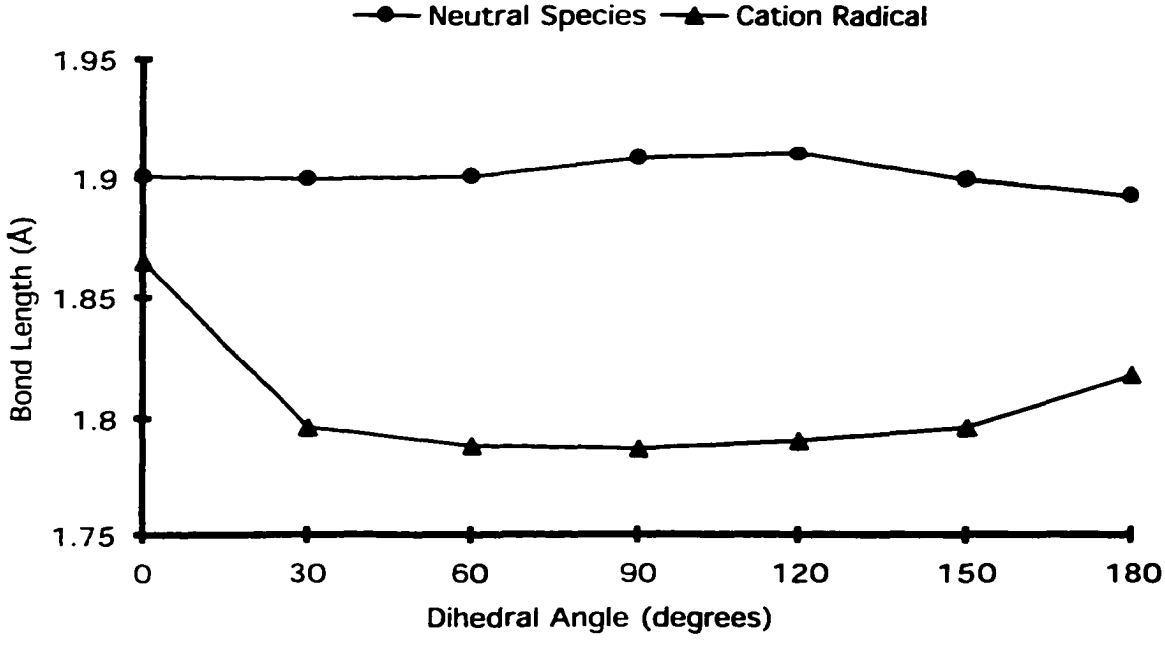

Figure 6.7. α-Carbon-Sulfur Bond Length.

In Figure 6.6, the C-Sn bond is slightly lengthened at 0°, but becomes much longer at larger angles. Likewise, the C-S bond is slightly shortened at 0°, but becomes much shorter at larger angles. The Sn-C-S bond angle is much larger in the cation radical (121.1°) than in the neutral species (115.9°) for the 90° dihedral conformer, while for the 0° dihedral conformer the difference between the cation radical (112.4°) and the neutral species (111.8°) is much smaller. The C-S-H bond angle also increases going from the neutral species to the cation radical (≈2° at all geometries).

The key to understanding these unique observations is the nature of the HOMO. For the 0° dihedral cation radical, the HOMO was found to be completely localized on tin, with the Sn-C-S plane being a node. However, the spin in this species was found to be entirely on the sulfur. This is unusual, since in most organic cation radicals the electron is expected to be removed from the HOMO of the neutral species, and the HOMO of the cation radical is generally expected to be the SOMO. By comparing stannylmethane neutral and cation radical species to methanethiol neutral and cation radical species, it was found that of the two compounds the methanethiol neutral species does possess the higher energy HOMO, in agreement with the spin being localized on the sulfur. The stannylmethane possesses the higher energy HOMO of the two cation radicals, in agreement with the nature of the stannylmethanethiol 0° cation radical HOMO. For the 0° conformer, there is no overlap of the sulfur p-type lone pair and the C-Sn bond, so there is no mixing of the two sets of orbitals, and not only the HOMO, but the SHOMO, etc., are composed of tin and tin-hydrogen orbitals. The orbital bearing the spin (the SOMO) is the highest MO of the set of MOs centered on sulfur, and is not the HOMO. In the case of the 90° dihedral, the spin was found to be more widely distributed within the molecule. Additionally, the HOMO was discovered to be much more delocalized, involving all the heavy atoms and oriented in the Sn-C-S plane.

From these electronic and geometric parameters a picture develops of a fragmenting ion, in which the fragmentation is much more advanced at 90° than at 0°. It can be seen in the 90° cation radical as C-Sn bond elongation, C-S bond shortening, changes in C-S-H bond angle indicating a shift to lesser p-orbital content in the σ-bonds, and movement of the tin away from the incipient π-orbital. The fragmentation is much less advanced in the 0° dihedral because the sulfur and carbon orbitals which will form the thione π system are orthogonal. This type of fragmentation is known for α-stannylated thioethers, but there has been some confusion as to the distribution of charge and spin in the fragmenting ion. These data seem to indicate, at least for dialkyl thioethers, that the spin remains with the developing thione system, while the tin group departs as a cation. These data also provide the first evidence that this fragmentation process participates in lowering the adiabatic ionization potential.

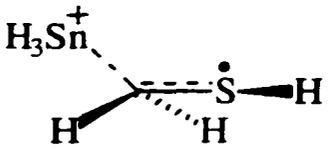

Figure 6.8. Cleavage of the C-Sn Bond as the Thione System Develops.

Although the predictions of the Hydrogen Model are almost certainly correct in the qualitative sense, better quantification was desired, so the Methylated Model was employed. Also, in light of the fragmentation process observed for the Hydrogen Model, the question of the magnitude of the non-adiabatic (vertical) ionization potential became important. The non-adiabatic ionization potential should not be affected by factors requiring geometric change, as the cation radical geometry is fixed to match the neutral species geometry. This type of calculation more closely matches the type of data which would be obtained in a photoelectron spectroscopy study.

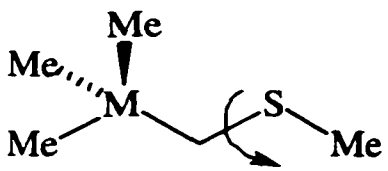

Figure 6.9. Methylated Model of α -Stannylated Thioethers, Illustrating the Varied Dihedral Angle (M = C, Si, Sn).

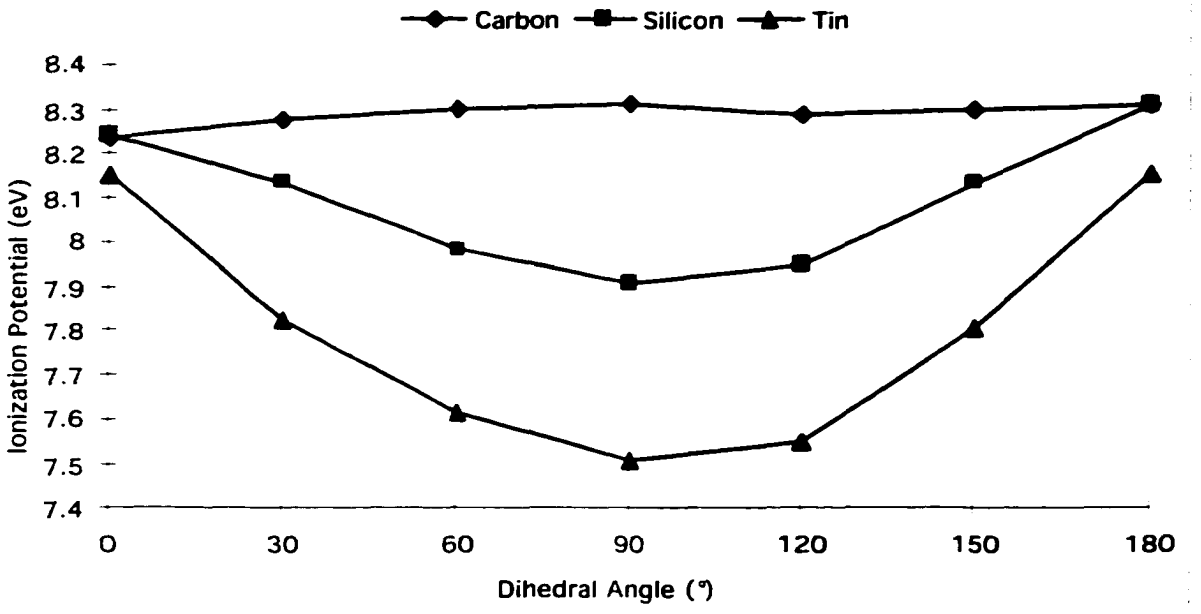

Figure 6.10. Methylated Model Adiabatic Ionization Potentials.

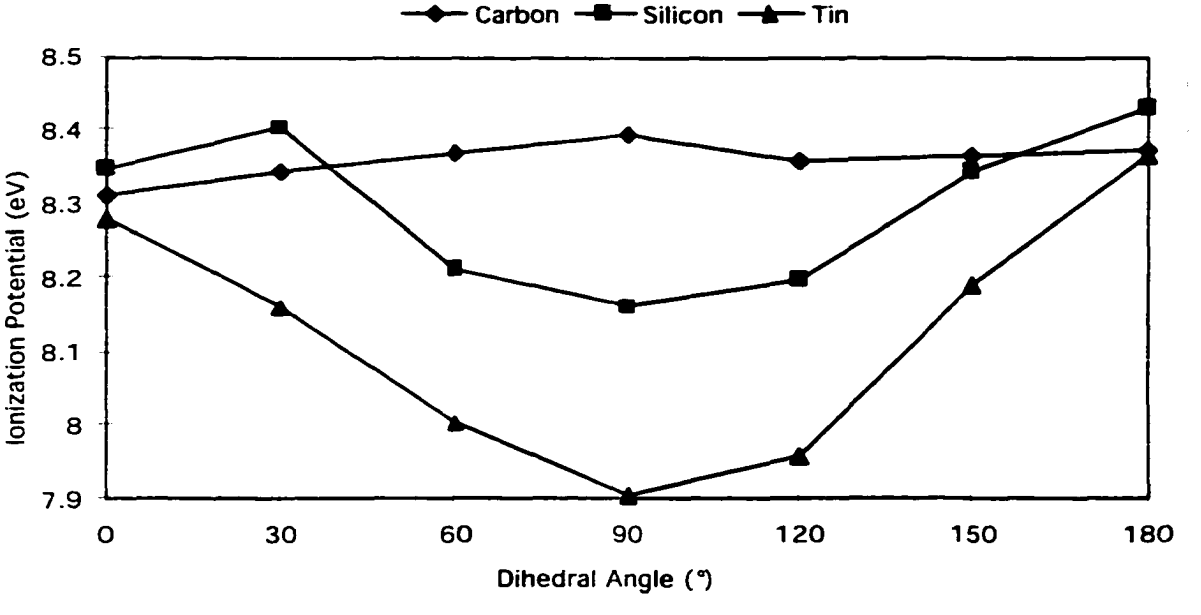

Figure 6.11. Methylated Model Non-Adiabatic (Vertical) Ionization Potentials.

As can be seen in Figure 6.12, the geometry of an α-carbon has little effect on the adiabatic ionization potential, while the potential-lowering effect of α-silicon varies a little more than 0.3 eV with the C-S-C-Si dihedral angle. As was expected, the adiabatic ionization potential is affected the most by, and shows the strongest geometric dependence on an α-tin substituent, which lowers the ionization potential of the sulfide by more than 0.6 eV at 90° (in the C-S-C-Sn dihedral) compared to 0 or 180°. It is interesting to note that there is a small (0.1-0.15 eV) effect of tin which does not seem to be geometry-dependent and appears to be absent in silicon. This may be due to progress of the fragmentation process discussed for the Hydrogen Model. One would expect it to be more advanced for tin due to tin's enhanced ability to accomodate the positive charge, but it is strange to see it completely absent from the silicon; silicon is known to also have a fair capacity for accommodating positive charge. The effect probably comes from some other source entirely.

This conclusion is supported by examination of the non-adiabatic ionization potentials in Figure 6.11. The small difference in potential at a dihedral angle of 0° is still present, though the stabilizing effects of the partial fragmentation cannot affect the non-adiabatic potential. Though the variation of ionization potential for α-carbon is slightly greater than for the adiabatic case, the α-silicon potential depression is decreased to about 0.2 eV at maximum. In a like fashion, the effects of α-tin decrease to little more than 0.4 eV. The effects also become somewhat steeper with respect to angle, which is to be expected for the loss of the stabilizing effects of the incipient fragmentation on the cation radical. The fragmentation affected all angles nearly equally except very near 0 and 180°, and the superimposition of this effect would round out the curve of the ionization potential versus dihedral angle, as is seen for the adiabatic potential in Figure 6.10. A rough comparison with Table 6.4 shows that the values appear to be about 0.1 eV low overall,

though this is uncertain due to the variation with geometry and the free rotation of the acyclic sulfides.

The variation in ionization potential was fitted, by multiple linear regression, to Karplus-like equations. The adiabatic potential was fitted to $IP_{adiabatic}$ (eV) = 0.3190 cos 2θ + 0.0903 cos 4θ + 7.7433 with an r^2 = 0.9786, where θ is the value of the C-S-C-Sn dihedral angle in degrees. The non-adiabatic (vertical) potential was fitted to $IP_{non\text{-}adiabatic}$ (eV) = 0.2117 cos 2θ - 0.0576 cos 0.5θ + 8.1291 with an r^2 = 0.9752, where θ is the value of the C-S-C-Sn dihedral angle in degrees.

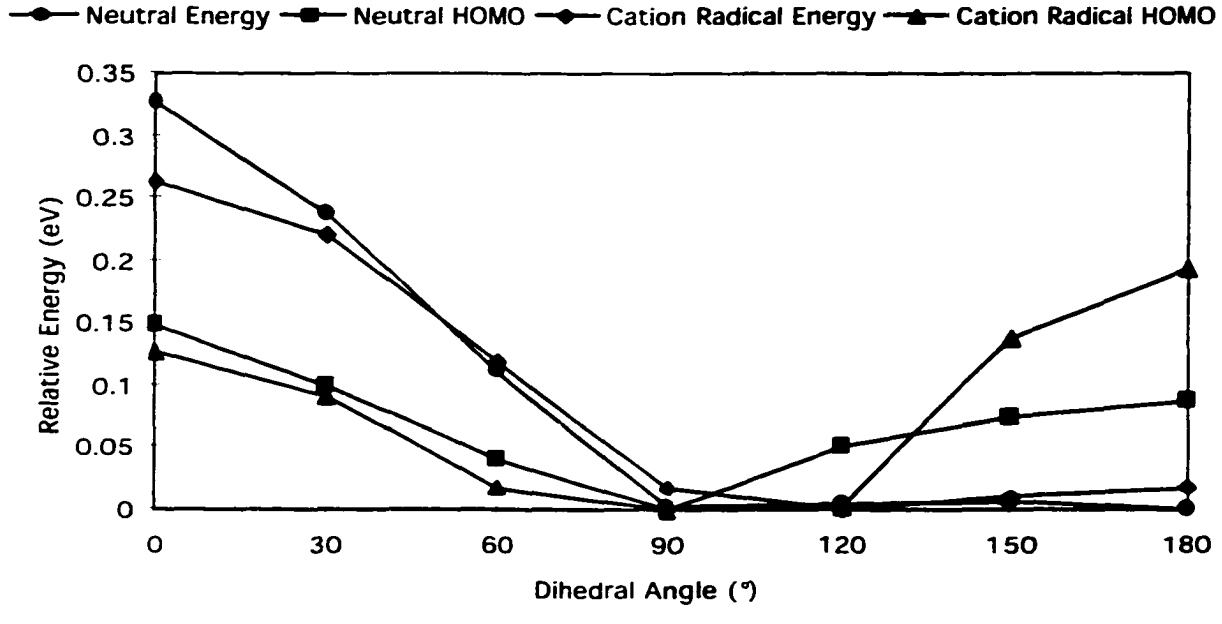

Figure 6.12. Effects of α-Carbon on the Energy of the Sulfide, Sulfur Radical Cation and Corresponding HOMOs.

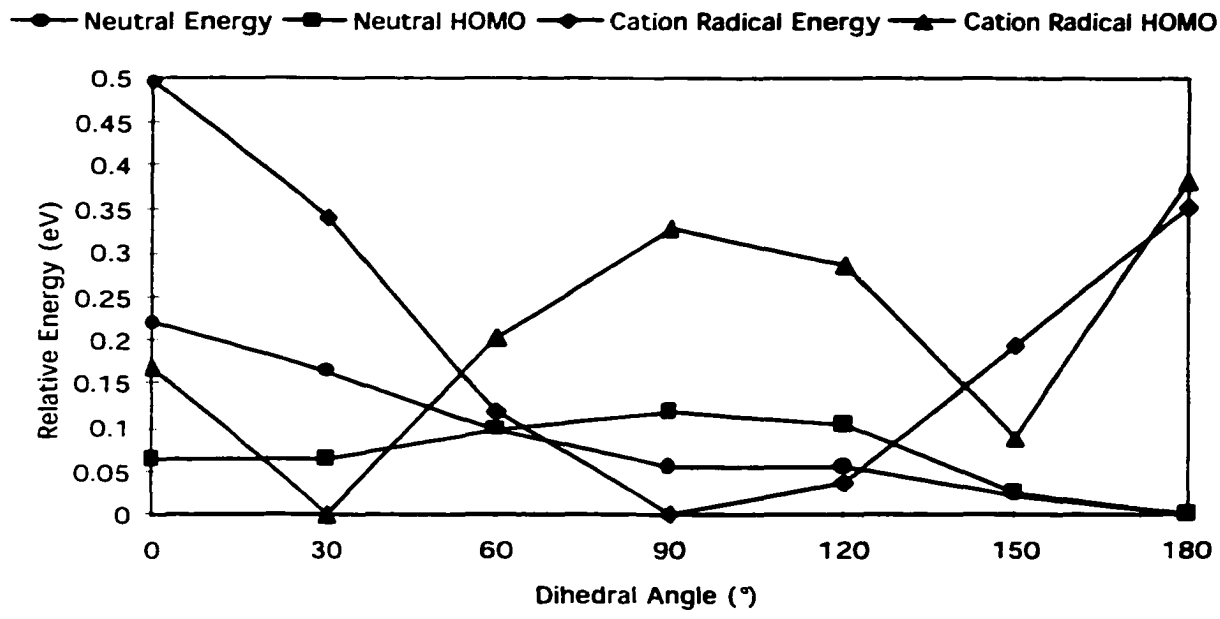

Figure 6.13. Effects of α-Silicon on the Energy of the Sulfide, Sulfur Radical Cation and Corresponding HOMOs.

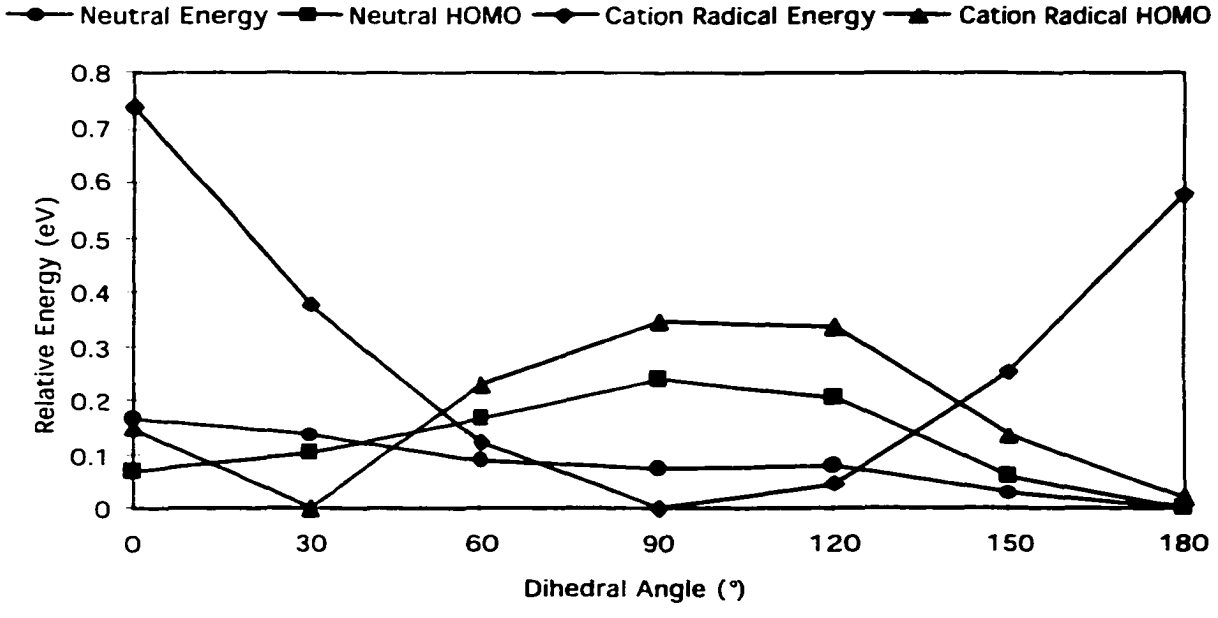

Figure 6.14. Effects of α-Tin on the Energy of the Sulfide, Sulfur Radical Cation and Corresponding HOMOs.

Figures 6.12 through 6.14 detail the various contributing effects that comprise the Methylated Model adiabatic ionization potentials. Considering first the case of α-carbon, it is surprising to note that the HOMO of the neutral species is actually stabilized when the C-C bond is parallel to the sulfur 3p orbital. From orbital energy considerations, the interaction between these orbitals should be the weakest of the three substituents considered, but it is expected to either have no effect or a destabilizing effect like the others. However, one can clearly see that the HOMO is stabilized in a geometry-dependent fashion, the stabilization being 0.15 eV at 90° as compared to 0°. It is almost as if the sulfur 3p lone pair is donating electron density into the C-C σ* orbital, though that explanation is not supported by the geometric features. The C-C bond length does not alter significantly through its entire rotation in the neutral molecule, though is does lengthen 0.05 Å from 0 to 90° in the cation radical. Even granting the antibonding orbital interaction, it does not explain why there should be any difference in the HOMO energy at 0 and 180°. This smaller effect could be due to steric effects, as can be observed in the overall energy variation, and at any rate, the variation of the HOMO is small, especially compared to that for α-silicon and α-tin. The overall neutral energy varies as one would expect, demonstrating that the large steric repulsion between the methyl and *tert*-butyl groups falls off rapidly with the varying dihedral angle and is essentially relieved at a dihedral angle greater than 90°. It is clear that this steric interaction is also the governing factor in the energy of the cation radical, and its energy variation tracks that of the neutral species almost exactly. The cation radical HOMO, which is also the SOMO, varies in a similar fashion to the neutral HOMO, and from this it is suggested that these variations are the result of the fragmentation process described for α-tin; it is known that sulfides such as methyl *tert*-butyl sulfide oxidize by irreversible electrochemical processes and these effects may be the only interactions available to alter the HOMO and SOMO, though one would expect a larger change in the C-C bond length.

The case of the α-silicon is even more peculiar. In Figure 6.13 one can see the expected destabilization of the HOMO in the neutral molecule, with the familiar overlay of steric repulsion altering the symmetry between 0 and 180°. Likewise, the familiar steric repulsion governing the total energy of the neutral species. The case of the cation radical is more interesting. The cation radical total energy shows the expected, though still unaccounted-for, stabilization at 90°, reaching a maximum variation between a dihedral angle of 0 and 90° of 0.5 eV. It is clear that once again this effect is not due to stabilization of the cation radical HOMO, since it is destabilized at 90°. Even more bizarre is an effect hinted at in the calculations done by Yoshida's method on the O-Si model compound. The cation radical HOMO varies strongly with the dihedral angle, but possesses minima near 30 and 150° rather than 0 or 90°. The source of these minima is unknown. Though the effects of the incipient fragmentation are observed in various geometric parameters (the C-Si bond lengthens 0.1 Å from 0 to 90° and the α-C-S bond shortens 0.07 Å over the same angle) this could not be responsible for the geometry of the observed effect, and the effect, unlike all the others, is actually greater at 180°. The only suggestion to be offered is interaction with empty orbitals of significant d-character, such orbitals being the only possible source of a four-fold set of minima over 360° rotation. This effect is observed in slightly altered form for α-tin (*vide infra*). The absence of the effect in the α-carbon substituted sulfide and its presence in the α-tin substituted sulfide support the d-orbital argument.

For the final case of α-tin substituted sulfides, we find the situation to be very similar to that seen for α-silicon. The destabilization of the neutral HOMO is almost identical, except for the doubling of magnitude expected for the better orbital energy match. The neutral total energy shows the same trend for all three molecules, being governed by steric effects. The only difference is a falling-off of the steric effect magnitude, which is expected since the C-M bond length increases going from M = C to M = Si, and finally to M = Sn. The steric effect falls from a maximum (at 0° C-S-C-M dihedral angle) of over 0.3

eV for carbon to less than 0.25 eV for silicon, reaching a minimum at less than 0.2 eV for tin. The stabilization of the cation radical is present, and as expected in greater magnitude than for silicon (for Si, max. of 0.5 eV; for Sn, max. of 0.75 eV). The strange variation in cation radical HOMO observed for silicon is also present, in about the same magnitude. The only difference seems to be that where for silicon the effect was greatest at 180°, where the HOMO was destabilized by 0.4 eV versus 30°, in tin 180° is a minimum, being affected about equally as compared to the minimum of 30°. This is probably due to an effect similar to that in operation in silicon, with some additional effect in operation which stabilizes the cation radical HOMO greatly at a dihedral angle of 180°.

ELECTROCHEMICAL RESULTS

Table 6.6. Oxidation Potentials of Selected Sulfides and Derivatives.

Compound	E_{peak} (V)	Electrode[a]	Solvent[b]
thietane	1.47	carbon	MeCN
thiolane	1.33	platinum	MeCN
	1.37	carbon	MeCN
	1.42	carbon	DCM
thiane	1.45	platinum	MeCN
	1.43	carbon	MeCN
	1.49	carbon	DCM
2-thiabicyclo[2.2.2]octane	1.30	platinum	MeCN
	1.31	carbon	DCM
2-triisopropylsilylthiolane	1.16	carbon	DCM
3-trimethylsilyl-2-thiabicyclo[2.2.1]heptane[c]	1.07	carbon	MeCN
tricyclohexylstannylmethyl methyl sulfide	0.78	carbon	MeCN
tricyclohexylstannylmethyl isobutyl sulfide	0.86	carbon	DCM
tricyclohexylstannylmethyl n-decyl sulfide	0.84	carbon	DCM
1-tricyclohexylstannylethyl ethyl sulfide	0.86	carbon	DCM
2-trimethylstannylthiolane	0.49	platinum	MeCN
	0.66	carbon	DCM
2-tricyclohexylstannylthiolane	0.66	carbon	DCM
2-trimethylstannylthiane	0.70	platinum	MeCN
	0.83	carbon	DCM
2-tricyclohexylstannylthiane	0.83	carbon	MeCN
2-trimethylstannyl-4-*tert*-butylthiane	1.17	carbon	DCM
3-trimethylstannyl-2-thiabicyclo[2.2.1]heptane[c]	0.72, 0.6	carbon	DCM

[a] The electrodes used were either 1.6 mm diameter Teflon-jacketed planar platinum electrodes (designated "platinum") or 3 mm diameter Teflon-jacketed planar glassy carbon electrodes (designated "carbon").

[b] The solvents used were either 0.1 M tetra-n-butylammonium hexafluorophosphate in degassed acetonitrile (designated "MeCN") or 0.1 M tetra-n-butylammonium hexafluorophosphate in dried degassed dichloromethane (designated "DCM").

[c] These compounds were analyzed as unseparated mixtures of exo and endo isomers, in which the endo isomer predominated.

The variation in the methods employed to obtain electrochemical oxidation potentials was a matter of necessity. Compounds substituted with tri(cyclohexyl)stannyl groups adsorbed to platinum and required glassy carbon for analysis. Many compounds were not soluble in acetonitrile, particularly the aforementioned tri(cyclohexyl)stannyl substituted compounds. The acyclic compounds had to be synthesized with tri(cyclohexyl)stannyl substitution as the trimethylstannyl derivatives were too volatile to be

isolated. The cyclic compounds were derivatized with tri(cyclohexyl)stannyl in an effort to get X-ray crystallographic data; the effort has not yet born fruit, but is ongoing.

Nevertheless it is clear that α-stannylation works as well for one sulfur as it does for two (see Table 6.5). There is a 0.82 V drop in oxidation potential from thiolane to 2-trimethylstannylthiolane and a 0.75 V drop from thiane to 2-trimethylstannylthiane. It is also interesting to note that going from the very small methyl group in trimethylstannyl to the much larger cyclohexyl group does not alter the oxidation potential.

ELECTROCHEMICAL DISCUSSION

Though the electrochemical data are extensive, relatively few conclusions can be drawn from them due to the shortage of compounds with constrained C-S-C-Sn dihedral angles. However, they do possess several significant features. It can be seen for the case of thiolane that the oxidation potential drops from 1.42 V for the parent compound to 1.16 V for the silylated compound, to 0.66 V for the stannylated compounds. This is in keeping with the general trends which were computed, but since the ring geometry is fluxional, the data cannot be more directly compared.

The dangers of such a comparison can be seen in the case of thianes. One would expect 2-trimethylstannylthiane and 2-tricyclohexylstannylthiane to exist in the chair conformation with the substituents equatorial. This would cause the C-S-C-Sn dihedral angles to be approximately 180°, a nadir of the potential-lowering effect. Yet there is observed a 0.75 V drop in potential for the compound. Only when cis-4-*tert*-butyl-2-trimethylstannylthiane was analyzed was the truth known. The latter compound has an oxidation potential of 1.17 V, a drop of only 0.32 V. Since the *tert*-butyl group locks the geometry of the ring, we can be sure that this effect is the actual value for equatorial α-tin, and it is probably only so high as 0.32 V because electrochemical oxidation potentials can be shifted by following fast chemical processes like the incipient fragmentation previously

discussed. The unlocked 2-trialkylstannylthianes oxidize at low potential due to another electrochemical phenomenon, in which sometimes very minor conformers can be oxidized exclusively if the equilibrium between them is fast, and the minor conformer oxidizes at a sufficiently lower potential. It is, after all, known for stannylated cyclohexanes that the A value for tin is small (4 kcal/mole; See Table 6.3), and the population of the axial conformer is fairly large. The A value for thianes would not be expected to be identical (it is known that the value for 1,3-dithianes is not), but qualitatively it is likely to be similar. Since the C-S-C-Sn dihedral angle should be closer to 60°, the α-tin effect should be much larger. Indeed, the neutral geometries of the chair conformers of the two isomers of 4-*tert*-butyl-2-trimethylstannylthiane were calculated using the same methods as with the Methylated Model. The C-S-C-Sn dihedral angles were found to be 84° for the trans (axial tin) isomer and 177° for the cis (equatorial tin) isomer. The adiabatic ionization potentials calculated for these geometries using the aforementioned Karplus-like fits are 7.51 and 8.15 eV, respectively. These potentials are, of course, not directly comparable to electrochemical potentials for a host of reasons, but the magnitude of the difference is nevertheless similar. It is not known why a similar equilibrium does not make the potential of 2-trimethylstannyl-1,3-dithiane lower, though it is suspected that the 1,3-dithiane anomeric effect is at least partially responsible.

Using the same methods, predictions were made for the endo and exo isomers of 3-trimethylstannyl-2-thiabicyclo[2.2.1]heptane. The predicted adiabatic ionization potentials are 7.65 and 7.51 eV, respectively, and these too match well to the observed difference in the endo/exo mixture, which yielded oxidation potentials of 0.72 and approx. 0.6 V, respectively.

The final point to be made is that the potentials for the acyclic α-stannylated sulfides are essentially the same as for 2-trimethylstannylthiane; since the thiane is probably a mixture of gauche and trans conformers, this is not unexpected.

CONCLUSIONS

Though the source of the potential-lowering effect of α-silicon and α-tin in ethers and thioethers is not attributable to any simple, discrete factor, its geometric nature and quantitative value have been explored and several possible contributors have been excluded. A prominent remaining possible contributor is the incipient fragmentation of the α-substituted thioether into a protonated/methylated thione radical and a trialkylsilyl or trialkylstannyl cation. This is supported by the irreversible nature of the electrochemical oxidation of these species. The electrochemical behavior of these compounds was found to be in agreement with the computational theory. Several previous claims and theories pertaining to the subject have been evaluated. and most were found to be more or less flawed.

CHAPTER 7

COLLECTED METHODS

COMPUTATIONAL METHODS

Gaussian 94[103] was used for all calculations except molecular mechanics and those requiring the visualization of orbitals. Molecular mechanics were performed with Spartan.[104] For the latter, the geometry of interest was optimized with Gaussian 94 and input to Spartan for orbital plotting, using the same method and basis set as in Gaussian 94 to compute the wavefunction. All Gaussian 94 calculations in Chapter 5 were executed on an IBM RSC6000-590 running AIX 3.2, while those for Chapters 2 and 3 were executed on a SGI Origins 2000 running IRIX 6.4. Spartan was run on an SGI Iris workstation under IRIX 4.0.5.

Most of the basis sets employed were of the standard extended-sp type. These basis sets are generally designated X-YZ(Z)G where X is the number of Gaussian functions used in linear combination to describe the inner shell functions, while there are as many valence shells as numbers following the dash, and each shell is composed of a linear combination of that number of Gaussian functions. Therefore, for the basis set 6-31G, there are six Gaussians in linear combination comprising the inner shell functions, and there are two valence shells (a "split valence"), the inner valence shell being composed of three Gaussians in linear combination, while the outer consists of a single Gaussian function. The exponents and expansion coefficients of the Gaussian functions are optimized to match the experimental energies of heavy atom hydrides (XH_{n+1}) when used with the Hartree-Fock (HF) method. The single exception is the 6-311G** basis set (6-311G with polarization functions on all atoms), which was optimized to reproduce experimental energies at the second-order Møller-Plesset perturbation level (MP2).

These basis sets are often augmented by polarization functions and/or diffuse functions. Polarization functions are able to describe non-uniform displacement of charge from the nuclear center, which is vital when describing molecules with delocalized or non-classical bonding or with very polar bonds. Polarization functions are designated by the addition of asterisks (*); one asterisk indicates the addition of polarization functions on heavy atoms only (not hydrogen or helium), while two asterisks indicate the addition of polarization functions on all atoms. For 6-31G basis sets, this entails the addition of six d-type Gaussian primitives to heavy atoms (for * and **) and three p-type Gaussian primitives to hydrogen and helium (** only). For 6-311G, however, the heavy atoms only gain five d-type Gaussian primitives, while the augmentation of the light atoms is identical. Diffuse functions are essentially extra valence functions which allow the description of loosely-held electrons, such as those in lone pairs, especially in anions or on atoms with significant negative charge, or electrons in orbitals with significant antibonding character. Diffuse functions are designated by the addition of plus signs (+); again + means diffuse functions on heavy atoms only, while two ++ means diffuse functions on all atoms. With diffuse functions, all atoms which are augmented are augmented in the same way: they receive one extra s-type Gaussian and three extra p-type Gaussian primitives, with the exponents and expansion coefficients optimized to match experimental energies of the various elements' heavy atom hydride monoanions (XH_n^-).[141]

Unfortunately, computational work with tin was limited by the basis sets which could accurately describe the heavy element. Although it was found to yield inferior answers as compared to the higher Gaussian-type basis sets (See Chapters 2 and 6), the LANL2DZ basis set was used for all calculations in Chapter 5; it was the best choice for computational modeling of tin-containing compounds, and of course the rest were also computed with LANL2DZ for consistency, as the error introduced by the basis set is

certainly less than that which would be introduced by using various basis sets and trying to directly compare the results. The LANL2DZ basis set is the Dunning-Hunziga double-zeta valence basis set employing Wadt-Hay relativistic effective core potentials.[142]

Various methods were used for the computing of geometries, energies, and properties in these studies. As necessary they will be discussed in more detail (*vide infra*), but here they are mentioned for the sake of clarity in abbreviation. The fundamental method is the Hartree-Fock method, abbreviated HF. This method has little consideration for electron correlation. To improve electron correlation, particularly important when working with non-localized molecular orbitals, several higher methods were employed, but each was based on the Hartree-Fock method. The one found to be most successful in the applications of these studies was the second-order Møller-Plesset perturbation method (MP2), which begins with the Hartree-Fock result and improves it by making a series of minor alterations. Also of this type is the Configuration Interaction, Singles method (CIS); while explicit configuration interaction calculations are not as efficient as Møller-Plesset perturbations (CIS is approximately equivalent to "MP1.5"), the method is linked in Gaussian 94 to the calculation of excited-state properties, and was used exclusively for this purpose. Finally, there are the hybrid density-functional theory methods, of which the Becke-3 Perdew-Wang 91 method was chosen. These methods start with a Hartree-Fock core, and add to its fundamental equation terms for the explicit consideration of electron correlation (both local and non-local) and pairing energy. They have the advantage of using less CPU time, less active RAM, and less disk space, and therefore larger atoms and molecules can be modeled.

Chapters 2-4: 1,2-Dichalcogenins

All neutral and cation radical species were optimized from both C_2 and C_{2v} symmetries. For the electrochemical cycles, energies were calculated for the optimized

neutral species, the neutral species at the optimized cation radical geometry, the optimized cation radical, and the cation radical at the optimized neutral species geometry. Apart from the method/basis set study conducted with 1,2-dithiin, all compounds were calculated with the MP2/6-31+G* method/basis set combination.

The CIS/6-31+G* method/basis set was used to calculate electronic transition properties (wavelengths, probabilities, symmetries, etc.). It was also used to calculate the frequency of the S-S bond stretch and ring-flattening pseudotorsions of the first singlet excited state and to optimize the geometry of the first excited singlet state. The frequencies were also calculated at the optimized geometry. The frequencies of the ground state had to be calculated with the Hartree-Fock method, though the geometries were optimized with MP2; the data were checked carefully for consistency and no negative frequencies were found, indicating that the approximation was suitable. The geometry of the lowest triplet state were calculated using the unrestricted MP2 method, and once again the HF method was used to estimate the frequencies, with the same checks as for the ground state.

Chapter 6: α-Substituted Sulfides

Except as specifically noted in the text (as for Yoshida's model), all calculations were conducted with B3PW91/LANL2DZ. For the Hydrogen Model, all calculations were geometry optimized with the Sn-C-S-H dihedral frozen at intervals of 30° and values from 0 to 180° (inclusive); all other parameters were allowed to optimize. Calculations were carried out on both the neutral and cation radical species of stannylmethanethiol trihydride. The calculation employed 37 basis functions and 73 primitive gaussians (22 valence electrons for the neutral species)

For the Methylated Model, all calculations were geometry optimized with the X-C-S-C dihedral frozen at intervals of 30° and values from 0 to 180° (inclusive) where X = C, Si, Sn. Calculations were carried out on both the neutral and cation radical species of methyl neopentyl sulfide, methyl trimethylsilylmethyl sulfide, and methyl

trimethylstannylmethyl sulfide. The calculations on the first employed 90 basis functions composed of 218 primitive gaussians (56 valence electrons in the neutral species); the calculations on latter two employed 89 basis functions composed of 205 primitive gaussians (54 valence electrons in the neutral species).

Appendix A: Tetrathiatetraasterane

No special application of the standard computational routines was made in the case of asterane, except that once again frequencies were calculated from the MP2 geometry with HF. However, Spartan was not used to visualize the orbitals; due to the high molecular symmetry (D_{4h}) it possible to derive the orbital plots by hand directly from the Gaussian 94 populations. Molecular mechanics were employed via the MM3 force field.

SYNTHETIC METHODS

NMR spectra were obtained on a Varian Unity 300 instrument (299.954 MHz for ^{1}H; 75.431 MHz for ^{13}C). All spectra were reported relative to deuterochloroform (^{1}H NMR residual shift: 7.24 ppm; ^{13}C NMR, center peak of triplet: 77.0 ppm), which was also used as the solvent. The sample was prepared 1:4 v/v in deuterochloroform to a total volume of 1 mL. The spectra were obtained at room temperature (approx. 21°C). Standard proton and broadband-proton-decoupled carbon pulse programs were employed. The proton spectrum was processed with an exponential multiplier window function (line broadening = 0.1 Hz); the carbon spectrum was zero-filled once and processed in two different ways by an exponential multiplier window function (line broadening = 1 Hz and -1 Hz). The proton digital resolution was 0.27 Hz/pt.; the carbon digital resolution was 1.10 Hz/pt. Electron impact mass spectra for the product study were obtained by injection on a Hewlett-Packard 5988A GC/MS system using a HP-5 column eluting with helium gas at 15 psig with the injector port heated to 200°C and the following column oven temperature program: 1 minute at 70°C, heating to 300°C at 20°C/minute, and 8 minutes at 300°C.

Synthesis of Starting Sulfides

***tert*-Butyl Cyclohexyl Sulfide by Nucleophilic Substitution.** *tert*-Butyl thiol (0.6 mL, 5.3 mmol) and cyclohexyl bromide (0.6 mL, 4.9 mmol) were mixed in a 50 mL round-bottom flask equipped with a magnetic stir bar and a reflux condenser. The apparatus was purged with argon and fitted with a septum through which was applied a positive pressure of argon. Sodium hydroxide (0.2 g, 5 mmol in approximately 1.5 mL of water) was diluted with 5 mL of absolute ethanol and added to the reaction mixture. The reaction was refluxed with stirring for 24 h. Upon cooling, the reaction mixture was poured into 150 mL of water. Sodium hydroxide was added until the pH of the water was 10-12, then the mixture was extracted with 3x100 mL hexanes. Due to a slight tendency to emulsion, 100 mL of saturated aqueous sodium chloride was added to the mixture and one further extraction was made with 100 mL hexanes. The hexanes solution was dried over anhydrous magnesium sulfate, filtered, and the solvent was removed by rotary evaporation. *tert*-Butyl cyclohexyl sulfide was obtained (92 mg, identified by GC/MS), corresponding to a 10% yield.[143]

***tert*-Butyl Cyclohexyl Sulfide by Photoreaction.** In a modification of Weibull's method,[144] *tert*-butyl thiol (0.6 mL, 5.3 mmol) and cyclohexene (0.5 mL, 4.9 mmol) were placed in a quartz phototube and stoppered with a septum. The phototube was placed in a circulating-water jacket and the whole apparatus was placed in a Srinavasan-Griffin photoreactor for 365 nm irradiation. The mixture was irradiated with ice-water circulation for 40 h, and an aliquot was taken. Irradiation continued to a total time of 98 h. By ^{1}H NMR analysis, at 40 h the reaction had converted 71%, and at 98 h the reaction had only progressed to 77% conversion. Solvent and starting materials were removed by rotary evaporation to yield an essentially pure product. In a scaled-up reaction, cyclohexene (2.5 mL, 24.7 mmol) and *tert*-butyl thiol (3 mL, 26.6 mmol) were reacted in

the same fashion for 48 h. *tert*-Butyl cyclohexyl sulfide (2.20 g) was obtained in 52% yield.

Diisobutyl Sulfide from Sodium Sulfide. Due to the sporadic availability of isobutyl thiol, some of the diisobutyl sulfide used was synthesized from sodium sulfide and isobutyl iodide. Sodium sulfide nonahydrate (2 g, 8.2 mmol) was placed in a 15 mL flask with 37 mL of water. A Claisen head was attached with an addition funnel on one side and two stacked reflux condensers on the other side. Water circulation and stirring was initiated. When the sodium sulfide had mostly dissolved, isobutyl iodide (2 g, 10.9 mmol) was added from the addition funnel. Aluminum foil was used to exclude light (as the iodide is photosensitive). After 30 min stirring, heat was applied and the mixture was brought to reflux between 100 and 110°C. The reaction was allowed to reflux for 23 h. A fair quantity of white crystals had formed (presumably sodium iodide) along with some blue-black gelatinous precipitate. The flask was rinsed with both dichloromethane and water, saturated aqueous sodium chloride was added to the mixture, and the mixture was extracted with dichloromethane. The organic extract was dried over anhydrous sodium sulfate and filtered. The solvent was removed by rotary evaporation at approximately 30°C and 25 torr. In this fashion a small quantity of a pale yellow liquid was obtained, which was determined by GC/MS to be 85% diisobutyl sulfide. The reaction was scaled up to 4.1 g of sodium sulfide nonahydrate (17.1 mmol) in 10 mL of water. The solution was sonicated to aid in the dissolution of the sodium sulfide (a more concentrated solution was desired); this opportunity was taken to also degas the aqueous solution. Isobutyl iodide (4.2 g, 22.8 mmol) was added and the reaction was refluxed with stirring for 20.5 h. The reaction was worked up as before, and 1.04 g (31%) crude diisobutyl sulfide was obtained. Crude diisobutyl sulfide was purified by short-path vacuum distillation from lithium aluminum hydride.[145]

Diisobutyl Sulfide from Isobutyl Thiol. Using a modification of Vecera's method[146], sodium metal (0.89 g, 38.6 mmol) was dissolved in 15 mL absolute ethanol under argon. Isobutyl thiol (4 mL, 36.9 mmol) was added dropwise by syringe. When the color became no more intense, isobutyl bromide (4 mL, 36.8 mmol) was added dropwise by syringe. The mixture was refluxed under argon overnight with a West condenser. A copious white precipitate (presumably sodium bromide) formed and settled. The mixture was decanted into a separatory funnel and enough water was added to dissolve it. The water-ethanol mixture was extracted with 4x50 mL hexanes. The hexanes solution was dried over anhydrous magnesium sulfate, filtered, and the solvent was removed by rotary evaporation. After accounting for GC/MS purity (99%), diisobutyl sulfide was obtained in 88% yield. Crude diisobutyl sulfide was purified by short-path vacuum distillation from lithium aluminum hydride.

Dineopentyl Sulfide from Thiourea. Thiourea (0.21 g, 2.7 mmol) was dissolved in 10 mL absolute ethanol (0.27 M). Neopentyl bromide (0.75 g, 1.5 mmol) was added, and the mixture was refluxed under static argon pressure for 7 days. After this time sodium hydroxide (0.11 g, 2.8 mmol) was added directly to the reaction mixture. The reaction mixture was refluxed for 10 additional days. The final product was worked up by the addition of 40 mL of water and extraction with 4x50 mL n-pentane. A few drops of product were obtained, and were found to be dineopentyl sulfide by GC/MS.[146]

Methylation of Alkyl Mercaptans. Using a modification of Vogel's method,[147] 10% aqueous sodium hydroxide (165 mL, 0.41 mol) was degassed by bubbling argon through the solution with stirring. The solution was then set up with a septum and placed under positive argon flow. With vigorous stirring, isopropyl thiol (14 mL, 0.15 mol) was dripped into the reaction mixture by syringe. After the addition was complete and the intensity of the yellow color stabilized, dimethyl sulfate (14 mL, 0.148

mol) was dripped in by syringe. As the addition progressed, sufficient heat was evolved to reflux the more volatile components of the reaction mixture. When the addition was complete, the positive argon flow was replaced by positive argon static pressure and the reaction was allowed to stir for approximately 20 h. The stirring was then stopped and after 1 h of standing a golden layer had separated out on top of the reaction mixture. This layer was removed by Pasteur pipette and analyzed by GC/MS. The liquid was found to be 89% pure methyl isopropyl sulfide, contaminated with isopropyl thiol and diisopropyl disulfide. The yield, accounting for the purity, was 72%.

Using the same method, 10% aqueous sodium hydroxide (85 mL) and isobutyl thiol (12 mL) were used with dimethyl sulfate (10 mL) to form methyl isobutyl sulfide in 96% yield (99% pure). Ten percent aqueous sodium hydroxide (100 ml), *tert*-butyl thiol (15 mL), and dimethyl sulfate (16 mL) were used to make methyl *tert*-butyl sulfide in 89% yield (98% pure). The crude methyl alkyl sulfides were purified by short-path vacuum distillation from lithium aluminum hydride.

Synthesis of 4-*tert*-Butylthiane[148]

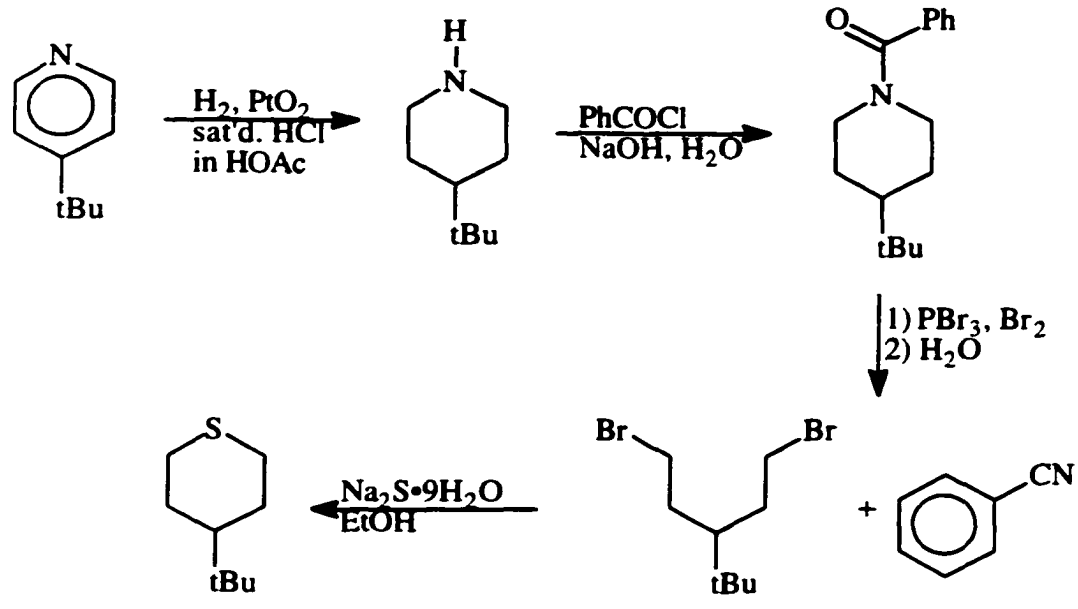

Scheme 7.1. 4-*tert*-Butylthiane.

4-*tert*-Butylpiperidine. A method of hydrogenating 4-*tert*-butylpyridine was devised. Several attempts were required to find suitable conditions. A Parr medium-pressure shaker-hydrogenation apparatus was used. First, a solution of 4-*tert*-butylpyridine in glacial acetic acid was used with PtO_2 catalyst. In 3.25 h, the hydrogen pressure dropped from 54 to 18 psig. However, there was found to be only 28% conversion to 4-*tert*-butylpiperidine. The same catalyst (now converted to finely divided Pt metal) was washed with glacial acetic acid and reused, to determine if the catalyst had been poisoned over the course of the reaction. Despite the fact that the catalyst was already reduced (which normally accounts for some of the hydrogen uptake), hydrogen uptake was much slower in the second trial; the pressure dropped from 56 to 36 psig over 3.75 days. The conversion was 21%. A solution of absolute ethanol saturated with HCl gas was prepared, and upon titration was determined to be 6.125 M in acid. A solution of 4-*tert*-

butylpyridine in HCl sat'd. ethanol was prepared and used with fresh catalyst. Over 1.8 days the pressure dropped from 57 to 21 psig. The solution was removed from the catalyst and the ethanol was removed by rotary evaporation. The residue was dissolved in water and brought to a pH of about 12 with 3N aqueous NaOH. The resulting solution was extracted with ether, dried over anhydr. $MgSO_4$, and the ether was removed by rotary evaporation. The yield was 37%.

Finally, glacial acetic acid saturated with hydrogen chloride gas was prepared by bubbling the gas through for approximately 10 min. The HCl sat'd. HOAc was titrated with 3N NaOH to a canary yellow endpoint using Thymol Blue (pK_a 1.65, endpoint reported to be approximately pH 1.5). This endpoint should reflect the dissolved hydrogen chloride without being significantly affected by the presence of acetic acid. The mixture was found to be 2.1 M HCl in HOAc. A solution of 7.4 mmol 4-*tert*-butylpyridine in 20 mL of glacial acetic acid was prepared and charged with approximately 5 mol% PtO_2 catalyst. Acid-saturated HOAc (5.4 mL) was added to the mixture and it was hydrogenated for 18.5 h. Over this time the pressure dropped from 62 to 13 psig. The vessel was then repressurized to 59 psig and allowed to react for 2 additional hours. The solution was washed off the catalyst with 50 mL HOAc. Then 50 mL of water were added and the mixture was iced and brought to pH 12 with 6N aqueous NaOH. The cloudy mixture which resulted was extracted with 3x150 mL Et_2O. The ether solution was dried over anhydrous magnesium sulfate and the solvent was removed by rotary evaporation. The conversion was determined to be 100% by ^{1}H-NMR. The reaction was scaled up to 10 g of pyridine using the same catalyst from the successful small-scale trial (now reduced to platinum). The reaction was in this case run open to the main reservoir of the Parr hydrogenation apparatus. The reaction was closely monitored and repressurized as necessary. Due to a lack of significant conversion after 4 days, another 5 mol% catalyst was added. This was done with extreme care, as the catalyst reduces very quickly upon

contacting the hydrogen-saturated solution in the hydrogenation vessel. Workup and analysis as above showed 86% conversion at an estimated 126 turnovers for the platinum catalyst (assuming no product from the initial 5 mol%).

N-Benzoyl-4-*tert*-butylpiperidine. The entire product from the previous step was placed in a 500 mL round-bottom flask equipped with a magnetic stirrer. Sodium hydroxide (3.9 g) was dissolved in 30 mL water and added to the flask. When the mixture had become homogenous, benzoyl chloride (8.8 mL, 1.01 eq) was added. The mixture was stirred for 1.25 h. The reaction mixture was diluted with 17 g sodium hydroxide in 100 mL water and was extracted with toluene. The toluene solution was then washed with 10% aqueous HCl, dried over anhydrous magnesium sulfate, and the toluene was removed by rotary evaporation with gentle heating.[149]

1,5-Dibromo-3-*tert*-butylpentane. Crude benzoylpiperidine (3.5 g) from the previous step was distilled under reduced pressure to yield pure N-benzoyl-4-*tert*-butylpiperidine (3.43 g, 14.0 mmol). Phosphorus tribromide (5 g, 18.7 mmol) was added to the pure N-benzoyl-4-*tert*-butylpiperidine after purging the distillation receiver with argon. The flask was then heated under static argon pressure until the benzoylpiperidine dissolved. Stirring was begun with cooling in an ice bath, and then liquid bromine (2.8 g, 17.5 mmol) was added. After a few minutes, the flask was connected to a distillation head with a vacuum adapter and a receiver cooled with a dry ice-acetone bath. The flask was heated with stirring, but no gas evolved as per the literature procedure. Vacuum was applied and all the volatile components were distilled into the receiver as a bright yellow solid. The solid was melted into a large excess of water and stirred under static argon pressure for a few days. The $POBr_3$ was decomposed into phosphoric and hydrobromic acids. The acid hydrolyzed some of the benzonitrile produced by the cleavage, forming benzoic acid. The water-product mixture was extracted with pentane, dried over anhydrous

magnesium sulfate, and the pentane was removed by rotary evaporation at the maximum pressure which would remove pentane at room temperature.[150] The residue was examined by GC/MS and found to consist of 24 mol% benzonitrile, 6 mol% benzoic acid, and 71 mol% 1,5-dibromo-3-*tert*-butylpentane. This mixture was used without further purification in the next step.

4-*tert*-Butylthiane. The mixture from the previous step (1.64 g, 5 mmol dibromopentane) was placed in a 50 mL round-bottom flask. Sodium sulfide nonahydrate (1.8 g, 7.5 mmol) was heated in 8 mL absolute ethanol. A fine suspension and yellow precipitate formed. Absolute ethanol (4 mL) was added to the flask containing the dibromopentane, along with a magnetic stirrer, and the system was fitted for reflux. The system was purged with argon. The sodium sulfide suspension was added and the mixture was refluxed for 24 h. The mixture was then diluted with 240 mL 10% aqueous NaOH and was extracted with 4x75 mL pentane. The extract was dried over anhydrous magnesium sulfate and the pentane was removed by rotary evaporation. An oily yellow residue was obtained and was analyzed by GC/MS. It was found to be pure 4-*tert*-butylthiane, but due to the yellow color this result was deemed untrustworthy. The sulfide was distilled under reduced pressure from a small quantity of lithium aluminum hydride; the distillate was colorless. Crude product (0.48 g) was distilled to produce 0.22 g of pure 4-*tert*-butylthiane.[148]

2-Trimethylstannyl-4-*tert*-butylthiane. Purified 4-*tert*-butylthiane (0.22 g, 1.4 mmol) was placed in a large test tube with a magnetic stir bar. Potassium *tert*-butoxide (0.22 g, 2.0 mmol) was added, and the tube was capped with a septum. The tube was purged with argon, then cooled to -40°C in an acetonitrile-dry ice bath with stirring. Anhydrous tetrahydrofuran (1 mL) and then 2.5 M n-butyllithium in hexanes (0.7 mL, 1.75 mmol) were added. The solution immediately became dark orange. After 1 h stirring

at -40°C, trimethylstannyl chloride (0.40 g, 2.0 mmol) in 1 mL anhydrous tetrahydrofuran was added. After brief stirring outside the bath (made necessary due to a large increase in viscosity upon addition of the stannyl chloride), the reaction mixture was allowed to stir for 2 h at -40°C. The test tube was removed from the bath and when it reached room temperature, 10 mL of distilled water were added. The reaction was allowed to stir at room temperature overnight, then was extracted with 4x50 mL hexanes. The solution was dried over magnesium sulfate, filtered, and the hexanes removed by rotary evaporation. An oily residue (0.37 g) was obtained. The residue was analyzed by GC/MS and found to be 85 mol% 2-trimethylstannyl-4-*tert*-butylthiane, with 4 mol% 1-trimethylstannylbutane and 11 mol% 4-*tert*-butylthiane remaining. Two isomers were found in a 38:1 ratio, and the more abundant isomer (0.34 g, 74%) was determined to be the cis-2-trimethylstannyl-4-*tert*-butylthiane by ^{13}C NMR (see the explanation in the Results).

MS: (peaks containing tin are reported for the ^{120}Sn isotope) 322 ($M^{+\cdot}$), 307 (-Me), 183, 165 (Me_3Sn^+), 157 (base peak, -$SnMe_3$), 135 ($MeSn^+$), 101 (-[Me_2SnCH_2 & tBu]), 87, 57 (tBu^+), 41.

HRMS ($M+H^+$) Calculated: 323.0855. Found: 323.0856.

^{13}C NMR (^{119}Sn-^{13}C couplings reported where observed): δ49.58 (C4, 47.13 Hz), 32.84 (C3, 14.5 Hz), 32.70 ($Me_3\underline{C}$, <2 Hz), 32.25 (C6, 43.03 Hz), 28.92 (C5, 5.5 Hz), 27.07 ($C(\underline{C}H_3)_3$), 25.76 (C2, 341.59 Hz), -11.26 ($Sn(\underline{C}H_3)_3$, 332.01 Hz).

^1H NMR: δ2.48 (H6a and H6e, m, 2H), 1.97 (H3e and H5e, bd, J = 12.6 Hz, 2H), 1.12-1.37 (H2a, H3a, and H5a; 3H), 0.85 (H4a, tt, J = 2.4, 10.7 Hz, 1H), 0.70 ($C(C\underline{H}_3)_3$, s, 9H), -0.01 ($Sn(C\underline{H}_3)_3$, s, 9H).

General Procedure for the Trial Deprotonation of Sulfides

All synthetically produced starting sulfides were distilled from a small quantity of lithium aluminum hydride shortly before use. This procedure guarantees a dry sample free

from both disulfides and thiols, which are the major contaminants in the synthesis. The distillations were conducted at reduced pressure and were run at the minimum temperature possible (down to room temperature, where the vacuum was adjusted such that the material boiled at ambient temperature). A dry ice-cooled receiver was employed. Those sulfides not synthesized were purchased from Aldrich and were used without further purification.

Freshly sublimed potassium *tert*-butoxide (approximately 140 mg) in a test tube was cooled under argon to the reaction temperature with an appropriate solvent-dry ice bath (for -40°C, acetonitrile was used as the solvent; for -78°C, acetone was used as the solvent). A measured amount of the sulfide was then added (approximately 1 mmol), followed by the addition of 1 mL anhydrous THF, after which stirring was initiated. After 5 min, 2.5 M n-butyllithium in hexanes (0.5 mL, 1.25 mmol) was added rapidly. Stirring was continued at low temperature for a measured time, then 0.4 mL tri-n-butylstannyl chloride was added via syringe. The mixture was stirred for an additional measured time at low temperature, and then allowed to warm to room temperature with stirring. The reaction was quenched with 10 mL of water and extracted with 3x30 mL pentane. The combined organic layer was dried over magnesium sulfate. The solvent was carefully removed on a rotary evaporator and the crude product was used for the GC/MS product study.

Summary of Previous Work

All of the materials used for the electrochemical studies in Chapter 5, with the exception of the cis-4-*tert*-butyl-2-trimethylstannylthiane, were made previously by a postdoctoral associate. Some of these syntheses have been published,[76] but those based on a modification of the method introduced by Vedejs and co-workers[151] have not been published. As they are not the work of the author, they will merely be summarized here.

2-Thiabicyclo[2.2.2]octane was synthesized by the Diels-Alder cycloaddition of thiophosgene to 1,3-cyclohexadiene, followed by reduction with lithium aluminum

hydride. 3-Trialkylstannyl-2-thiabicyclo[2.2.1]heptane was made as shown in Scheme 7.2.

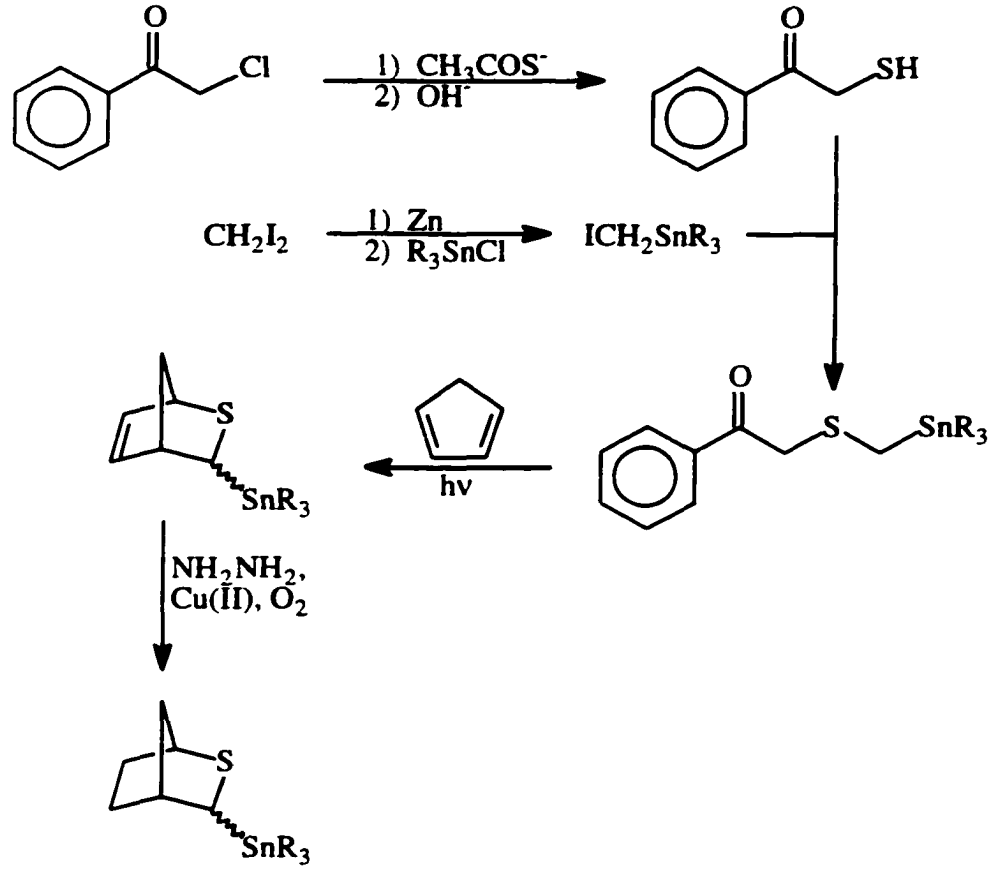

Scheme 7.2. Synthesis of 3-Trialkylstannyl-2-thiabicyclo[2.2.1]heptane.

ELECTROCHEMICAL METHODS

General Electrochemical Procedure for 1,2-Dichalcogenins and Thioethers

The solutions necessary for the cyclic voltammetric measurements (a reference solution of 0.1 M $AgNO_3$ in acetonitrile and supporting electrolyte solutions of 0.1 M tetra-n-butylammonium hexafluorophosphate in acetonitrile or dichloromethane) were always made the day of the experiment and were not stored. The exact concentration of analyte

varied somewhat from compound to compound and run to run, but was maintained near 1 mM. Acetonitrile was found to be best used as received from the supplier (Fisher), but dichloromethane was distilled under flowing argon gas from P_2O_5 immediately before use. The acetonitrile was degassed using a sonicating bath and a flow of argon to remove expelled air. Degassing the solutions was found to be critical to obtaining low residual currents in the supporting electrolyte solutions. Both a 1.6 mm diameter planar platinum working electrode and a 3 mm diameter planar glassy carbon working electrode (both from BioAnalytical Systems) were employed for various of the α-stannylated sulfides, as some showed adsorption behavior with platinum. The platinum electrode was polished on an emery pad with dry polishing alumina prior to use, while the glassy carbon electrode was polished on lint-free laboratory tissue paper with the solvent to be used (without supporting electrolyte). A 0.5 mm diameter platinum wire was used as the counter-electrode; the wire was heated to incandescence before use. The reference electrode used was a silver wire immersed in a solution of 0.1 M $AgNO_3$ in acetonitrile, which was separated from the solution by two Vycor frits (new for each day of use) sealed to the glass with heat-shrink Telfon tubing. The interstitial solution was also 0.1 M $AgNO_3$ in acetonitrile. The diffusion progress of the interstitial solution could be observed by the deposited silver in the Vycor frit; in this fashion it was assured that the solution did not change significantly over the period of use and that no silver entered the sample chamber. The entire electrochemical cell was kept under a positive pressure of argon. In the case of the 1,2-dichalcogenins, the cell was also purged in advance with argon, and before the analyte was introduced the cell was wrapped in black cloth. The electrochemistry room was also kept dark for the duration of the studies. Stirring between cyclic voltammetric sweeps was accomplished by swirling the entire cell. The potentiostat used was a Cypress Systems Model 1 computer-controlled electrochemical apparatus. Peak potentials were always reported at 100 mV/s, though data were usually acquired at a variety of sweep rates.

General Electrochemical Procedure for Tetrathiatetraasterane

Asterane electrochemistry done in dichloromethane was executed as detailed above, but many other solvents were also attempted for asterane. In addition to a variety of solvents, asterane consumption was kept to a minimum by employing a smaller cell volume. To accomodate these needs, a modified electrochemical system was used. Data collected by this method are referred to in the text as data collected with the "bundle" electrode. This electrode was constructed from the aforementioned 1.6 mm diameter Teflon-jacketed planar platinum electrode from BAS. Two 0.5 mm diameter platinum wires, cleaned in advance by heating to incandescence, were bound to either side of the Teflon jacket with PTFE (polytetrafluoroethylene) tape. This "bundle" electrode just fit inside a 1 mL volumetric vial, with the PTFE tape binding making a loose stopper in the mouth of the vial. Solutions in the vial, which were often viscous due to the nature of the solvent, were agitated by pistoning the electrode in the vial.

Solvents such as dichloromethane and liquid sulfur dioxide were used with tetra-n-butylammonium hexafluorophosphate (TBAHFP) as supporting electrolyte, at 0.1 M when the concentration could be accurately controlled. A mixture of dichloromethane and trifluoroacetic anhydride was used to determine the effect of lowered water content; this mixture was produced by adding two drops of TFAA to a 5 mL solution of 0.1 M TBAHFP. Ninety-eight percent sulfuric acid and 20% fuming sulfuric acid were used without a supporting electrolyte. Fluorosulfonic acid and triflic acid were converted into 0.1 M solutions of acid and conjugate potassium salt by adding the prerequisite amount of potassium chloride and removing the hydrogen chloride gas with gentle vacuum.

Asterane was also analyzed by both carbon-paste electrode and thin-layer electrode. The former was constructed by mixing a spatula-full of carbon black (from acetylene, 50% compressed, APS, <1 μm, 99.9+% [metals basis], Alfa) with a solution of 1.5 mg of asterane in 15 mL of dichloromethane. This mixture was allowed to evaporate, and then

the asterane-impregnated carbon black was mixed with boiling-point-grade silicone oil until a oily-clay texture was acheived. The mixture was packed into a Pasteur pipette and a heavy-gauge copper wire (cleaned with nitric acid, washed, and dried) was inserted into the mixture to act as an electrical contact. The mixture was extruded slightly to make contact with the supporting electrolyte solution, and the surface could be refreshed by cutting it off with a razor blade and extruding a fresh amount of mixture. The supporting electrolyte was 0.1 M lithium perchlorate in water, and the data were acquired versus a Ag/0.1 M $AgNO_3$ in acetonitrile reference electrode, with a 0.5 mm diameter platinum wire (cleaned by heating to incandescence) as counterelectrode. Comparison electrodes of thianthrene and ferrocene were made similarly, except the analytes were mixed in a mortar and pestle directly with the carbon black.

The thin-layer electrode was constructed by placing a drop at a time of a saturated solution of asterane in dichloromethane on the upturned face of the 3 mm diameter planar Teflon-jacketed glassy carbon electrode (BAS) until a film was visible. This was used with a supporting-electrolyte solution of 0.1 M TBAHFP in acetonitrile, versus a Ag/0.1 M $AgNO_3$ in acetonitrile reference electrode, with a 0.5 mm diameter platinum wire (cleaned by heating to incandescence) as counterelectrode.

APPENDIX A

ASTERANE: COMPUTATIONAL SIMULATION, ANALYSIS, AND EXPLORATORY ELECTROCHEMICAL STUDIES

SIGMA AROMATICITY

The idea that compounds with electrons possessing cyclic σ-type overlap might also display characteristics more typically associated with cyclically-conjugated π electron systems is not new. This concept has been used to explain the low strain energy of cyclopropane (as compared to calculations of what it should be, based on angle strain).[152-154] It is a more recent concept that lone pair electron systems might also share in aromatic or anti-aromatic properties.[155,156] Such systems are particularly interesting since they present an opportunity to investigate electron delocalization interactions without interference from bonding electrons.

An excellent example of this concept is hexaiodobenzene. Hexaiodobenzene possesses six iodine atoms, and each atom possesses one p-type lone pair orbital of the proper alignment to overlap with both its neighboring iodines. Six such filled orbitals comprise a system of 12 electrons overlapping in a σ-type fashion. However, 12 electrons should be Hückel antiaromatic (4n e^-). If two electrons are removed, the system would be expected to display aromatic characteristics, and indeed it does. It is unusually easy to remove two electrons from hexaiodobenzene, and an unusually stable dication is formed. Unlike the NMR spectra of most cationic species, in which the carbon chemical shifts are greatly increased due to a drop in electron density, the carbon chemical shifts of hexaiodobenzene dication are upfield of its neutral parent. This is interpreted as indicating the presence of a 10 electron ring current through the iodines, thereby placing the carbon atoms in the shielding zone. The NMR also demonstrated that the dication is a singlet

species.[157] A similar experiment conducted with hexachlorobenzene, created a triplet species of lower symmetry than the parent which showed no evidence of aromaticity.[158] Presumably this is because the chlorine orbitals are too small for effective overlap and and the chlorine electrons are too tightly held for efficient delocalization, while the iodine orbitals are large enough for good overlap and the electrons are loosely held.

More recently, evidence has emerged for the dication of hexakis(methylthio)benzene as a transient species in the Pummerer-type rearrangement of the monoxide. The dication was computationally predicted (B3LYP/6-31G*) to be σ-delocalized, in a fashion very similar to the aforementioned hexaiodobenzene dication.[159] In contrast, the ring in the dication of hexakis(dimethylamino)benzene was found to be highly twisted.[160] Of course, there is no evidence yet that the ring in hexakis(methylthio)benzene is not similarly deformed in the dication.

In search of an example even less contaminated by complications (such as the aromatic π system in hexaiodobenzene), tetrathiatetraasterane (heretoafter referred to simply as asterane) was synthesized.[161] This molecule possesses four sulfur atoms in fairly close proximity, and enforces a geometry which requires the highest energy orbitals, the sulfur p-type lone pairs, to be co-planar and in good alignment for overlap.

HÜCKEL VS. MÖBIUS AROMATICITY[162-164]

When considering aromatic systems it is important to remember that orbital symmetry plays a large role in the nature of the cyclically conjugated system. Most chemists are familiar with Hückel aromaticity. With this type of aromaticity, 4n+2 electrons are stabilized, while 4n electrons are destabilized. However, many chemists may not be familiar with the orbital overlap requirements of Hückel aromaticity. It requires that the orbital overlap possesses an even number of interatomic nodes. Since inverting a p-

orbital, for example, which was in phase with its neighbors creates two nodes (an even number), it can be demonstrated that the precise assignment of signs is irrelevant, so long as one considers the oddness or evenness of the number of interatomic nodes. All orbitals engaged in π-type overlap automatically qualify as Hückel systems, since all of the contributing p-type orbitals can be phased "up" or "down" and thereby have no nodes between atoms (zero being considered an even number for the purposes of this discussion).

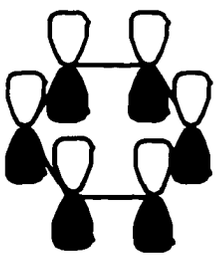

Figure A.1. p-Type Orbitals in Benzene: π-Type Overlap with No Interatomic Nodes.

Note that there are nodes in this maximum-overlap picture; they are atomic orbital nodes (in the plane of the ring), and are therefore not interatomic nodes.

Unlike π-type overlap, in σ-type overlap it is possible to have nodes in the maximum overlap model. For example, barrelene has some overlap between each ethylenic unit; this overlap cannot be arranged in such a fashion as to have no interatomic node.

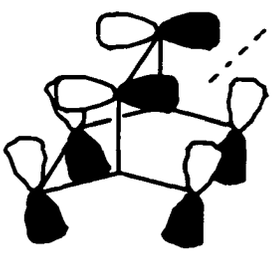

Figure A.2. Barrelene Maximum Overlap Model.
(dashed line indicates the interatomic node)

Molecules for which the maximum overlap model must possess one node (or for which any atomic orbital arrangement possesses an odd number of nodes) have Möbius aromaticity. Möbius aromaticity stabilizes molecules with 4n electrons, while destabilizing systems of 4n+2 electrons.

For this reason, lone-pair systems are Hückel systems if they are comprised of an even number of lone-pair centers (2n centers), while they are Möbius systems if they are comprised of an odd number of lone-pair centers (2n+1 centers). In addition, since neutral systems will have twice the number of electrons as centers, all neutral Hückel lone-pair systems would be expected to be anti-aromatic (4n electrons), and all neutral Möbius lone-pair systems would also be expected to be anti-aromatic (4n+2 electrons). The neutral states of both hexaiodobenzene and tetrathiaasterane should be destabilized, while the dication states should be stabilized.

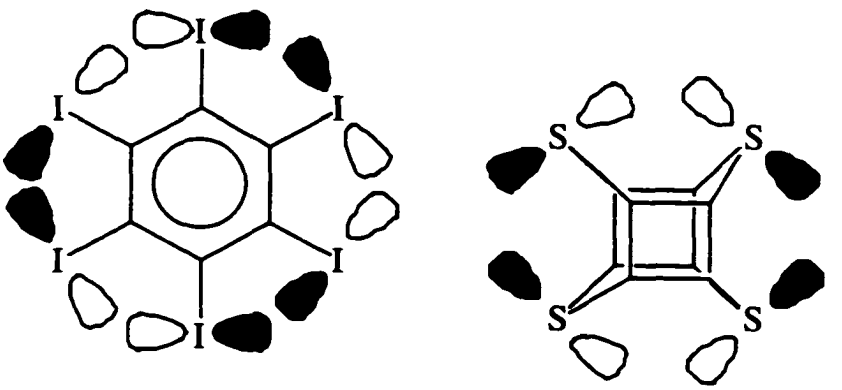

Figure A.3. Hexaiodobenzene and Tetrathiaasterane Maximum Overlap.

COMPUTATIONAL RESULTS

The first step of any good in-depth computational study is an educated choice of method and basis set. Methods which are good for certain types of calculations are not

always best for others, especially since the definition of "best" must include such factors as whether the available computational resources are capable of completing a calculation done in the "best" way possible. It has also been demonstrated (See Chapter 3) that the largest basis set does not always yield the most accurate result. To determine the best compromise of computational efficiency and accuracy, a survey of asterane optimized geometries was conducted by a few of the better methods using basis sets proven reliable for other purposes. The results were compared to the data obtained from X-ray crystallographic analysis of asterane.

Two things should be noted. The X-ray data showed a geometry very close to the expected D_{4h} symmetry, but very slightly asymmetric; for the purposes of this analysis it is assumed that this distortion is due to crystal packing effects. This explanation seems reasonable given the very small deviation from true D_{4h} symmetry. It is also not expected that there would be any symmetry-lowering distortion due to a Jahn-Teller effect since all computations predict a non-degenerate HOMO. This is particularly significant since the geometry optimization calculations were started from a D_{4h} structure; due to the nature of the diagonalization procedure used in essentially all computational chemistry programs, this starting symmetry will be preserved by the computer even if symmetry-breaking could lead to a lower energy. To check the validity of this assumption, Hartree-Fock vibrational frequency calculations were also carried out, and in fact the D_{4h} symmetry assumption was found to be incorrect for asterane dication. The actual species was located by examining the negative frequency found for the D_{4h} symmetry and then applying a corresponding distortion to the neutral geometry before re-optimizing for the dication species. The neutral and radical cation species were found to be vibrationially stable. The high symmetry of those species made possible calculations which would otherwise have been beyond reach.

Table A.1. Comparison of Asterane Geometric Parameters.

Parameter	Experimental[a]	MP2 6-31+G*	B3PW91 6-31+G*	B3PW91 LANL2DZ
Bond Length (Å)				
C-S	1.793-1.798	1.80	1.81	1.87
C-C	1.553-1.559	1.56	1.56	1.57
C-H	0.9800 [b]	1.10	1.10	1.09
S-S Distance (Å)	3.29	3.25	3.25	3.31
Bond Angle (°)	110.1-110.2	105.3	105.3	104.4
H-C-S				
H-C-C	110.1-110.2	112.8	112.9	113.5
C-C-S	117.19-117.70	117.9	117.8	117.8
C-C-C	89.73-90.24	90.0	90.0	90.0
C-S-C	98.48-98.50	97.1	97.5	97.4
Dihedral Angle (°)	0.10	0.0	0.0	0.0
C-C-C-C				
C-S-C-C	52.63-52.92	53.2	53.1	53.1
S-C-C-C	121.07-121.70	122.0	121.8	121.8
S-C-C-S	0.02-0.54	0.0	0.0	0.0
C-S-C-H	180.0	180.0	180.0	180.0
C-C-C-H	109.4	114.8	115.0	115.8
H-C-C-H	0.0	0.0	0.0	0.0
S-C-C-H	126.8	123.2	123.2	122.4

[a] Experimental data are taken from X-ray crystallographic analysis; range is due slight deviation from D_{4h} symmetry.

[b] Carbon-hydrogen bond lengths are routinely underestimated by X-ray crystallographic analysis since hydrogen possesses no core electrons to deflect X-rays in the region of the nucleus; the result is that the only deflection demonstrating the presence of hydrogen is that from the bonding electrons in the X-H bond, which are obviously not located at the same distance as the hydrogen.

As can be seen in Table A.1, the MP2 and the B3PW91 methods yielded nearly identical results when both were used with the augmented split-valence basis set 6-31+G*; the LANL2DZ basis set, used to account for relativistic effects in heavy atoms, gave poor results. The features of these methods and basis sets are discussed in greater detail in Chapters 3 and 7. Since the B3PW91 method seemed to be as good as, if not slightly better than, the MP2 method for asterane, and since the MP2 method was so computationally costly that no more complicated calculations could be executed with it, the B3PW91 method with the 6-31+G* basis set was chosen for all further calculations.

However, since MP2 eigenvalues have a reputation for being more accurate (the evidence considered, a relative advantage only), they are reported rather than the DFT eigenvalues.

Table A.2. Asterane Eigenvalues and PES Comparison.

Orbital	Symmetry	Degeneracy	Eigenvalue (eV)	PES Orbital Energy (eV)
HOMO	B_{2G}	1	9.13	8.188
HOMO-1	A_{2G}	1	9.20	8.288
HOMO-2	E_U	2	9.50	8.19-8.56
HOMO-3	B_{2U}	1	11.62	10.25
HOMO-4	E_U	2	11.69	10.62
HOMO-5	B_{1G}	1	12.40	11.29
HOMO-6	E_G	2	13.60	11.91
HOMO-7	A_{1G}	1	13.71	12.32-13.00
HOMO-8	E_G	2	13.90	14.06
HOMO-9	A_{1G}	1	14.73	14.69
HOMO-10	E_G	2	16.10	15.32
HOMO-11	B_{1U}	1	16.49	

The same calculations were used to visualize the orbitals, and simplified diagrams are included below.

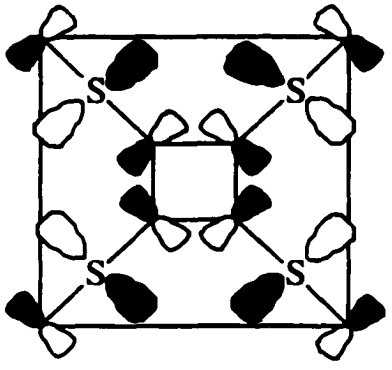

Figure A.4a. Exploded Overhead View: HOMO.

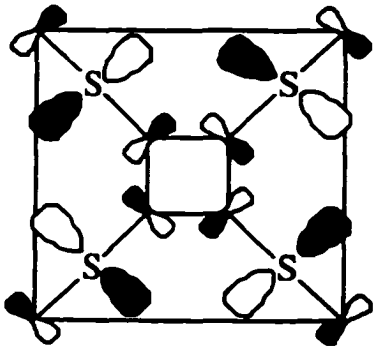

Figure A.4b. Exploded Overhead View: HOMO-1.

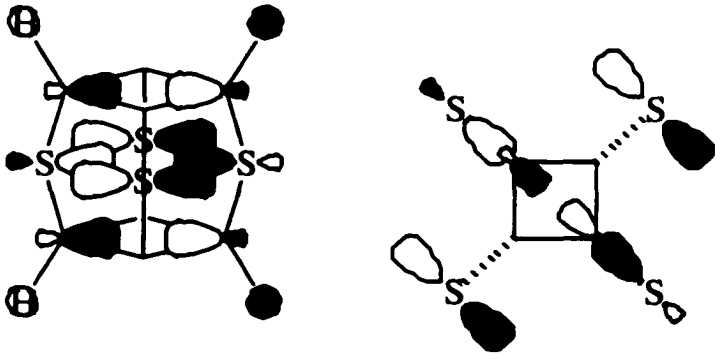

Figure A.4c. Elevated Side View (left) and Overhead View (right): Doubly-Degenerate HOMO-2.
The two E_u molecular orbitals differ by a 90° rotation about the four-fold axis.

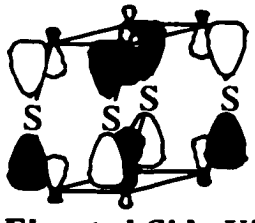

Figure A.4d. Elevated Side View: HOMO-3.

As the MP2 calculations were too computationally expensive for calculation of states other than the ground, B3PW91/6-31+G* was employed to calculate the relative energies and geometries of the cation radical (both adiabatic and non-adiabatic) and dication.

Table A.3. Asterane Ionization Potentials and Oxidized State Geometries.

Parameter	Neutral Species	Cation Radical
Bond Length (Å):		
C-C	1.56	1.55
C-H	1.09	1.09
C-S	1.81	1.82
S-S Distance (Å):	3.25	3.20
Bond Angle (°):		
C-C-C	90.0	90.0
C-C-S	117.8	116.9
C-S-C	97.5	100.4
H-C-C	112.9	114.1
H-C-S	105.3	104.9
Dihedral Angle (°):		
C-C-C-S	121.8	120.5
C-C-C-H	115.0	116.6
S-C-C-H	123.2	122.9
C-S-C-C	53.1	52.5
S-C-C-S	0.0	0.0
H-C-C-H	0.0	0.0
C-C-C-C	0.0	0.0
H-C-S-C	180.0	180.0
Energy (eV)	0.00	7.92 (8.31[a])

[a] Non-adiabatic ionization potential.

The HF method was used to simulate the vibrational spectrum of asterane at the MP2 geometry. This is not an altogether sound method, as is discussed in Chapter 7, but the reliability of the result can be tested by examining the number of predicted negative vibrations; if one or more negative vibrations are found, the MP2 structure is too far from the minimum structure calculated by the HF method for reliable simulation, but if all vibrations are positive the minima coincide sufficiently to allow analysis.

The vibrations of asterane are interesting due to the high molecular symmetry. They occur as sets of motions in which, in most cases, all allowed symmetries are present, though only some are active. Below, the vital statistics of the vibrations are tabulated, then the motions are described. As was found in general for asterane, transitions of E symmetry are doubly-degenerate while all others are singly degenerate.

Table A.4. Vibrational Frequencies of Asterane.

Symmetry	Frequency (cm^{-1})	Infrared Intensity (KM/mol)	Raman Scattering Activity (A^4/amu)	Raman Depolarization Ratio
B_{2G}	257.9	0	1.2871	0.7500
E_U	259.2	1.9089	0	0
B_{2U}	310.0	0	0	0
A_{1G}	372.7	0	8.3703	0.2147
B_{1G}	431.3	0	9.9650	0.7500
E_G	436.0	0	6.6173	0.7500
A_{1U}	457.1	0	0	0
A_{2G}	554.4	0	0	0
E_U	615.7	1.9414	0	0
A_{1G}	637.1	0	53.2166	0.0068
A_{2U}	646.3	5.3020	0	0
E_U	729.1	21.9299	0	0.7407
E_G	731.4	0	5.8283	0.7500
B_{2U}	889.7	0	0	0
B_{1G}	939.3	0	2.5706	0.7500
B_{2U}	972.2	0	0	0
B_{1U}	1007.2	0	0	0
B_{2G}	1019.7	0	22.1753	0.7500
B_{1G}	1039.1	0	0.1330	0.7500
E_G	1071.1	0	0.3914	0.7500
E_U	1078.1	4.9688	0	0.7199
A_{2U}	1118.6	3.6412	0	0
A_{1G}	1122.1	0	9.8041	0.4543
B_{2G}	1267.2	0	0.1195	0.7500
B_{1U}	1270.6	0	0	0
E_G	1344.1	0	2.5833	0.7500
A_{2U}	1383.5	0.2124	0	0
A_{2G}	1387.6	0	0	0
A_{1U}	1389.6	0	0	0
E_U	1394.7	1.0378	0	0
E_G	1417.6	0	8.5651	0.7500
B_{2U}	1441.2	0	0	0
E_U	1449.5	0.1363	0	0
A_{1G}	1469.4	0	7.6841	0.7497
B_{1G}	1491.8	0	20.6624	0.7500
B_{1G}	3123.3	0	31.7394	0.7500
B_{2U}	3125.8	0	0	0
E_U	3139.1	14.3672	0	0
E_G	3141.6	0	172.3255	0.7500
A_{1G}	3159.5	0	643.1623	0.1365
A_{2U}	3160.3	112.9213	0	0

The vibrational motions may be fairly easily grouped. To describe them, it will be necessary to introduce a few conventions. The symmetries of the molecule are such that

the motions may be grouped into "radially symmetric", meaning that the motion would be identical if the molecule were rotated through 90° about the four-fold axis, and "radially antisymmetric". They may also be grouped into "+/-z symmetric" and "+/-z antisymmetric", referring to whether the atomic motions are in the same or opposite sense or direction in both cyclobutane rings. Other, lesser, symmetries will be described as necessary.

Starting with the higher frequencies, the first set is, of course, the C-H stretches. If one assigns the x- and y-axes to the two orthogonal axes passing through two diagonally-opposite sulfur atoms, the C-H stretches can be easily described by noting whether the hydrogen atoms oriented along each axis are in phase (+) or antiphase (-). The C-H stretches come in "+/-z symmetric/antisymmetric" pairs; the symmetric motion will be listed first, then the antisymmetric: all hydrogens attached to each ring in phase (+xy), 3159.5 cm^{-1} symm., 3160.3 cm^{-1} antisymm.; (+x, no y) and (+y, no x) doubly-degenerate pair, 3139.1 cm^{-1} symm., 3141.6 cm^{-1} antisymm.; and (+x,-y), 3123.3 cm^{-1} symm., 3125.8 cm^{-1} antisymm.

The next set is the C-H bends. These are a little more complex, since two bending motions need to be considered. The first are twisting bends that keep the hydrogen atom at a fairly constant distance from the four-fold axis; these motions are labelled clockwise (+°) and counterclockwise (-°). There are also bends which move along one of axes discussed in the previous paragraph, which move the hydrogen atoms towards and away from the four-fold axis. When the hydrogens on the x-axis move toward the four-fold axis in phase, this will be denoted +x, and so forth as above. Also as above, the "+/-z symmetric" motion will be listed first, then the "+/-z antisymmetric" motion: (+x,+y), 1469.4 cm^{-1} symm., 1383.5 cm^{-1} antisymm.; (+x,-y), 1491.8 cm^{-1} symm., 1441.2 cm^{-1} antisymm.; (+°x,+°y), 1387.6 cm^{-1} symm., 1389.6 cm^{-1} antisymm.; (+°x,-°y), 1267.2 cm^{-1} symm., 1270.6 cm^{-1} antisymm. There are also several doubly-degenerate motions in which

hydrogens along one axis move in a disrotatory fashion while hydrogens on the other axis move toward the four-fold axis in an antiphase fashion. The direction of displacement of disrotatory hydrogens on the x-axis, for example, will be denoted by + or -y (since they are being displaced parallel to the y-axis), and vice versa for disrotatory hydrogens on the y-axis. The previous convention of denoting the motion of hydrogens toward the four-fold axis will be retained. This will not cause confusion due to the limitations of symmetry. The "z symmetric" convention will be employed as above: (+x,+x) and (+y,+y), 1449.5 cm^{-1} symm., 1417.6 cm^{-1} antisymm.; (+x,-x) and (+y,-y), 1394.7 cm^{-1} symm., 1344.1 cm^{-1} antisymm.

The next category is C-C stretches. These are very simple, and fall into three groups: totally symmetric, in which the cyclobutane rings simply shrink and expand without distorting shape; a doubly-degenerate pair of kite-shaped distortions caused by the contraction of adjacent C-C bonds antiphase to the expansion of the opposite pair of adjacent C-C bonds (one of the doubly-degenerate motions is a 90° rotation of the other); and a rectangular distortion caused by the contraction of opposite C-C bonds antiphase to the expansion of the other pair of opposite C-C bonds. The "z symmetric" convention will be employed as before: radially in-phase, 1122.1 cm^{-1} symm., 1118.6 cm^{-1} antisymm.; kite-shaped distortions, 1078.1 cm^{-1} symm., 1071.1 cm^{-1} antisymm.; and rectangular distortion, 1019.7 cm^{-1} symm., 1007.2 cm^{-1} antisymm.

The C-S stretches are somewhat confused due to some coupling between the C-S stretches and C-C-C bends. They can be classified into the singly-degenerate radially-symmetric C-S stretches, and both a singly-degenerate and two doubly-degenerate motions best described by viewing asterane along an axis perpendicular to the four-fold axis which passes two diagonally-opposite sulfur atoms. From this point of view, atomic motions in the singly degenerate case are mirrored left and right, while in the doubly-degenerate motions the atomic motions on the left are antiphase to those on the right; in both cases the

atoms in the plane containing the view axis and the four-fold axis do not move. This viewpoint will be referred to in later paragraphs as the "sulfur-axis" view. In the first category, the simplest motion is the completely symmetric C-S stretch at 637.1 cm^{-1}, accompanied by its "z antisymmetric" analogue at 646.3 cm^{-1}. In the more complex category, the simplest is a singly-degenerate motion in which the four C-S bonds in motion are all in phase (at 972.2 cm^{-1}). The action of this motion on the cyclobutane rings cause it to be coupled effectively with a "z antisymmetric" mode of cyclobutane ring pucker. In the doubly-degenerate cases, where the left-hand motions are antiphase to the right-hand motions, there are two pairs. Each pair is related by a 90° rotation about the four-fold axis. In the first, both left-hand C-S bonds contract as the right hand bonds stretch (615.7 cm^{-1}), while in the second the upper-left-hand and lower-right-hand C-S bonds contract as the lower-left-hand and upper-right-hand C-S bonds stretch (731.4 cm^{-1}).

There is only one degenerate pair of C-C-S bending motions. If one views asterane down an axis perpendicular to the four-fold axis which passes through the center of one the 1,4-dithiane rings, the motions may be described as the upper left and lower right C-C-S bond angles opening, while the lower left and upper right C-C-S bond angles close (antiphase motion). From this viewpoint, the bonds in the front and rear of the molecule are in phase. The two doubly-degenerate motions, at 436.0 cm^{-1}, are related by a 90° rotation about the four-fold axis. Related to this motion is the C-C-S wagging, which causes a twisting motion of the molecule when "z antisymmetric" and an apparent wagging of the sulfur atoms when "z symmetric". The twist motion is found at 457.1 cm^{-1}. The other motions will be described as for the twisting motions of hydrogens above. There are two singly-degenerate conrotatory motions and one doubly-degenerate disrotatory motion. The (+°x,+°y) conrotatory motion is found at 554.1 cm^{-1}, while the (+°x,-°y) conrotatory motion is found at 257.9 cm^{-1}. The pair of doubly-degenerate disrotatory motions involve

the disrotatory motion of only sulfur atoms on the x-axis and only sulfur atoms on the y-axis. They are found at 259.2 cm^{-1}.

The C-C-C bends, one of which is already described as coupled to a C-S stretch, involve the rhomboidal distortion of the cyclobutane rings. This forces them to couple efficiently to the cyclobutane puckering motion. The two pure cyclobutane puckers are the "z symmetric" motion at 310.0 cm^{-1} and the "z antisymmetric" motion at 1039.1 cm^{-1} (similar to the previously described coupled motion, and also slightly coupled). The true "z symmetric" rhomboidal distortion is found at 939.3 cm^{-1}, but the "z antisymmetric" rhomboidal distortion is coupled to a "z symmetric" puckering motion, and is found at 889.7 cm^{-1}.

Finally there are the C-S-C bends. There are two singly-degenerate motions: the fully in-phase motion at 372.7 cm^{-1}, and the (+x,-y) antiphase motion at 431.3 cm^{-1}. There is also a doubly-degenerate motion best discussed using the previously mentioned "sulfur-axis" viewpoint. The pair is related by a 90° rotation about the four-fold axis, and the motion consists of the left-hand C-S-C bond angle opening as the right-hand bond angle closes, and the motion is found at 729.1 cm^{-1}.

To assess an possible evidence for sulfur-sulfur bonding interaction in the radical cation, the vibrational frequencies of the radical cation were compared to those of the neutral species.

Table A.5. Vibrational Frequency Comparison.

Symmetry	Neutral Frequency (cm^{-1})	Radical Cation Frequency (cm^{-1})	ΔFrequency (cm^{-1})
B_{2G}	257.9	201.2	-57
E_U	259.2	253.8	-5
B_{2U}	310.0	312.1	+2
A_{1G}	372.7	353.4	-19
B_{1G}	431.3	439.5	+8
E_G	436.0	433.9	-2
A_{1U}	457.1	449.9	-7
A_{2G}	554.4	534.2	-20
E_U	615.7	594.6	-21
A_{1G}	637.1	619.1	-18
A_{2U}	646.3	648.4	+2
E_U	729.1	707.6	-22
E_G	731.4	721.8	-10
B_{2U}	889.7	887.3	-2
B_{1G}	939.3	923.2	-16
B_{2U}	972.2	952.9	-19
B_{1U}	1007.2	1027.3	+20
B_{2G}	1019.7	1036.2	+17
B_{1G}	1039.1	1044.6	+6
E_G	1071.1	1082.5	+11
E_U	1078.1	1096.2	+18
A_{2U}	1118.6	1136.3	+18
A_{1G}	1122.1	1136.5	+14
B_{2G}	1267.2	1277.0	+10
B_{1U}	1270.6	1273.9	+3
E_G	1344.1	1352.3	+8
A_{2U}	1383.5	1390.5	+7
A_{2G}	1387.6	1391.6	+4
A_{1U}	1389.6	1391.3	+2
E_U	1394.7	1410.6	+16
E_G	1417.6	1418.1	+1
B_{2U}	1441.2	1433.1	-8
E_U	1449.5	1458.5	+9
A_{1G}	1469.4	1477.7	+8
B_{1G}	1491.8	1499.1	+7
B_{1G}	3123.3	3172.1	+49
B_{2U}	3125.8	3173.3	+48
E_U	3139.1	3182.9	+44
E_G	3141.6	3184.6	+43
A_{1G}	3159.5	3197.2	+38
A_{2U}	3160.3	3198.0	+38

Configuration-interaction by single excitation (CIS) with 6-31+G* was used to analyze the electronic transitions of asterane. All transitions were found to be forbidden; of course, in the realm of forbidden transitions, the spin-forbidden transitions should exhibit a larger molar absorptivity than the symmetry-forbidden transitions, due to the fairly large spin-orbit coupling of sulfur atoms. The experimental value was found to be λ_{max} = 230 nm (ε = 600).

Table A.6. Electronic Transitions of Asterane: Symmetries, Energies, Oscillator Strengths, and Contributing Transitions.

Transition Symmetry[a]	Transition Energy (nm)	Contributing MOs and Coefficients[b]
$^3A_{1U}$	237	HOMO-1 → LUMO+9, -0.31808
		HOMO → LUMO+8, 0.19198
$^3B_{1U}$	234	**HOMO-1 → LUMO+8, 0.21163**
		HOMO → LUMO+9, -0.30518
^3E_G	232	**HOMO-1 → LUMO+30, 0.18635** and
		HOMO-1 → LUMO+2, 0.19679
$^1A_{1U}$	211	HOMO-1 → LUMO+9, -0.32629
		HOMO → LUMO+8, 0.21305
$^1B_{1U}$	207	**HOMO-1 → LUMO+8, 0.23034**
		HOMO → LUMO+9, -0.31730
$^3B_{2G}$	206	**HOMO → LUMO, 0.36644**
		HOMO → LUMO+6, -0.33291
^1E_G	205	**HOMO-3 → LUMO+9, 0.26795** (both)
$^3A_{2G}$	205	**HOMO-1 → LUMO, 0.34021**
		HOMO-1 → LUMO+6, -0.35292
$^1B_{2G}$	188	**HOMO → LUMO, 0.52708**
$^1A_{2G}$	186	**HOMO-1 → LUMO, 0.50299**

[a] All E symmetry transitions are doubly-degenerate. All other transitions are singly degenerate.

[b] The largest positive contribution is always listed in bold, along with any other contributor with a magnitude greater than 0.3.

Calculations on the asterane dication showed that the D_{4h} species possessed a negative-fequency vibration in which a carbon-carbon bond in the cyclobutane ring expanded. The neutral species geometry was taken as a starting point, and the carbon-carbon bond was manually lengthened. This led to a C_S-symmetry species in which the cyclobutane ring on one end of the molecule was opened (Table A.7). The asterane dication non-adiabatic ionization potential was calculated to be 20.59 eV.

Table A.7. Asterane Dication Calculated Geometric Parameters and Heavy-Atom Charges.

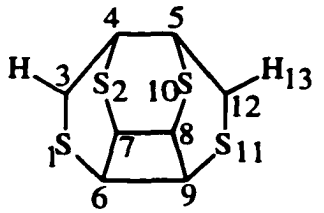

Parameter	Location	Value
C-H Bond Length (Å)	Opened Ring	1.09
	Closed Ring	1.10
C-C Bond Length (Å)	3-4	1.48
	4-5	1.55
	6-7	1.58
	7-8	1.56
	6-9	1.55
C-C Distance (Å)	3-12	3.31
C-S Bond Length (Å)	1-3	1.68
	1-6	1.80
	2-4	1.84
	2-7	1.80
S-S Distance (Å)	1-2	3.23
	2-10	3.24
	1-11	3.49
C-C-C Bond Angle (°)	3-4-5	126.6
	6-7-8	89.9
	7-6-9	90.1
C-C-S Bond Angle (°)	1-3-4	132.1
	2-4-5	117.3
	4-5-10	91.3
	1-6-7	115.9
	1-6-9	2.5
	2-7-6	118.5
	2-7-8	117.8
C-S-C Bond Angle (°)	3-1-6	101.1
	4-2-7	95.8
Charge: Carbon	3	-0.08
	4	+0.13
	6	-0.01
	7	-0.03
Charge: Sulfur	1	+0.52
	2	+0.47

Due to the great interest in the possibility of cyclic delocalizing interaction of electrons in the sulfur 3p lone pair orbitals, calculations were undertaken to simulate

various asterane analogues where the conjugation was interrupted with various structural features. Geometric features pertinent to the comparison, along with ionization potentials, are summarized below.

Table A.8. Parameters of Various "Interrupted" Asteranes.

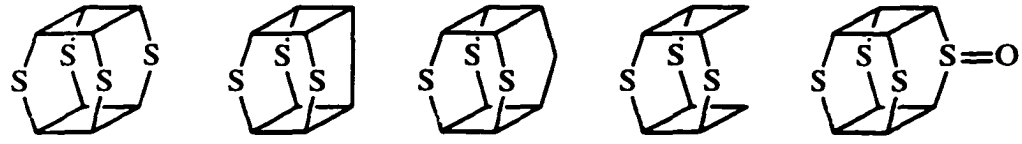

A B C D E

Parameter	A	B	C	D	E
Neighboring S-S Distance (Å)	3.25	3.21	3.24	3.33	3.25[a]
C-C Bond Length (Å) between cyclobutadiene rings		1.54	1.53		
S-H Distance (Å) from methylene			2.99		
C-C Distance (Å) between methylenes				3.43	
H-H Distance (Å) between methylenes				2.15	
S-SO Distance (Å)					
syn to oxygen					3.35
anti to oxygen					3.18
S-O Bond Length (Å)					3.37
Ionization Potential (eV):					
Adiabatic	7.92	7.80	8.01	8.18	7.57
Non-Adiabatic	8.31	7.90	n/a[b]	n/a[b]	7.85

[a] This is the distance between neighboring sulfide sulfur atoms.
[b] Data not available.

As a useful preliminary for experimental work in the area, the concept of obtaining compound B (see Table A.8) from asterane was explored. Such a transformation has the additional potential of proceeding all the way to cubane, and would represent a significant advance in cubane synthetic technology if it worked (Scheme A.1).

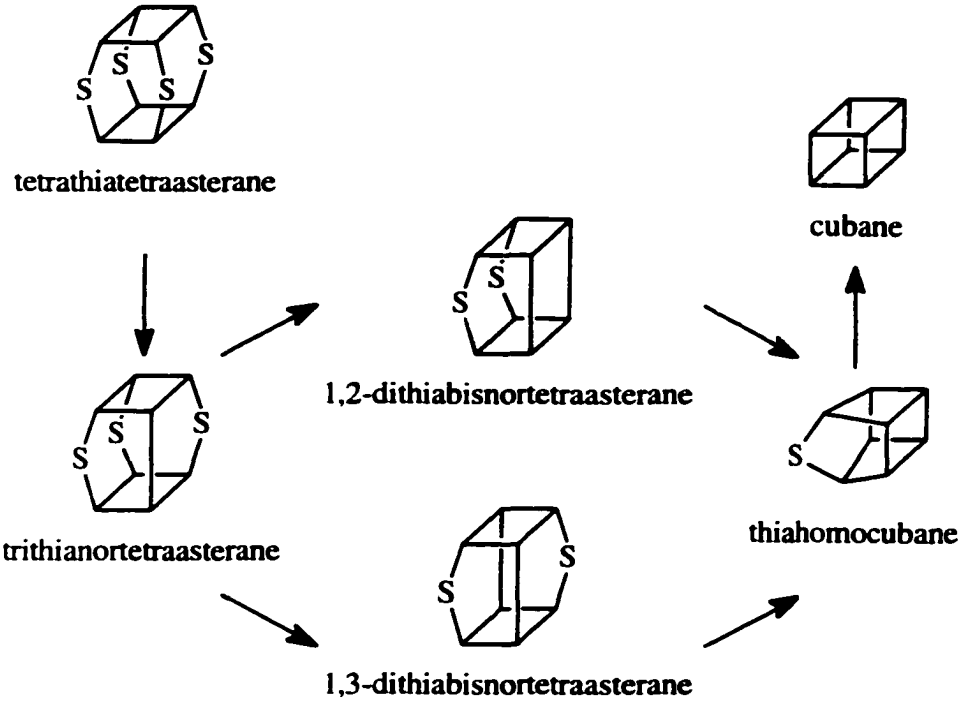

Scheme A.1. Asterane Desulfuration Pathways.

An important consideration in the process of desulfurating a cage compound such as asterane to form carbon-carbon bonds is the change in strain energy as successive sulfurs are removed. This strain energy was investigated by MM3 molecular mechanics calculations.

Table A.9. Strain Energy in the Desulfuration of Tetraasterane.

Compound	Strain Energy (kcal/mol)
Tetraasterane	98.8
Trithianorasterane	92.1
1,2-Dithiabisnorasterane	113.3
1,3-Dithiabisnorasterane	95.2
Thiahomocubane	132.6
Cubane	170.1

As can be seen from Table A.9, the mono-desulfurated product is actually the lowest in strain, and the 1,3-di-desulfurated product is lower than asterane in strain energy, while the

1,2-di-desulfurated product is considerably higher in strain energy. This is to be expected since the 1,3 product contains four five-membered rings where there were four six-membered rings, while the 1,2 product contains a four-membered ring, two five-membered rings and a six-membered ring where there were four six-membered rings. This difference results in a testable path prediction; additionally, this behavior may disfavor the use of chelating agents which remove two sulfur atoms in concert.

EXPERIMENTAL RESULTS

Asterane is a very difficult compound with which to work. It was found to be very insoluble in most organic solvents (greatest organic solubility is approximately 10^{-4} M in dichloromethane), and so the oxidation data which are so important to the investigation of delocalization of charge and spin was very difficult to obtain. During the course of attempted electrochemical analysis, a wide variety of systems were attempted. Ninety-eight percent sulfuric acid was used (as strong acids seemed to be able to dissolve asterane without altering it). The auto-ionization of the acid was sufficient for conductivity. The data in strong acids were acquired with a platinum working electrode versus a platinum pseudo-reference electrode (see Chapter 7). Asterane was found to have an irreversible oxidation wave at 0.43 V; for comparison, thianthrene under identical conditions gave a reversible redox couple with an oxidation wave at 0.47 V and a reduction wave at 0.39 V. Fluorosulfonic acid was attempted with the same electrode system, but provided no useful data. To increase conductivity, potassium chloride was added and hydrogen chloride gas removed by vacuum. The residual current was decreased, but no redox activity was observed. Twenty percent oleum (98% sulfuric acid with 20% dissolved sulfur trioxide) was used. Once again, auto-ionization was sufficient for conductivity. An oxidation shoulder was observed at 0.42 V. Triflic acid with potassium triflate was generated as for fluorosulfonic acid (created in the same fashion as the potassium fluorosulfonate above).

The results were unreliable, but on one scan there was obtained a peak at -0.23 V with the usual direction of current displacement (relative to the sweep direction) and two peaks (at 0.398 and -0.024 V).

After at best mixed results with strong acids, further work was attempted with dichloromethane, which (due to solubility limits) proved recalcitrant in preliminary studies. Distilled degassed dichloromethane was treated with trifluoroacetic anhydride (two drops in 1 mL) to further reduce the residual current curve. Immediately after the addition of TFAA to a saturated solution of asterane in dichloromethane, an oxidation wave at 0.64 V and two reduction waves at 0.45 and 0.18 V were observed. The solution was given five minutes to react, since without an acid catalyst, TFAA reacts fairly slowly with water. After five minutes, the peak at 0.18 V had disappeared, while the oxidation wave was still present, as was the reduction wave, although shifted slightly to 0.41 V. Since the data was acquired versus a platinum pseudo-reference, ferrocene was added, and a redox couple with an oxidation wave at 0.23 V and a reduction wave at 0.11 V was observed.

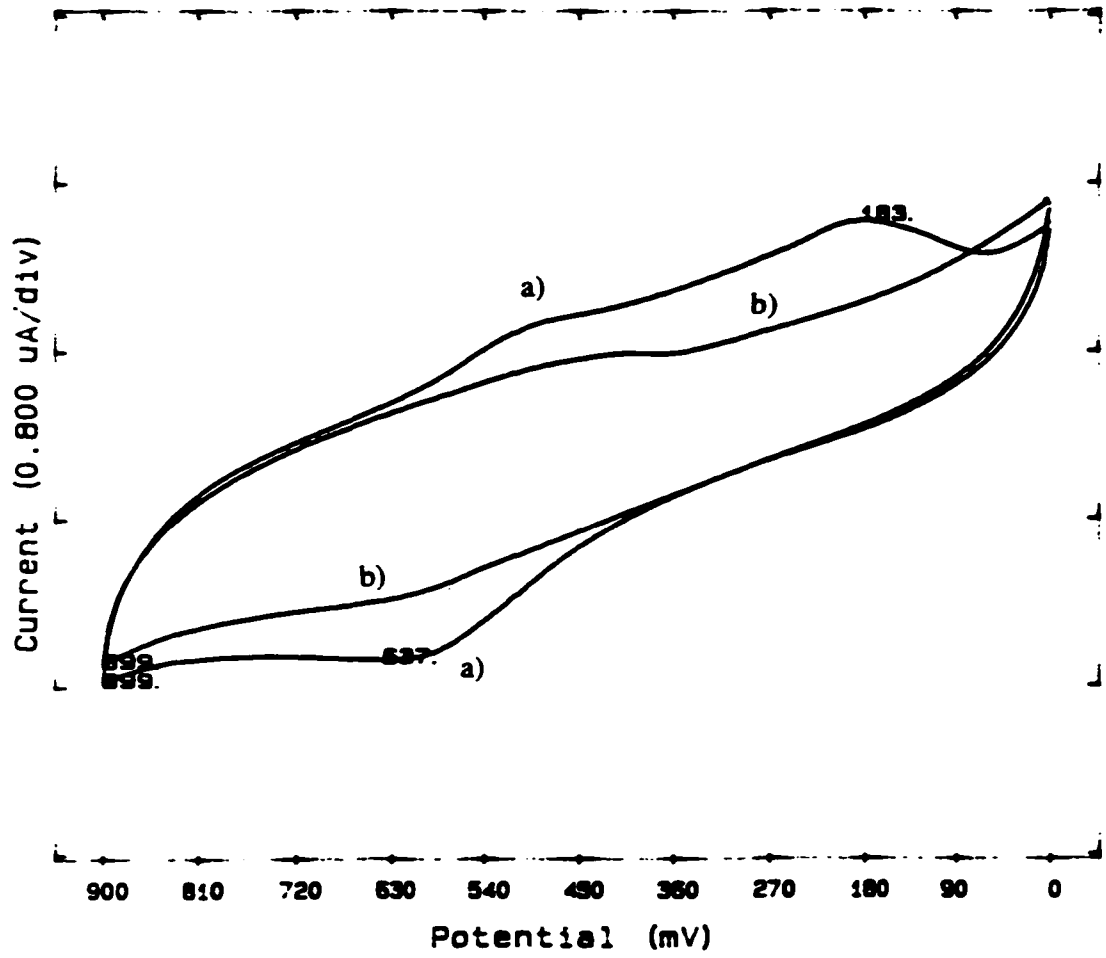

Figure A.5. Cyclic Voltammograms of Asterane in Dichloromethane with Trifluoroacetic Anhydride.
a) Immediately After Addition of TFAA; b) After Five Minutes.
Full scale = 4 μA, acquired at 100 mV/s.

Carbon paste electrodes were constructed. Both asterane and thianthrene showed the distortion typical of a carbon paste electrode into which the counterions have difficulty penetrating. Asterane was observed to have an oxidation wave at 0.11 V and a reduction wave at -0.20 V (versus Ag/0.1 M $AgNO_3$ in MeCN with a conducting solution of 0.1 M $LiClO_4$). This redox couple, although highly distorted by adverse diffusion effects, was probably reversible. Under the same conditions the thianthrene was observed to have a very similar redox couple, with an oxidation wave at 0.06 V and a reduction wave at -0.36 V. It also displayed a second oxidation wave at 0.51 V. Ferrocene, unlike the other two compounds, displayed a fairly normal reversible cyclic voltammogram, although slightly distorted. The oxidation wave was found at 0.04 V and the reduction wave at -0.10 V.

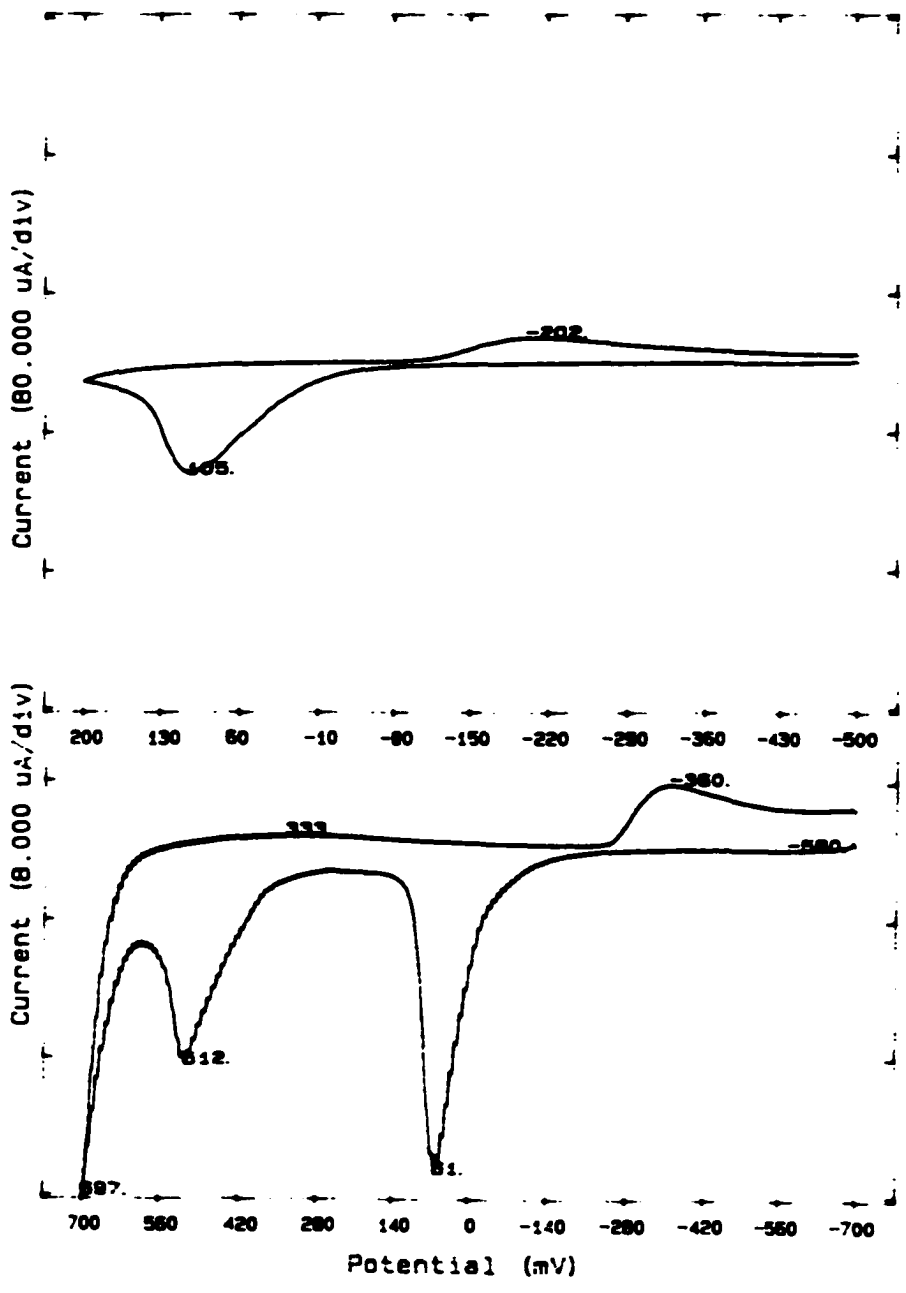

Figure A.6. Carbon-Paste Cyclic Voltammograms.
a) Asterane; b) Thianthrene.

Thin-layer electrochemistry was also attempted, but no results were obtained.

Charge-transfer spectroscopy with tetracyanoethylene was also attempted, but did not yield a charge-transfer band.

DISCUSSION

It should be mentioned as a preliminary to the discussion of asterane ionizations that the assignments seen in Table A.2 are fairly rough; the computational nature of many of the orbitals is not well known, and though He(I) and He(II) data were acquired for asterane, the analysis of orbital contributions proved difficult and somewhat ambiguous. The proposed fit is based mainly on the groupings of signals observed in the computational simulation of the eigenvalues and on similar groupings of signals in the photoelectron spectrum. The match may be confused by the existence of observable vibrational progressions.

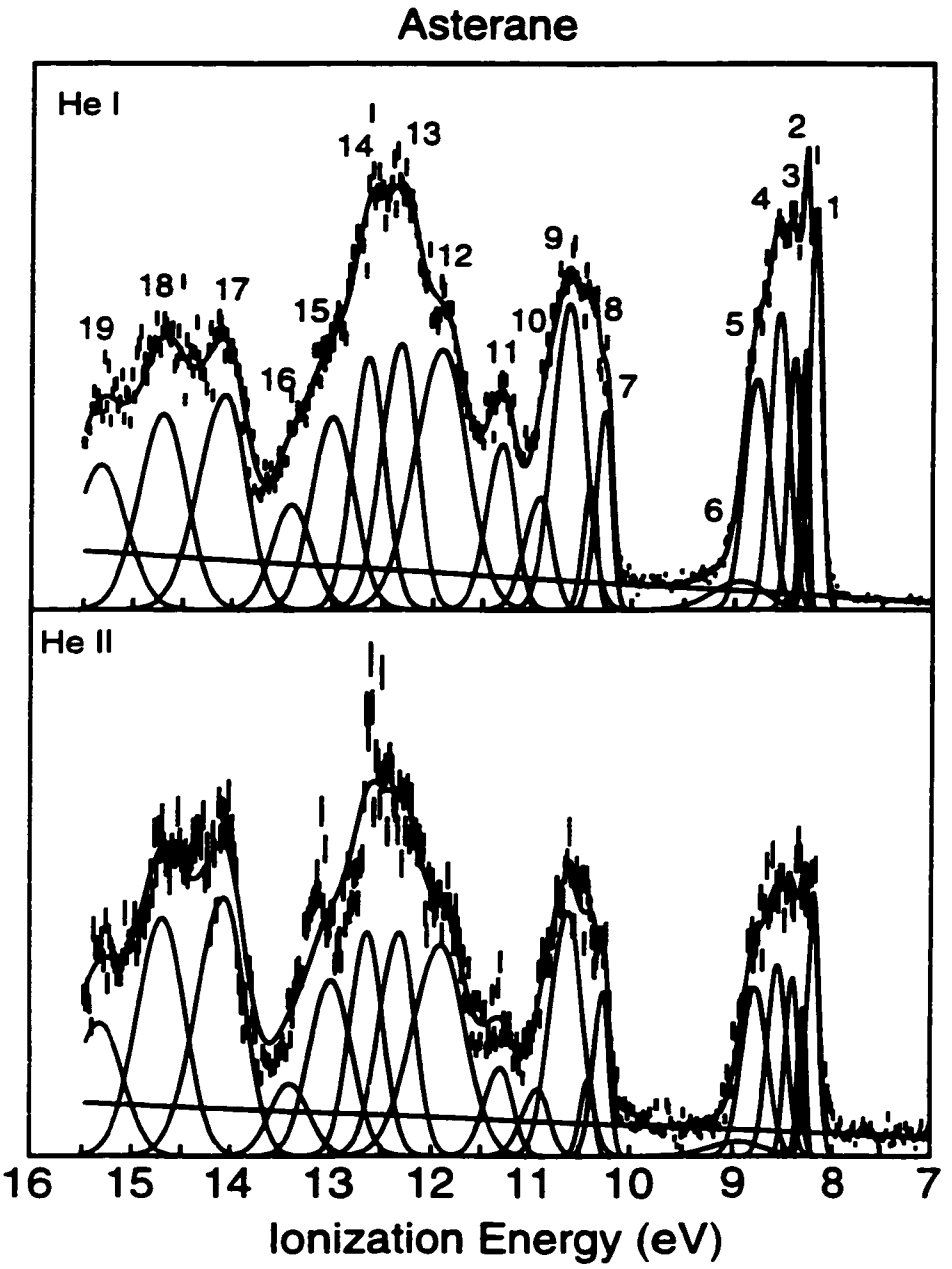

Figure A.7. Photoelectron Spectra of Asterane.
a) He(I) Spectrum; b) He(II) Spectrum.

One such potential confusion is in the first peak grouping. Two very sharp bands are visible at the leading edge of ionization. The splitting was found to be 0.100 ± 0.003 eV, which, if vibrational, would correspond to 810 ± 24 cm^{-1}. The most likely explanation is that these peaks are actually the HOMO and SHOMO, which have a computationally predicted splitting of 0.07 eV. They could be so sharp due to the small geometric relaxation energy predicted for asterane (0.39 eV). Of course, they might also be vibrational. According to the computational simulation of the vibrational spectrum of asterane radical cation (Table A.5), candidates for the coupled vibrational motion (on the basis of matching the observed splitting) include the doubly-degenerate E_U transitions at 708 cm^{-1}, the doubly-degenerate E_G transitions at 722 cm^{-1}, the singly-degenerate B_{2U} transition at 887 cm^{-1}, and the singly-degenerate B_{1G} transition at 923 cm^{-1}.

It can be said, at the very least, that the non-adiabatic (vertical) ionization potential is known with certainty. This value (8.19 eV) compares well with the ΔSCF-computed value of 8.31 eV. It is not expected to compare well to the HOMO eigenvalue, but the error between the two is in the expected direction (Chapter 3).

Interesting effects are observed in the comparison of neutral asterane and the radical cation. While most geometric parameters remain similar, the S-S non-bonded distance is seen to shrink a bit; this is achieved mainly by opening up the C-S-C bond angle. This result would seem peculiar on its own, since the charge and spin are shared over the sulfurs and they should desire to be farther from one another; however, viewed in terms of relieving the anti-aromatic interaction of the sulfur atoms and replacing it with a more favorable seven-electron interaction (see Chapter 2), this is to be expected, as increased S-S 3p overlap increases the stabilizing interaction.

Apparently, the potentially aromatic interaction of six sulfur 3p electrons does not outweigh the destabilization of two full positive charges over four sulfur atoms, and upon oxidation to the dication asterane undergoes gross structural alterations, which are

summarized in Table A.6. Notable among the geometric changes are the carbon-carbon and carbon-sulfur bond contractions. When taken along with the interesting distribution of charge, they paint a picture of a pair of thionium ions which may be tending toward a second carbon-carbon bond cleavage to form a dithioethylene unit and a dithionium unit (indicated by the contraction of the carbon-carbon bond adjacent to the cleaved bond). There is still certainly a large sulfur-sulfur interaction, as evidenced by the large charge on the sulfur atoms not adjacent to the cleaved bond, but the nature of that interaction is different from that in the radical cation.

Due to the large number of predicted transitions near the experimental transition, it would be easy to pick one which fits the experimental data very closely. None of the transitions are predicted to be allowed. Given that the molecule is of high symmetry and contains many sulfur atoms which participate in the highest occupied molecular orbitals, it is possible that a triplet transition may be observable though theoretically disallowed. This has been seen for other sulfur-bearing molecules (Chapter 3). Considering this, the first four transitions are all triplets and are all within 7 nm of the experimental value, which is probably less than the indeterminate solvent correction. The actual transition is most likely a composite of the $^3B_{2G}$ HOMO $\rightarrow$ LUMO and $^3A_{1G}$ HOMO-1 $\rightarrow$ LUMO transitions (205-206 nm). This conclusion is based on the aforementioned transitions' orbital composition, even though the error in CIS calculations is usually to predict a longer wavelength than is observed. Without experiments in which the absorbance is measured along the crystal axes and compared, it is impossible to say for certain, and may be impossible even with such experiments.

The nature of the cyclic delocalization of sulfur 3p electrons was explored in greater depth with preliminary studies on "interrupted" asteranes (See Table A.8). Though it was expected that these compounds should have much higher ionization potentials due to the lack of cyclic conjugation, it was found not to be true. Most of the compounds exhibited

ionization potentials very similar to that of asterane, and the sulfoxide was substantially easier to ionize. The S-S non-bonded distance was found to be similar for all the molecules, the largest variation being for compound D (where one sulfur was removed and the open valences replaced with hydrogen) and the sulfoxide. In compound D, the sulfurs seem to have merely taken advantage of the open space to relieve repulsive interactions and move around toward the unoccupied position. In compound C, where a methylene unit replaces one sulfur atom, the hydrogens cause the reverse effect, and there is a fairly close approach between sulfur and methylene hydrogen. The sulfoxide is a particularly interesting case, since the S-S non-bonded distance syn to the oxygen is 3.35 Å, but the S-S non-bonded distance anti to the oxygen is 3.18 Å. The fact that some of the molecules have an ionization potential near asterane's is explainable; for example, the highly-strained C-C bond in compound B could be participating in the cyclic conjugation. This is less believable for compounds C and D. It must be concluded that, although the charge and spin in asterane are cyclically delocalized, this cyclic delocalization is not necessary to lower the ionization potential, and indeed is not the best method of lowering the ionization potential, as seen in the asterane analogues. It is interesting that asterane has by far the largest predicted geometric relaxation energy (0.39 eV). Perhaps this indicates a greater importance in the proximity of the sulfur atoms (which move slightly closer in the radical cation) than would be suspected from a preliminary comparison with the "interrupted" asteranes.

Unfortunately, the most that can be said about asterane electrochemistry is that asterane behaved very similarly in potential and current-voltage response to the first redox couple of thianthrene. The most promising results were definitely the carbon-paste cyclic voltammograms. They showed that the oxidation potential of asterane is only 0.04 V more positive than thianthrene ($E^{\circ\prime} = 0.30$ in 0.1 M tetra-n-butylammonium perchlorate/SO_2

versus Ag/saturated $AgNO_3$ in SO_2 at -40°C[165]), though the "center" of the redox "couple" is certainly more positive yet (the reduction wave observed for asterane was 0.16 V more positive than that of thianthrene). Under the same conditions, the asterane oxidation wave was also 0.07 V more positive than the center of the ferrocene redox couple (more symmetric, so presumable more reliable). Ferrocene is known to have an $E^{\circ\prime} = 0.307$ V in 0.2 M lithium perchlorate in acetonitrile versus a saturated calomel electrode.[165]

CONCLUSIONS

It is difficult to draw many conclusions from the current data, but it seems fairly certain that asterane does indeed possess a cyclically delocalized electronic structure, primarily based on sulfur 3p orbitals engaged in σ-type overlap, with Walsh-like contributions from carbon 2p orbitals. Although this electronic structure does delocalize the charge and spin, it does not seem to lend any unusual ease of ionization or stability to the radical cation. Asterane would be an interesting candidate for more involved spectrophotometric experiments involving the solid state, and these would have the advantage of not being forced to deal with asterane in solution, quite a tricky prospect. Asterane electrochemistry did not yield spectacular results, but some reliable data were obtained. It is not judged likely, in the author's opinion, that any further results will be obtained from any conventional means, and many unconventional techniques have already been explored. The field may hope to be furthered by synthetic means in which more soluble asterane analogues might be obtained by desymmetrizing the molecule via substitution.

REFERENCES

1) Block, E.; Birringer, M.; DeOrazio, R.; Fabian, J.; Glass, R. S.; Guo, C.; He, C.; Lorance, E.; Qian, Q.; Schroeder, T. B.; Shan, Z.; Thiruvazhi, M.; Wilson, G. S.; Zhang, X. *J. Am. Chem. Soc.* **2000**, *122*, 5052-5064.

2) Mortensen, J. T.; Sørensen, N. A. *Acta Chem. Scand.* **1964**, *18*, 2392-2394.

3) Bohlmann, F.; Kleine, K.-M. *Chem. Ber.* **1965**, *98*, 3081-3086.

4) Bohlmann, F.; Zdero, C. In *The Chemistry of Heterocyclic Compounds*; Gronowitz, S., Ed.; Wiley: New York, 1985; Vol. 44, Chapter 3.

5) Norton, R. A.; Finlayson, A. J.; Towers, G. H. N. *Phytochemistry* **1985**, *24*.

6) Rodriguez, E. In *Biologically Active Natural Products*; Cutler, H. G., Ed.; ACS Symposium Series; American Chemical Society: Washington, D.C., 1988; Vol. 380, pp 432-437.

7) Ellis, S. M.; Balza, F.; Constabel, J. B.; Towers, G. H. N. In *Light-Activated Pest Control*; ACS Symposium Series; American Chemical Society: Washington, D.C., 1995; Vol. 616, pp 165-178.

8) Page, J. E.; Huffman, M. A.; Smith, V.; Towers, G. H. N. *J. Chem. Ecol.* **1997**, *23*, 2211-2226.

9) Guillet, G.; Philogene, B. J. R.; O'Meara, J.; Durst, T.; Arnason, J. T. *Phytochemistry* **1997**, *46*, 495-498.

10) De Vaila, S. S.; Brodi, B. B.; Rodriguez, E.; Gibson, D. M. *J. Nematol.* **1998**, *30*, 192-200.

11) Bierer, D. E.; Dener, J. M.; Dubenko, L. G.; Gerber, R. E.; Litvak, J.; Peterli, S.; Peterli-Roth, P.; Truong, T. V.; Mao, G.; Bauer, B. E. *J. Med. Chem.* **1995**, *38*, 2628-2648.

12) Rathore, R.; Lindeman, S. V.; Kumar, A. S.; Kochi, J. K. *J. Am. Chem. Soc.* **1998**, *120*, 6931-6939.

13) Matsue, T.; Evans, D. H. *J. Electroanal. Chem.* **1984**, *168*, 287-298.

14) Hammerich, R.; Parker, V. D. *Acta Chem. Scand. Ser. B* **1981**, *35*, 395-402.

15) Olsen, B. A.; Evans, D. H. *J. Am. Chem. Soc.* **1981**, *103*, 839-843.

16) Olsen, B. A.; Evans, D. H.; Agranat, I. *J. Electroanal. Chem.* **1982**, *136*, 139-148.

17) Matsue, T.; Evans, D. H.; Agranat, I. *J. Electroanal. Chem.* **1984**, *163*, 137-143.

18) Gillies, J. Z.; Gillies, C. W.; Cotter, E. A.; Block, E.; DeOrazio, R. *J. Mol. Spectrosc.* **1996**, *180*, 139-144.

19) Glass, R. S.; Gruhn, N. E.; Lichtenberger, D. L.; Lorance, E.; Pollard, J. R.; Birringer, M.; Block, E.; DeOrazio, R.; He, C.; Shan, Z.; Zhang, X. *J. Am. Chem. Soc.* **2000**, *122*, 5065-5075.

20) Sandman, D. J.; Ceaser, G. P.; Nielsen, P.; Epstein, A. J.; Holmes, T. J. *J. Am. Chem. Soc.* **1978**, *100*, 202-206.

21) Bock, H.; Brahler, G.; Dauplaise, D.; Meinwald, J. *Chem. Ber.* **1981**, *114*, 2622-2631.

22) Zweig, A.; Hoffman, A. K. *J. Org. Chem.* **1965**, *30*, 3997-4001.

23) Aso, Y.; Yui, K.; Miyoshi, T.; Otsubo, T.; Ogura, F.; Tanaka, J. *Bull. Chem. Soc. Jpn.* **1988**, *61*, 2013-2018.

24) Hine, J. *Structural Effects on Equilibria in Organic Chemistry*; John Wiley and Sons, Inc.: New York, 1975.

25) Ehrenson, S.; Brownlee, R. T. C.; Taft, R. W. *Prog. Phys. Org. Chem.* **1973**, *10*, 1.

26) Gillespie, R. J.; Ireland, P. R.; Vekris, J. E. *Can. J. Chem.* **1975**, *53*, 3147-3152.

27) Roesky, H. W.; Hamza, A. *Angew. Chem. Int. Ed. Engl.* **1976**, *15*, 226.

28) Gillespie, R. J.; Kent, J. P.; Sawyer, J. F. *Inorg. Chem.* **1981**, *20*, 3784-3799.

29) Cameron, T. S.; Haddon, R. C.; Mattar, S. M.; Parsons, S.; Passmore, J.; Ramirez, A. P. *J. Chem. Soc. Chem. Commun.* **1991**, 358-360.

30) Cameron, T. S.; Haddon, R. C.; Mattar, S. M.; Parsons, S.; Passmore, J.; Ramirez, A. P. *J. Chem. Soc. Dalton Trans.* **1992**, 1563-1572.

31) Cameron, T. S.; Haddon, R. C.; Mattar, S. M.; Parsons, S.; Passmore, J.; Ramirez, A. P. *Inorg. Chem.* **1992**, *31*, 2274-2279.

32) Wolmerhäuser, G.; Heckmann, G. *Angew. Chem. Int. Ed. Engl.* **1992**, *31*, 779-780.

33) Ogawa, S.; Kikuchi, T.; Niizuma, S.; Sato, R. *J. Chem. Soc. Chem. Commun.* **1994**, 1593-1594.

34) Ogawa, S.; Kikuchi, T.; Sasaki, A.; Chida, S.; Sato, R. *Tetrahedron Lett.* **1994**, *35*, 5469-5472.

35) Ogawa, S.; Kikuchi, T.; Sasaki, A.; Chida, S.; Sato, R. *Tetrahedron Lett.* **1999**, *40*, 4375-4378.

36) Lide, D. R. *CRC Handbook of Chemistry and Physics*; 72 ed.; Lide, D. R., Ed.; CRC Press: Boca Raton, 1992.

37) Turner, D. W.; Baker, C.; Baker, A. D.; Brundle, C. R. *Molecular Photoelectron Spectroscopy*; Wiley-Interscience: London, 1970.

38) Moyano, A.; Paniagua, J. C. *J. Mol. Struct. (THEOCHEM)* **1996**, *369*, 39-52.

39) Krygowski, T. M.; Cyranski, M. K.; Czarnocki, Z.; Hafelinger, G.; Katritzky, A. R. *Tetrahedron* **2000**, *56*, 1783-1796.

40) Simkin, B. Y.; Minkin, V. I.; Glukhovtsev, M. N. "The Concept of Aromaticity in Heterocyclic Chemistry", *Adv. Heterocycl. Chem.*; 1993; Vol. 56, pp 303-428.

41) King, R. B. *Russ. Chem. Bull.* **1993**, *42*, 1283-1291.

42) Jug, K. *Chem. Listy* **1993**, *87*, 749-753.

43) Zhou, Z. X. *Int. Rev. Physi. Chem.* **1992**, *11*, 243-261.

44) Box, V. G. S. *Heterocycles* **1991**, *32*, 2023-2041.

45) Katritzky, A. R.; Karelson, M.; Malhotra, N. *Heterocycles* **1991**, *32*, 127-161.

46) Gorelik, M. V. *Usp. Khim.* **1990**, *59*, 197-228.

47) Randic, M.; Nikolic, S.; Trinajstic, N. *Coll. Czech. Chem. Commun.* **1988**, *53*, 2023-2054.

48) Juric, A.; Sabljic, A.; Trinajstic, N. *J. Heterocycl. Chem.* **1984**, *21*, 273-282.

49) Rabinovitz, M.; Willner, I.; Minsky, A. *Acc. Chem. Res.* **1983**, *16*, 298-304.

50) Tomoda, S.; Nomura, Y. *J. Synth. Org. Chem. Jpn.* **1979**, *37*, 197-206.

51) Perlstein, J. H. *Angew. Chem. Int. Ed. Engl.* **1977**, *16*, 519-534.

52) Dewar, M. J. S. *Angew. Chem. Int. Ed. Engl.* **1971**, *10*, 761-&.

53) Volpin, M. E. *Russ. Chem. Rev.* **1960**, *29*, 129-160.

54) Garratt, P. J. *Aromaticity*; Wiley-Interscience: New York, 1986.

55) Minkin, V. I.; Glukhovtsev, M. N.; Simkin, B. I. *Aromaticity and Antiaromaticity: Electronic and Structural Aspects*; John Wiley and Sons: New York, 1994.

56) *Aromaticity: An International Symposium held at Sheffield on 6th-8th July 1966*; Chemical Society: Sheffield, England, 1966.

57) Badger, G. M. *Aromatic Character and Aromaticity*; Cambridge University Press: London, 1969.

58) Bergmann, E. D.; Pullman, B. *Aromaticity, Pseudo-Aromaticity, Anti-Aromaticity*; Bergmann, E. D.; Pullman, B., Ed.; Israel Academy of Sciences and Humanities: Jerusalem, Israel, 1970; Vol. 3.

59) Lewis, D. *Facts and Theories of Aromaticity*; Macmillan Press: London, 1975.

60) Shukla, D.; Wan, P. *J. Am. Chem. Soc.* **1993**, *115*, 2990-2991.

61) March, J. *Advanced Organic Chemistry: Reactions, Mechanisms, and Structure*; 4th ed.; John Wiley and Sons: New York, 1992.

62) Zimmermann, R. *J. Mol. Struct.* **1996**, *377*, 35-46.

63) Jas, G. S.; Kuczera, K. *Chem. Phys.* **1997**, *214*, 229-241.

64) Koseki, S.; Toyota, A. *J. Phys. Chem. A* **1997**, *101*, 5712-5718.

65)*The Sadtler Standard Spectra*; Sadtler Research Laboratories: Philadelphia, 1969.

66) Moore, T. L.; O'Connor, D. E. *J. Org. Chem.* **1966**, *31*, 3587-3592.

67) Krief, A. *Tetrahedron* **1980**, *36*, 2531-2640.

68) Ogura, K. "Sulfur Stabilization", In *Comprehensive Organic Synthesis*, Trost, B., Ed.; Pergamon Press: Oxford, 1991; Vol. 1, pp 505-539.

69) Streitwieser, A., Jr.; Juaristi, E.; Nebenzahl, L. L.; In *Comprehensive Carbanion Chemistry*; Elsevier: Amsterdam, 1980, pp 372-374.

70) Corey, E. J.; Seebach, D. *J. Org. Chem.* **1966**, *31*, 4097-4099.

71) Peterson, D. J. *J. Org. Chem.* **1967**, *32*, 1717-1720.

72) Shirley, D. A.; Reeves, B. J. *J. Organomet. Chem.* **1969**, *16*, 1-6.

73) Trost, B. M.; Keeley, D. E.; Arndt, H. C.; Rigby, J. H.; Bogdanowicz, M. J. *J. Am. Chem. Soc.* **1977**, *99*, 3080-3087.

74) Block, E.; Aslam, M. *J. Am. Chem. Soc.* **1985**, *107*, 6729-6731.

75) McDougal, P. G.; Condon, B. D.; Laffosse, M. D.; Lauro, A. M.; Vanderveer, D. *Tetrahedron Lett.* **1988**, *29*, 2547-2550.

76) Liu, Y. Q.; Glass, R. S. *Tetrahedron Lett.* **1997**, *38*, 8615-8618.

77) Taylor, R. D.; Wardell, J. L. *J. Organomet. Chem.* **1974**, *77*, 311-323.

78) McDougal, P. G.; Condon, B. D. *Tetrahedron Lett.* **1989**, *30*, 789-790.

79) Reich, H. J.; Bowe, M. D. *J. Am. Chem. Soc.* **1990**, *112*, 8994-8995.

80) Wartski, L.; El Bouz, M.; Seyden-Penne, J.; Dumont, W.; Krief, A. *Tetrahedron Lett.* **1979**, 1543-1546.

81) Kitteringham, J.; Mitchell, M. B. *Tetrahedron Lett.* **1988**, *29*, 3319-3322.

82) Parham, W. E.; Kalnins, M. A.; Theissen, D. R. *J. Org. Chem.* **1962**, *27*, 2698-2700.

83) Parham, W. E.; Motter, R. F. *J. Am. Chem. Soc.* **1959**, *81*, 2146-8.

84) Wiberg, K. B.; Castejon, H. *J. Am. Chem. Soc.* **1994**, *116*, 10489-10497.

85) Wolfe, S.; LaJohn, L. A.; Bernardi, F.; Mangini, A.; Tonachini, G. *Tetrahedron Lett.* **1983**, *24*, 3789-3792.

86) Bernardi, F.; Csizmadia, I. G.; Mangini, A.; Schlegel, H. B.; Whangbo, M.-H.; Wolfe, S. *J. Am. Chem. Soc.* **1975**, *97*, 2209-2218.

87) Cuevas, G.; Juaristi, E. *J. Am. Chem. Soc.* **1997**, *119*, 7545-7549.

88) Bernasconi, C. F.; Kittredge, K. W. *J. Org. Chem.* **1988**, *63*, 1944-1953.

89) Shatenshtein, A. I.; Gvozdeva, H. A. *Tetrahedron* **1969**, *25*, 2749-2755.

90) Oae, S.; Tagaki, W.; Ohno, A. *Tetrahedron* **1964**, *20*, 427-436.

91) Bordwell, F. G.; Bares, J. E.; Bartmess, J. E.; Drucker, G. E.; Gerhold, J.; McCallum, G. J.; Vanier, N. R.; Matthews, W. S. *J. Org. Chem.* **1977**, *42*, 326-332.

92) Eliel, E. L.; Hartmann, A. A.; Abatjoglou, A. G. *J. Am. Chem. Soc.* **1974**, *96*, 1807-1816.

93) Hartmann, A. A.; Eliel, E. L. *J. Am. Chem. Soc.* **1971**, *93*, 2572.

94) Seebach, D.; Gabriel, J.; Hassig, R. *Helv. Chim. Acta* **1984**, *67*, 1083-1099.

95) Hoffmann, R. W.; Julius, M.; Chemla, F.; Ruhland, T.; Frenzen, G. *Tetrahedron* **1994**, *50*, 6049-6060.

96) Hoffmann, R. W.; Dress, R. K.; Ruhland, T.; Wenzel, A. *Chem. Ber.* **1995**, *128*, 861-870.

97) Aggarwal, V. K. *Angew. Chem. Int. Ed. Engl.* **1994**, *33*, 175-177.

98) Dress, R. K.; Rolle, T.; Hoffmann, R. W. *Chem. Ber.* **1995**, *128*, 673-677.

99) Eliel, E. L. *Angew. Chem. Int. Ed. Engl.* **1972**, *11*, 739.

100) Schäfer, H.; Schöllkopf, N.; Walter, D. *Tetrahedron Lett.* **1968**, 2809-2814.

101) Wright, A.; West, R. *J. Am. Chem. Soc.* **1974**, *96*, 3222-3232.

102) Kuivila, H. G.; Considine, J. L.; Sarma, R. H.; Mynott, R. J. *J. Organomet. Chem.* **1976**, *111*, 179-196.

103) Frisch, M. J.; Trucks, G. W.; Schlegel, H. B.; Gill, P. M. W.; Johnson, B. G.; Robb, M. A.; Cheeseman, J. R.; Keith, T.; Petersson, G. A.; Montgomery, J. A.; Raghavachari, K.; Al-Laham, M. A.; Zakrzewski, V. G.; Ortiz, S. V.; Foresman, J. B.; Peng, C. Y.; Ayala, P. Y.; Chen, W.; Wong, M. W.; Andres, J. L.; Replogle, E. S.; Gomperts, R.; Martin, R. L.; Fox, D. J.; Binkley, J. S.; Defrees, D. J.; Baker, J.; Stewart, J. P.; Head-Gordon, M.; Gonzalez, C.; Pople, J. A. *Gaussian 94*; Revision E.2; Gaussian, Inc.: Pittsburgh, 1995.

104) *Spartan*; Version 4.0.2 GL ed.; Wavefunction, Inc.: Irvine, 1995.

105) Schaefer, T.; Kunkel, J. P.; Schurko, R. W.; Bernard, G. M. *Can. J. Chem.* **1994**, *72*, 1722-1727.

106) Jankowski, K. *Org. Mag. Res.* **1977**, *10*, 50-51.

107) van Berkel, W. W.; de Koning, L. J.; Nibbering, N. M. M. *J. Am. Chem. Soc.* **1987**, *109*, 7602-7608.

108) Biellmann, J.-F.; d'Orchymont, H.; Schmitt, J.-L. *J. Am. Chem. Soc.* **1979**, *101*, 3283-3288.

109) McLafferty, F. W.; Turecek, F. "Theory of Unimolecular Ion Decompositions" In *Interpretation of Mass Spectra*; 4th ed.; University Science Books: Mill Valley, 1993, pp 115-134.

110) Bates, R. B.; Potter, D. E.; Kroposki, L. M. *J. Org. Chem.* **1972**, *37*, 560-&.

111) de Koning, L. J.; Nibbering, N. M. M. *J. Am. Chem. Soc.* **1988**, *110*, 2066-2073.

112) Glass, R. S.; Guo, Q.; Liu, Y. Q. *Tetrahedron* **1997**, *53*, 12273-12286.

113) Mahling, S.; Asmus, K. D.; Glass, R. S.; Hojjatie, M.; Wilson, G. S. *J. Org. Chem.* **1987**, *52*, 3717-3724.

114) Mahling, S.; Asmus, K. D.; Glass, R. S.; Hojjatie, M.; Wilson, G. S. *Abstr. Pap. Amer. Chem. Soc.* **1987**, *194*, 224-ORGN.

115) Glass, R. S.; Petsom, A.; Hojjatie, M.; Mahling, S.; Gobl, M.; Asmus, K. D.; Wilson, G. S. *J. Electrochem. Soc.* **1986**, *133*, C127-C127.

116) Glass, R. S.; Hojjatie, M.; Petsom, A.; Wilson, G. S.; Gobl, M.; Mahling, S.; Asmus, K. D. *Phosphorus Sulfur Silicon Relat. Elem.* **1985**, *23*, 143-168.

117) Glass, R. S.; Hojjatie, M.; Wilson, G. S.; Mahling, S.; Gobl, M.; Asmus, K. D. *J. Am. Chem. Soc.* **1984**, *106*, 5382-5383.

118) Glass, R. S. *Rev. Heteroatom. Chem.* **1996**, *15*, 1-24.

119) Glass, R. S. *Xenobiotica* **1995**, *25*, 637-651.

120) Glass, R. S.; Radspinner, A. M.; Singh, W. P. *Abstr. Pap. Amer. Chem. Soc.* **1992**, *204*, 266-ORGN.

121) Doi, J. T.; Musker, W. K. *Phosphorus Sulfur Silicon Relat. Elem.* **1988**, *35*, 173-182.

122) Russell, D. D.; Steffen, L. K.; Sabahi, M.; Hojjatie, M.; Glass, R. S.; Wilson, G. S. *J. Electrochem. Soc.* **1987**, *134*, C496-C496.

123) Doi, J. T.; Bharadwaj, P. K.; Musker, W. K. *J. Org. Chem.* **1987**, *52*, 2581-2584.

124) Doi, J. T.; Kessler, R. M.; Deleeuw, D. L.; Olmstead, M. M.; Musker, W. K. *J. Org. Chem.* **1983**, *48*, 3707-3712.

125) Glass, R. S.; Coleman, B. R.; Setzer, W. N.; Wilson, G. S. *J. Electrochem. Soc.* **1983**, *130*, C119-C119.

126) Hirschon, A. S.; Doi, J. T.; Musker, W. K. *J. Am. Chem. Soc.* **1982**, *104*, 725-730.

127) Wilson, G. S.; Swanson, D. D.; Klug, J. T.; Glass, R. S.; Ryan, M. D.; Musker, W. K. *J. Am. Chem. Soc.* **1979**, *101*, 1040-1042.

128) Glass, R. S.; Radspinner, A. M.; Singh, W. P. *Pure Appl. Chem.* **1996**, *68*, 853-858.

129) Glass, R. S. *Top. Curr. Chem.* **1999**, *205*, 1-87.

130) Yoshida, J.; Maekawa, T.; Murata, T.; Matsunaga, S.; Isoe, S. *J. Am. Chem. Soc.* **1990**, *112*, 1962-1970.

131) Yoshida, J.; Morita, Y.; Itoh, M.; Ishichi, Y.; Isoe, S. *Synlett* **1992**, *1992*.

132) Yoshida, J.; Ishichi, Y.; Nishiwaki, K.; Shiozawa, S.; Isoe, S. *Tetrahedron Lett.* **1992**, *33*, 2599-2602.

133) Yoshida, J.; Itoh, M.; Isoe, S. *J. Chem. Soc. Chem. Commun.* **1993**, *1993*, 547-549.

134) Yoshida, J. *Top. Curr. Chem.* **1994**; *170*, 39-81.

135) Yoshida, J.; Watanabe, M.; Toshioka, H.; Imagawa, M.; Suga, S. *Chem. Lett.* **1998**, *1998*, 1011-1012.

136) Glass, R. S.; Radspinner, A. M.; Singh, W. P. *J. Am. Chem. Soc.* **1992**, *114*, 4921-4923.

137) Kimura, K.; Katsumata, S.; Achiba, Y.; Yamazaki, T.; Iwata, S. *Handbook of He(I) PES Spectra of Fundamental Organic Molecules*; Halsted: New York, 1981.

138) White, J. M. *Austr. J. Chem.* **1995**, *48*, 1227-1251.

139) Block, E.; Yencha, A. J.; Aslam, M.; Eswarakrishnan, V.; Luo, J. Z.; Sano, A. *J. Am. Chem. Soc.* **1988**, *110*, 4748-4753.

140) Bock, H.; Meuret, J. *J. Organomet. Chem.* **1993**, *459*, 43-54.

141) Hehre, W. J.; Radom, L.; von Rague Schleyer, P.; Pople, J. A. *Ab Initio Molecular Orbital Theory*; John Wiley and Sons: New York, 1986.

142) Wadt, W. R.; Hay, P. J. *J. Chem. Phys.* **1985**, *82*, 284-298.

143) Schöberl, A.; Wagner, A. "Methoden zur Herstellung und Umwandlung von Sulfiden (Thioäthern)", Methoden der Organischen Chemie (Houben-Weyl), Ed.; Vol. IV 9, pp 93-148.

144) Weibull, B. *Ark. Kemi A* **1946**, *23*.

145) McAllan, D. T.; Cullum, T. V.; Dean, R. A.; Fidler, F. A. *J. Am. Chem. Soc.* **1951**, *73*, 3627.

146) Vecera, M.; Gasparic, J.; Snobl, D.; Jurecek, M. *Coll. Czech. Chem. Commun.* **1956**, *21*, 1284-1285.

147) Vogel, A. I.; Cowan, D. M. *J. Chem. Soc.* **1943**, 16-24.

148) Willer, R. L.; Eliel, E. L. *J. Am. Chem. Soc.* **1977**, *99*, 1925-1936.

149) Marvel, C. S.; Lazier, W. A. "Benzoyl Piperidine", *Organic Syntheses*; John Wiley and Sons, Incorporated: New York, 1941; Vol. 1, pp 99-101.

150) von Braun, J. "Pentamethylene Bromide", *Organic Syntheses*; John Wiley and Sons, Incorporated: New York, 1941; Vol. 1, pp 428-430.

151) Vedejs, E.; Eberlein, T. H.; Mazor, D. J.; McClure, C. K.; Perry, D. A.; Ruggeri, R.; Schwartz, E.; Stults, J. S.; Varie, D. L.; Wilde, R. G.; Wittenberger, S. *J. Am. Chem. Soc.* **1986**, *51*, 1556-1562.

152) Dewar, M. J. S. *Bull. Soc. Chim. Belg.* **1979**, *88*, 957-967.

153) Cremer, D.; Gauss, J. *J. Am. Chem. Soc.* **1986**, *108*, 7467-7477.

154) Furusaki, A. *J. Mol. Struct. (THEOCHEM)* **1996**, *362*, 365-377.

155) Lee, I.; Yang, K.; Kim, H. S. *Tetrahedron* **1985**, *41*, 5007-5010.

156) Lee, I. *Bull. Korean Chem. Soc.* **1985**, *6*, 178-179.

157) Sagl, D. J.; Martin, J. C. *J. Am. Chem. Soc.* **1988**, *110*, 5827-5833.

158) Wasserman, E.; Hutton, R. S.; Kuck, V. J.; Chandross, E. A. *J. Am. Chem. Soc.* **1974**, *96*, 1965-1966.

159) Kobayashi, K.; Takahashi, O.; Namatame, K.; Kikuchi, O.; Furukawa, N. *Chem. Lett.* **1998**, 515-516.

160) Chance, J. M.; Kahr, B.; Buda, A. B.; Toscano, J. P.; Mislow, K. *J. Org. Chem.* **1988**, *53*, 3226-3232.

161) Bojkova, N. V.; Glass, R. S. *Tetrahedron Lett.* **1998**, *39*, 9125-9126.

162) Heilbronner, E. *Tetrahedron Lett.* **1964**, 1923-1928.

163) Dewar, M. J. S. *The Molecular Orbital Theory of Organic Chemistry*; McGraw-Hill: New York, 1969.

164) Zimmerman, H. E. *Acc. Chem. Res.* **1971**, *4*, 272-280.

165) Bard, A. J.; Faulkner, L. R. *Electrochemical Methods: Fundamentals and Applications*; John Wiley and Sons: New York, 1980.